

Label-free, Isothermal DNA-DNA Strand Displacement Amplification: Application in
Bioanalysis

A Dissertation

Presented in Partial Fulfillment of the Requirements for the
Degree of Doctor of Philosophy

with a

Major in Chemistry

in the

College of Graduate Studies

University of Idaho

Md Mamunul Islam

Major Professor: Ray von Wandruszka, Ph.D.

Committee Members: I. Francis Cheng, Ph.D.; Sebastian Stoian, Ph.D.; Peter B. Allen, Ph.D.

Department Administrator: Ray von Wandruszka, Ph.D.

August 2021

Authorization to Submit Dissertation

This dissertation of Md Mamunul Islam, submitted for the degree of Doctor of Philosophy with a Major in Chemistry and titled "Label-free, Isothermal DNA-DNA Strand Displacement Amplification: Application in Bioanalysis," has been reviewed in final form. Permission, as indicated by the signatures and dates below, is now granted to submit final copies to the College of Graduate Studies for approval.

Major Professor: _____ Date: _____

Ray von Wandruszka, Ph.D

Committee Members: _____ Date: _____

I. Francis Cheng, Ph.D.

_____ Date: _____

Peter B. Allen, Ph.D.

_____ Date: _____

Sebastian Stoian, Ph.D.

Department

Administrator: _____ Date: _____

Ray von Wandruszka, Ph.D

Abstract

DNA is not just a carrier of genetic information; it is also a chemical. It is a molecule with certain properties, a specific arrangement of atoms, and a commercialized chemical synthesis pathway. DNA is widely used, manipulated and well-studied in bioanalysis. For instance, the current diagnostic assays for the SARS-CoV-2 virus rely upon DNA based bioanalysis. At a fundamental level, a DNA based bioanalysis takes the advantages of Watson-Crick base pairing. Adenine pairs specifically with thymine, guanine pairs with cytosine. This pairing is cooperative and specific. DNA is held together by many weak hydrogen bonds only when sequences are complementary. Together with the advance of many detection systems, enzymes, small molecule dyes, DNA based bioanalysis is a diverse and demanding research field in chemistry. We used these advantages to develop enzymatic and non-enzymatic reactions for cost effective, label-free, isothermal detection. Two isothermal systems, entropy driven amplifier (EDA) and strand displacement amplification (SDA), are developed to detect physiologically important miRNAs. This thesis includes three research chapters and one review.

Acknowledgements

I would like to express my deep and sincere gratitude to Dr. Peter B. Allen, who was my supervisor throughout my time in the department and my current supervisor Ray von Wandruszka for their continuous support, mentoring, insightful comments and encouraging directions. Without their direction this paper could not have been successfully written. In brief, words are not enough to express my gratitude for Dr. Allen and his tremendous support in letting me to grow up as a researcher. It was a great privilege and honor to work and learn under his guidance.

I would also like to acknowledge all of my committee members for their guidelines, academic supports and suggestions on writing this paper that has helped me immensely to improve this writing.

Finally, I am very much thankful to my family for their continuous support.

Dedication

To my beloved late father and sister

Table of Contents

Authorization to Submit Dissertation	ii
Abstract.....	iii
Acknowledgements.....	iv
CHAPTER 1: Recent advance in strand displacement amplification (SDA): A versatile tool in bioanalytical application	1
1.1 Introduction:	2
1.2 Linear SDA:	6
1.3 Exponential amplification reaction (EXPAR)	8
1.4 PEN toolbox:.....	11
1.5 RACTA (RNA aptamer involved cascade transcription amplification)	13
1.6 CRISPR/Cas based SDA	14
1.7 SDA signal reporting method	17
1.7.1 Fluorescence based reporting method.....	17
1.7.2 Colorimetric detection	22
1.7.3 Electrochemical detection	25
1.8 Analyte/target of SDA	27
1.9 Conclusion	30
1.10 Reference	32
CHAPTER 2: Towards label-free, non-enzymatic, and isothermal detection of DNA-DNA reactions: Application of Thioflavin T as light up dye	40
2.1 Introduction.....	40
2.2 Methods	43
2.2.1 Materials	43

2.2.2 ThT fluorescence sensitivity with PW17Ext and ThTSignal oligonucleotide	43
2.2.3 Binding Curve	44
2.2.4 Melt Curve Analysis of the PW17Ext and ThTSignal oligonucleotides	44
2.2.5 Circular Dichroism and PAGE Analysis of PW17Ext and ThTSignal.....	44
2.2.6 One-step strand (OSD) reaction with ThT detection	45
2.2.7 Effect of ThT dye on the rate of the OSD reaction	45
2.2.8 Comparison of OSD reaction between ThT and Fluor-Quencher detection system	45
2.2.9 Entropy Driven Amplifier with ThT readout	46
2.3 Results and Discussion	47
2.3.1 Discovery of a new fluorogenic oligonucleotide for ThT	47
2.3.2 Spectroscopic and PAGE analysis of ThT reporter oligonucleotides	48
2.3.3 A simple DNA-DNA reaction show fluorogenic activity with ThT	51
2.3.4 Entropy Driven Amplifier with ThT readout	54
2.4 Conclusion	57
2.5 Supplementary Information.....	60
2.6 AUTHOR INFORMATION.....	67
2.6.1 Corresponding Author	67
2.6.2 Author Contributions	67
2.7 Notes The authors declare no competing interests.....	67
2.8 Acknowledgment	67
2.9 References.....	67
CHAPTER 3: Graphene oxide assisted light-up aptamer selection against Thioflavin T for label-free detection of microRNA.....	72

3.1 Introduction.....	72
3.2 Methods	75
3.2.1 Materials	75
3.2.2 Aptamer selection.....	75
3.2.3 ThT Aptamer characterization	77
3.2.4 Circular dichroism analysis.....	78
3.2.5 Binding assay of ThT and the Apt5.9-32	78
3.2.6 Melt curve analysis of the Apt5.9-32.....	78
3.2.7 Strand displacement amplification optimization	79
3.2.8 SDA with different reporter system.....	80
3.2.9 In-vitro detection of miR-215	81
3.2.10 SDA specificity.....	81
3.2.11. PAGE analysis of SDA product.....	82
3.3 Results and Discussion	82
3.3.1 In Vitro Selection.....	82
3.3.2 Aptamer characterization and optimization.....	84
3.3.3 Isothermal Strand displacement amplification	88
3.3.4 SDA Characterization and Optimization	90
3.3.5 Aptamer SDA product confers reaction specificity.....	92
3.3.6 Optimization of Template-215 concentration for the detection of miR-215.....	93
3.3.7 Detection of miR-215.....	94
3.4 Conclusion	96
3.5 Oligonucleotides used in this study	98
3.6 Supporting information.....	99

3.7 Author contributions.....	109
3.8 Notes	109
3.9 Reference	109
CHAPTER 4: Simple, low-cost fabrication of acrylic based droplet microfluidics and its use to generate DNA-coated particles.....	114
4.1 Introduction.....	114
4.2 Materials and Methods.....	117
4.2.1 Microfluidic chip fabrication	117
4.2.2 Characterization of the droplet generator design performance.....	118
4.2.3 Particle generation by microfluidics	119
4.2.4 Particle generation by homogenization.....	120
4.3 Results and Discussion	120
4.3.1 Characterization of laser cutter performance	120
4.3.2 Development of acrylic device bonding protocol.....	122
4.3.3 Particle generator chip behavior	124
4.3.4 Effect of flow rate on droplet size	126
4.3.5 Generation of polyacrylamide particles containing DNA	127
4.4 Conclusions.....	129
4.5 Supplementary information.....	132
4.6 Acknowledgements.....	136
4.7 Author Contributions	136
4.8 Competing Interests.....	136
4.9 References.....	136
Appendix A: Copyright permission	141

List of Figures

Figure 1.1. Nucleic acid amplification. A) Sensitivity of target nucleic acid before and after amplification. B) Schematic of electronic operational amplifier. C) Polymerase chain reaction based non-isothermal nucleic acid amplification D) Strand displacement amplification based isothermal nucleic acid amplification.	4
Figure 1.2. Schematic of SDA using two different template A) Linear SDA using dsDNA Template B) Linear SDA using ssDNA Template.	6
Figure 1.3. Six common nicking endonuclease used in SDA ¹⁴	7
Figure 1.4. Schematic of a typical EXPAR: (A) Primer annealing- primer X binding to the complementary sequence at the 3'-end of the EXPAR template to form a transient duplex; (B) Primer extension- Using dNTPs, DNA polymerase extend the primer strand on the EXPAR template, forming EXPAR template/extended primer duplex with a nicking enzyme recognition site 5'-GAGTCNNNN-3' on the newly extended top strand; (C) Nicking by nick endonuclease Nt.BstNBI- the extended top strand is nicked at the site specific position; (D) Release of the "nicked" strand- the "nicked" primer strand is released from the EXPAR template. The remaining-cleaved duplex form of the EXPAR template continue the linear amplification cycle, through the cycle of primer extension, nicking, and release; (E) the newly formed primer oligonucleotides products activate additional EXPAR template sequences, giving rise to exponential amplification of the primer X. (Adapted from ⁸).....	9
Figure 1.5. PEN toolbox molecular program for the detection of microRNA. A four-template based amplification using three types of enzymes (polymerase, exonuclease, and endonuclease): The conversion template converts the target microRNA to a short DNA sequence; The autocatalytic template acts as amplification template to amplify input DNA strand, pseudo template is used to suppress the non-specific amplification; the reporting template reports the amplification of the system in fluorescence readout mode.	12
Figure 1.6. Schematic of SDA based RNA aptamer involved cascade transcription amplification (RACTA). RACTA involves two templates for two modules. Amplification module: Template 1	

contains three complementary sites- target miRNA binding site, nick site, input strand site for downstream amplification cycle. Signal reporting module- Template 2 contains two complementary sites- trigger binding promoter site and reporter generating spinach site (adapted from⁹). 14

Figure 1.7. Schematic reaction mechanism of CRISPR powered SDA in several steps. **Step 1:** Target recognition-ribonucleoprotein complexes, a pair of Cas9 enzyme guided by guide RNA (sgRNA) specifically recognize two ends of the target dsDNA resulted in a nick in both non-target strands. **Step 2:** Primer binding-introducing of two initiating (IP) primers resulted in hybridization with the nicked non-target strands. **Step 3:** Linear SDA starts - SDA mixture (Klenow Fragment (KF) polymerase (3'→5' exo⁻), Nb.BbvCI nikase, and single-stranded DNA binding protein (SSB),dNTPs) drives linear SDA from two primer binding sites resulted in the displacement of single strands, the Strand-for and Strand-rev. **Step 4:** Exponential SDA starts-upon reannealing with the primers, the displaced strands of step 3 generate exponential SDA. **Step 5:** Signal readout- the end products are reported based on fluorescence measurement by a biotin and cy5 labeled PNA probes in cooperation with streptavidin coated magnetic beads. (Figure reprinted with permission³⁷)..... 16

Figure 1.8. Schematic of intercalating dyes generating fluorescence interacting with DNA. A) Dye generates fluorescence only after binding to dsDNA. B) Fluorescence intensity increases as a function of time after the amount of dsDNA increases. 19

Figure 1.9. Schematic shows calorimetric-based SDA detection. A) Target initiated SDA on Probe/AuNPs platform. B) SDA products induced Probe/AuNPs aggregation.....23

Figure 1.10. Figure 1.10. Schematic shows electrochemical-based SDA/EXPAR detection. A) SDA with dual function duplex probe for electrochemical readout of G4 catalyzed redox reaction of hemin. B) SDA products interacts with methylene blue (MB) labeled hairpin probe (HP) immobilized on Au electrode.....26

Figure 1.11: Schematic shows versatile SDA targets detection via different readout mode..28

Figure 2.1. ThT fluorescence-activated by DNA. (A) ThTSignal and PW17Ext sequences with highlighted guanosine triplets. (B) Fluorescence enhancement comparison between ThTSignal and shortened versions of ThTSignal (names indicate the selected bases from the full sequence), and Aptamer ThT.2-2 (C) Fluorescence emission of 5 μ M ThT upon excitation with a blue transilluminator in the presence of the indicated concentrations of PW17Ext or ThTSignal DNA. (D) Fluorescence measurement of PW17Ext and ThTSignal upon excitation with a wavelength of 440 nm as a function of DNA concentration in the presence of 10 mM KCl. (E) Fluorescence measurement of PW17Ext and ThTSignal in the absence of potassium (The fluorescence is given as a fluorescence enhancement relative to ThT alone. Error bars represent the standard deviation of triplicate measurements). 48

Figure 2.2. Structural analysis of ThTSignal and PW17Ext using Circular dichroism (CD) and PAGE. (A) Background subtracted CD spectra from 220 nm-300 nm for both ThTSignal (dashed) and PW17Ext (solid). (B) Native PAGE analysis (no urea, 10% w/w polyacrylamide) of ThTSignal. The white box indicates slow migrating bands. (C) Native PAGE analysis (no urea, 10% w/w polyacrylamide) of PW17Ext. The white box indicates slow migrating bands. (D) Denaturing PAGE analysis (7M urea, 10% w/w polyacrylamide) of both ThTSignal and PW17Ext. The white box indicates the region where we do not see significant slow migrating species..... 51

Figure 2.3. A simple reaction shows fluorogenic activity (RFU) as a function of time with ThT. (A) Base abstraction of ThTSignal. (B) Schematic of one-step strand displacement reaction. (C) Label-free fluorescence measurement of a one-step strand displacement reaction. Overlapping “other controls” include Spine, Fuel, Fuel/Spine, ThT. Oligos were at 0.5 μ M in the presence of 5 μ M of ThT..... 52

Figure 2.4. ThT effect on reaction kinetics. (A) Effect of ThT dye on the rate of the One-step Strand Displacement (OSD) reaction. Graph shows fluorescence as a function of time in two conditions: (orange) where ThT is present in the reaction and (blue) where ThT was added at the specified reaction time. (B) Effect of ThT dye on the rate of the OSD reaction. Graph shows fluorescence as a function of time in two conditions: (orange) where ThT is present in the

reaction and (yellow) where a quenched fluorophore was used instead. Blue and gray are negative controls as labeled. Error bars are the standard deviation of triplicate reactions.. 53

Figure 2.5. Entropy Driven Amplifier with ThT reporting system. (A) Schematic of the entropy-driven amplifier system. (B) PAGE analysis of the EDA system. (C) Fluorescence readout of EDA reaction. Overlapping “other controls” include Spine-ThTSignal-Block, Spine-ThTSignal-Block + Catalyst, Fuel, Catalyst, Spine, mutCatalyst 1, mutCatalyst 2, mutCatalyst 3, Block, and ThT. (D) Comparison of EDA with various concentrations of Catalyst as labeled. 56

Figure 2.S1. Fluorescence comparison of ThTSignal (this work) and ThT.2-2 (Pei et al., Anal. Methods, 2016, 8, 8461) at several concentrations. (A) Fluorescence enhancement of ThT (F/F_0 where F_0 is ThT only) at our chosen wavelengths by ThTSignal and ThT.2-2. (B) Fluorescence enhancement of ThT at the wavelengths chosen by Pei et al. (C) Fluorescence emission spectrum of ThT with ThTSignal, ThT.2-2, and alone with excitation at 440 nm. (D) Fluorescence emission spectrum of ThT with ThTSignal, ThT.2-2, and alone with excitation at 425 nm. (E) Excitation spectrum of ThT with ThTSignal, ThT.2-2, and alone with emission [detection] at 510 nm. 60

Figure 2.S2. Binding studies of ThTSignal and PW17Ext via TFA using Open Spectramax iD3 platereader. Graphs show Fluorescence (RFU) as a function of (A) ThTSignal concentration, (B) PW17Ext concentration. The blue line is the best fit binding isotherm used to determine dissociation constant (K_d) between (A)ThTSignal and ThT, (B) PW17Ext and ThT 61

Figure 2.S3. Melt curve analysis of ThT interaction with oligonucleotides. Top graphs show the fluorescence as a function of temperature. Bottom graphs show the first derivative of fluorescence as a function of temperature. (A) Graphs show triplicate melt curves of TFTsignal in the absence of potassium. (B) Graphs show triplicate melt curves of PW17Ext in the absence of potassium. (C) Graphs show triplicate melt curves of TFTsignal in the presence of potassium and (D) Graphs show triplicate melt curves of PW17Ext in the presence of potassium. In each case, an inset show the temperature at which the fluorescence reached half its maximal value ($T_{1/2}$). 62

Figure 2.S4. Melt curve analysis of oligonucleotides structure with UV absorbance at 295 nm. Graphs show the absorbance as a function of temperature. (A) Graph shows melt curve of ThTsignal in the absence of potassium. (B) Graph shows melt curve of PW17Ext in the absence of potassium. (C) Graph shows melt curve of ThTsignal in the presence of potassium and (D) Graph shows melt curve of PW17Ext in the presence of potassium..... 63

Figure 2.S5. Illustration of ImageJ analysis of ThTSignal and PW17Ext gels. Low mobility band intensity is not proportional to DNA concentration. 64

Figure 2.S6. Composite image and source image for non-denaturing PAGE analysis of the EDA circuit (Figure 4B). In the false color image (left), blue indicates the fluorescence after staining with a nonspecific intercalating dye (GelRed). Yellow color indicates fluorescence after staining the same gel with ThT. Fluorescence after staining with GelRed (center) is shown as a black-and-white fluorescence photograph. Fluorescence after staining with GelRed and ThT (right) is shown as a black-and-white fluorescence photograph. 65

Figure 2.S7. Effect of reporter mechanism on DNA circuit kinetics. Reaction is equivalent to the reaction shown in Figure 5C-D, but with a fluorophore-quencher rather than ThT based detection. The reaction is very similar in kinetics. 66

Figure 3.1. *In vitro* selection of ThT aptamer. A) Schematic shows the process of GO assisted *in vitro* selection of ThT aptamer (created with BioRender.com). B) Fluorescence intensity (RFU) of five aptamer candidates and ThT only (blank). C) An image of fluorescence generated by ThT in the absence and presence of five aptamer candidates selected in this study. 83

Figure 3.2. NUPACK characterization of ThT aptamer candidates. A) NUPACK predicted secondary structure of the Apt5. B) The sequence of Apt5 and its fragments. C) NUPACK predicted secondary structures of five truncated versions of Apt5..... 85

Figure 3.3. Aptamer minimization. A) Fluorescence intensity of the best aptamer candidate Apt5 and five sub-sequences of Apt 5; 1-24, 5-28, 9-32, 13-36, and 17-40 at the concentration of 1 μ M. B) Image of fluorescence generated by Apt5 and five sub-sequences of Apt 5 C) Raw fluorescence melt curve of Apt5.9-32 (fluorescence as a function of temperature) analysis. D)

Negative 1 st derivative plot of thermofluorometric analysis of ThT Apt5.9-32 at the indicated concentrations from 0 to 5 μ M.....	86
Figure 3.4. SDA with ThT aptamer (Apt5.9-32) Reporter. A) Schematic of SDA with the ThT aptamer (Apt5.9-32) reporter system. B) SDA product analysis by 12% PAGE. The white boxes indicate Apt5.9-32 bands.....	89
Figure 3.5. Optimization of experimental parameters. SBR as a function of (A) temperature, (B) Bst polymerase concentration, (C) nicking endonuclease concentration, (D) dNTPs concentration, (E) magnesium, and (F) ThT. (Error bars represent the standard deviation of triplicate measurements).....	91
Figure 3.6. SDA product specificity. (A) A schematic diagram (top) shows how SDA (aptamer product) and nsSDA (SDA with the non-aptamer product) react in ThT. A bar graph shows fluorescence intensity at 50 min (bottom). (B) A schematic diagram (top) shows how SDA and nsSDA react in SYBR Green II. A bar graph shows fluorescence intensity at 50 min (bottom). (Error bars represent the standard deviation of triplicate measurements).	93
Figure 3.7. SDA Detection of miR- 215. A) Fluorescence intensity (RFU) of SDA reaction (with [Template- 215] =100 nM) as a function of miR- 215 concentration (indicated concentrations from 0 to 250 nM). Fluorescence intensity was measured at 50 min. B) Relationship between fluorescence intensity and miR- 215 concentrations (indicated concentrations from 0- 20 nM) in the SDA system (with [Template- 215] =100 nM). C) Endpoint fluorescence spectra (at 50 min of the SDA reaction) containing different concentrations of miR-215 (0, 0.5, 1, 2, 5, 10, 20, 40, 50, 60, 80, and 100 nM). D) Sequences of target oligonucleotides (a-i) used for SDA specificity including microRNA targets (a-d) and partially homologous DNA targets (e-i). Underlined bases indicate one or two bases alteration with respect to the target miR-215 sequence. E) SDA specificity with several target oligonucleotides, at 50 nM. F) SDA specificity with several target oligonucleotides, at 20 nM. F/F ₀ is defined as the ratio of fluorescence intensity of SDA in the presence of target sequence(F) to the fluorescence intensity of SDA mix with no target(F ₀ , reagent blank). Error bars represent the standard deviation of triplicate measurements in all cases.	95

- Figure 3.S1. Melt curve analysis of ThT interaction with Apt5.9-32. Top graphs show the fluorescence as a function of temperature. Bottom graphs show the first derivative of fluorescence as a function of temperature. (A) Graphs show triplicate melt curves of Apt5.9-32 in the absence of potassium. (B) Graphs show triplicate melt curves of Apt5.9-32 in the presence of 10 mM potassium. (C) Graphs show triplicate melt curves of PW17Ext in the absence of potassium and (D) Graphs show triplicate melt curves of PW17Ext in the presence of 10 mM potassium. In each case, an inset shows the temperature at which the fluorescence reached half its maximal value ($T_{1/2}$). 99
- Figure 3.S2. Melt curve analysis of aptamer structure with UV absorbance at 260 nm. Top graphs show the absorbance as a function of temperature. Bottom graphs show the first derivative of absorbance as a function of temperature. Graphs show the duplicate absorbance as a function of temperature of the aptamer, Apt5.932 (at 1 μ M) in two conditions: In selection buffer, no ThT(left) and in selection buffer, with 5 μ M ThT (right)..... 100
- Figure 3.S3. CD spectra of the Apt5.9-32 with controls: PW17Ext (as a G4DNA), blank (buffer-no DNA), ssDNA (random), dsDNA (random) 101
- Figure 3.S4. Binding studies of Apt5.9-32, using Spectrometer Id3 platereader. Graphs show fluorescence intensity (RFU) as function of (A) Apt5.9-32 concentration, trial 1, (B) Apt5.9-32 concentration, trial 2, and (C) Apt5.9-32 concentration, trial 3. The blue line is the best fit binding isotherm used determine dissociation constant (k_d) between Apt5.9-32 and ThT. Average $k_d = 6.28 \pm 1.78 \mu$ M. 102
- Figure 3.S5. Fluorescence enhancement of ThT comparison between Apt5.9-32(this work) and ThT.2-2 (Pei et al., Anal. Methods, 2016, 8, 8461) at several concentrations. (F0 is fluorescence of ThT only). 103
- Figure 3.S6. Fluorescence enhancement of ThT (at 5 μ M) by different oligonucleotides (at 1 μ M). Comparison of fluorescence generated by Apt5.9-32, Template-215, miR-215, and Primer-215 (F0 is fluorescence of ThT only). 104

- Figure 3.S7. SDA reaction time optimization. SDA was compared against necessary controls: Template, nsSDA, nsTemplate, Primer, and ThT. 105
- Figure 3.S8. Slope as a function of A) Temperature, B) Bst polymerase, C) Nick endo nuclease, D) dNTPs, E) Mg^{2+} , and F) ThT. SDA/nsSDA as a function of G) Temperature, H) Bst polymerase, I) Nick endo nuclease, J) dNTPs, K) Mg^{2+} , and L) ThT..... 106
- Figure 3.S9. Optimization of the Template-215 concentration. A) Fluorescence intensity of SDA reactions with four different concentrations of Template-215(100, 200, 50, and 25 nM) as a function of various Primer-215 concentration. Endpoint fluorescence intensity was collected at 50 min. B) Fluorescence-time curves as a function of different concentration of Primer-215 (0, 0.1, 1, 5, 10, 20, 25, 50, 100, 150, and 200 nM) where [Template-215] =100 nM. C) Linear relationship between fluorescence intensity and Primer-215 concentration in the SDA system where [Template-215] =100 nM (error bars represent the standard deviation of triplicate measurements in all cases)..... 107
- Figure 3.S10. SDA in two biofluids; saliva and serum. A) SDA comparison of 8 different oligonucleotides. Only the target miR-215 is detected both in saliva and serum. End point fluorescence intensity (F) was measured at 50 min. (error bars represent the standard deviation of triplicate measurements). B) Fluorescence-time curves as a function of 8 different oligonucleotides (triplicate measurements). Fluorescence intensity (F) from miR-215 is increased over the time in both saliva and serum sample (10% each). Other targets include miR-21, miR-656-3p, 1A5A, 1A3C, 1A, 8G, 5A, and blank in both saliva and serum samples. (F0 is fluorescence of SDA mix with no target) 108
- Figure 4.1. Characterization of laser etching process for generating microfluidic chips. (A) Flow diagram of the fabrication and thermal bonding process. (B) Cross-sectional images before and (C) after thermal bonding. (D) Micrographs show the measured depth of the channels in two test cases. (E) Graph shows the depth of the fluid channel as a function of laser head translation rate. 121
- Figure 4.2. Design and operation of the microfluidic particle generator. (A) Photograph shows the finished microfluidic particle generator. (B) A schematic shows the design and identity of

each fluid inlet and outlet. (C) Digital photographs show blue aqueous fluid (indicated by blue arrow) and clear or red oil (indicated by white and red arrows) flowing in the chip. Blue droplets are generated at the first junction. Red oil representing initiator is introduced at the second junction. A mixing region precedes the exit of the microfluidic chip. Dashed lines indicate margins of the channels..... 125

Figure 4.3. Effect of flow rate and channel size on droplet size. Droplet generator channels are shown at left. Scatter plots at right show the effect of oil and water flow rate on droplet diameter. A 200 μm scale bar is shown in the bottom right. The size of the outlet channel in which droplets were generated was (A) 210 μm , (B) 298 μm , and (C) 156 μm at the base of the triangular channel profile. Flow rate combinations that produced oscillating droplet diameters are represented as concentric circles in the scatter plot, with circle size proportional to the range of droplet sizes produced..... 126

Figure 4.4. Characteristics of droplets and particles. (A) Light microscope image shows consecutive droplets within the particle generator chip connected to syringe pumps. Acrylamide droplets were then polymerized into polyacrylamide particles. (B–E) Fluorescence micrographs show polyacrylamide particles containing fluorescein-modified DNA. (B) Microparticles were generated by a microfluidic chip with cholesterol modified DNA and (C) without cholesterol-modified DNA. Polyacrylamide microparticles were also generated using mechanical homogenization (D) containing DNA with cholesterol and (E) without cholesterol. (F) Histograms show the distribution of cholesterol-modified DNA at the surface of particles manufactured using the microfluidic generator and (G) those manufactured using mechanical homogenization. 128

Figure 4.S1. Heated press assembly. Top left shows a diagram of the assembly used in the heated press. Bottom left shows the assembly before being placed in the heated press. Right shows the assembly after being placed in the heated press..... 132

Figure 4.S2. Pressure after and before chip sealing. (A) Photograph of pressure sensitive film (28 - 85 PSI dynamic range) placed between the glass and the chip in the heated press after heat bonding the chip and cooling. Left is true color; right is false color to show contrast. (B)

Photograph of pressure sensitive film placed between the glass and the chip in the heated press before heat bonding the chip. Left is true color; right is false color to show contrast.

..... 133

Figure 4.S3. Success rate of channels at various conditions. (A) Graph of successful channels as a function cut rate used to fabricate channels. (B) Photograph of the 4-channel chip filled with blue dye. Successful channels filled through to the end; failed channels were blocked. (C) Successful channel % as a function of the channel depth calculated based on the cut rate and calibration curve described above..... 134

Figure 4.S4. Photograph of particle generation chip in operation. Left syringe contains the aqueous phase; top syringe contains the oil phase; right syringe contains the initiator solution. 135

List of Tables

Table 2.1. Sequences of all DNA	59
Table 3.1. ThT aptamer candidate sequences (1 μ M aptamer candidates and 5 μ M ThT in selection buffer).....	83
Table 3.2. Sequences of all DNA	98
Table 4.1 Comparison of alternative fabrication methods for droplet microfluidic devices..	117

CHAPTER 1: Recent advance in strand displacement amplification (SDA): A versatile tool in bioanalytical application

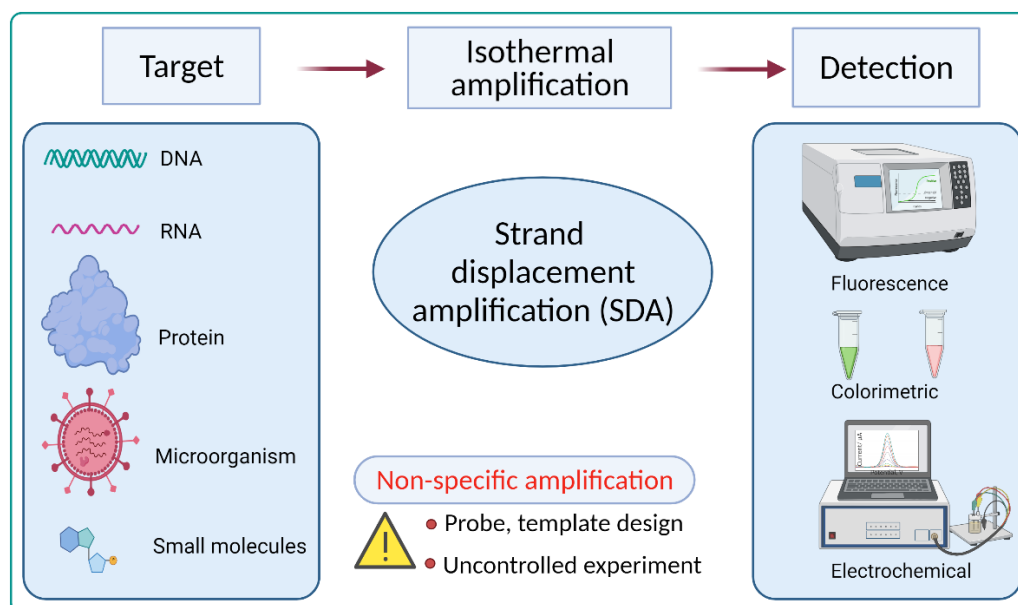
Md Mamunul Islam, Peter B. Allen*

University of Idaho, Dept. of Chemistry, 001 Renfrew Hall, 875 Perimeter Dr, Moscow, ID 83844- 2343

*pballen@uidaho.edu

(Manuscript in preparation)

Strand displacement amplification (SDA) is one of the first and simplest isothermal amplification reactions. Researchers have developed the SDA protocol for diverse applications in bioanalytical fields. In fact, SDA is currently playing a pioneering role in developing other types of isothermal amplification to overcome the limitations of the polymerase chain reaction (PCR).



PCR is the most well-known, researched, and applied nucleic acid amplification technique. Despite being by far the most widely used amplification method, PCR has inherent disadvantages in its operation and instrument requirements. The mechanism of PCR reaction involves three basic steps including denaturation, primer binding, and strand elongation.

These steps are temperature dependent. PCR result is very sensitive to minute quantities of inhibitor present in the surrounding environment. PCR requires a sophisticated instrument for repeated temperature cycling. PCR also requires well-trained personnel to perform efficient and sensitive amplification.

Isothermal amplification methods like SDA bring an alternative way to perform DNA amplification with low-cost instrumentation. This type of amplification method can be performed without expensive temperature cycle control and can make single-stranded DNA (ssDNA) product without any additional treatment. Like all amplification methods, it is possible for SDA to generate unwanted/nonspecific side products. We reviewed five different recent approaches to SDA with a strong emphasis on the origin of the non-specific amplification and different ways to minimize it.

1.1 Introduction:

Nucleic acid (NA) plays a central role in all known biology. This includes genetic information storage in deoxyribonucleic acid (DNA) and shorter-term direction of protein synthesis by ribonucleic acid (RNA). DNA can also be synthesized, manipulated to study living systems, and used for detecting pathogens. For instance, detecting food contamination by harmful pathogens in a simple and easy way is very important as a routine test to prevent food-borne disease. One of the most well-known bacteria is *Escherichia coli* (E. coli). Although most of this type of bacteria is innocuous, there are some type of E. coli that can cause diarrhea, severe food poisoning, and respiratory problems¹. Several methods exist to detect such harmful microorganisms such as antibody-based tests, bacterial culturing etc. However, these tests are time consuming and laborious. DNA-based tests can simplify and accelerate the process.

Analytically, detecting any pathogen is difficult. Nucleic acid based molecular assays have been developed to accomplish specific detection in these difficult circumstances. In a nucleic acid based molecular test, nucleic acid is used as an analyte or target. Detecting pathogenic DNA is a very difficult analytical problem due to the inherent matrix effect of the food on which the

bacteria could be growing. Detecting cancer-specific mutant DNA in a background of normal cellular matter is similarly difficult. In both cases, the analyte is chemically similar to the background. RNA and DNA are both nucleic acid and similar only difference is RNA contain ribose sugar where DNA contains deoxyribose sugar in their structure. Also, there are many sequences of DNA and RNA in the harmless bacteria and food-derived cells. To detect small quantities of pathogenic DNA or RNA in food can be accomplished quickly by detecting its specific DNA based on a unique sequence of the four nucleobases. This is still challenging: only a few bacterial cells are necessary to cause illness. Bacterial DNA must be detected in a background that is many orders of magnitude more abundant and chemically very similar.

DNA technology can help solve this challenging analytical problem. Easy synthesis, and well - developed modification chemistry of nucleic acid with different dyes and functional groups coupled with modern instrumentation are the driving force of this nucleic acid-based nanotechnology. Because of the central functional role of NA in living systems, accurate information about it, both quantitative and qualitative, is crucial to understand many physiological phenomena in molecular biology. This has direct application to human health and disease. It is generally accepted that inherited diseases are related to cellular dysregulation which can be traced back to the genetic information organization in the cell (genes and their expression network). As an example, mutations in genes occur with serious implications for the progression of cancer or other genetic diseases. It is therefore very important to monitor and detect any aberrant genetic marker or nucleic acid. The mutant DNA may be rare relative to normal DNA. One strategy to overcome this is to generate many copies of the analyte in a process called amplification. Through an amplification process, a small number of the specific analyte nucleic acid molecules are copied many times to generate a sufficient amount to reach detectable levels (**Figure 1.1A**). This process of reporting detectable signal by generating many copies of a small initial amount of specific target NA can be thought as nucleic acid amplification.

The term “amplification” in this context is an analogy to an electronic amplifier system such as an operational amplifier (**Figure 1.1B**). Operational amplifiers, of various size and shapes,

are used in circuitry to amplify an input voltage signal by many orders of magnitude to perform many useful operations in electronic circuits. A small input voltage produces a large output voltage. Similarly, in nucleic acid nanotechnology, nucleic acid amplification, of many types and processes, can be performed based on fundamental Watson-Crick base pairing using different enzymes and reagents. A small input concentration produces a large output concentration.

Nucleic acid amplification is a very important concept in both fundamental research as well as in real world application². Nucleic acid amplification has a wide range of applications including therapeutics, forensics, and disease diagnosis³. A specific example of disease diagnosis would be detecting circulating miRNA. Important cancer biomarker miRNAs are present in low abundance. Effective treatment can only occur if such a biomarker is successfully detected.

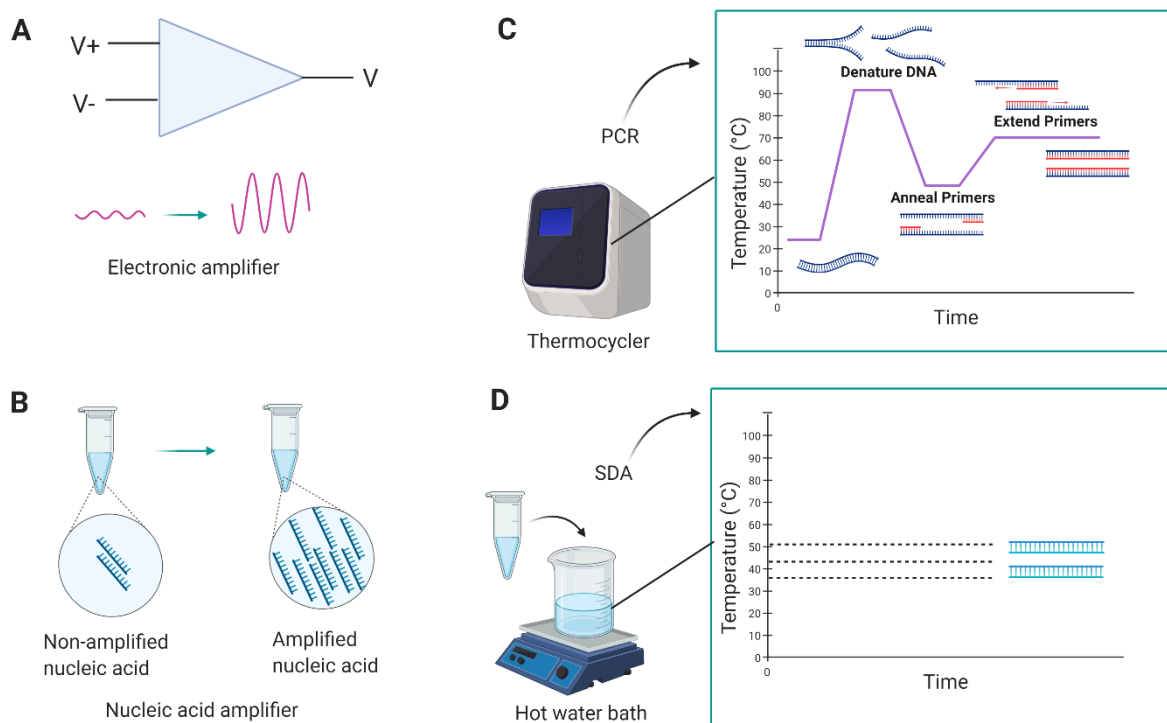


Figure 1.1. Conceptual diagram of nucleic acid amplification. A) Schematic of an electronic operational amplifier. B) Nucleic acid amplifier for comparison. C) Polymerase chain reaction is a non-isothermal nucleic acid amplification D) Strand displacement amplification (SDA) is an isothermal nucleic acid amplification.

Extracting accurate information about DNA and RNA in biological samples was made much easier by a revolutionary tool. Polymerase chain reaction (PCR) was discovered by Kary B.

Mullis in the late nineteen nineties⁴. PCR, called "molecular photocopying," is one of the most remarkable discoveries in molecular biology. Kary B. Mullis was awarded the Nobel prize for this revolutionary invention. By applying heat, an enzyme DNA polymerase and dNTPs, DNA copies can be obtained from small segments of initial DNA in a very short time^{5,6}. This reaction is invaluable to detect amplified nucleic acid, considering that the amount of nucleic acids in the biological sample is often very small. For example, to study a gene of interest in the cell, DNA first needs to be amplified by an *in vitro* amplification method. However, like every other technique in science, even this gold standard PCR amplification has its limits. PCR needs an expensive thermal cycler (**Figure 1.1C**) which often proves too costly for low resource laboratory settings. PCR is vulnerable to contamination, its efficiency is sensitive to inhibitors, and it requires a highly trained person to operate the experiment and get reproducible data. These limitations inspired isothermal nucleic acid amplification methods. This field continues to grow rapidly. Among them one of the most applied and oldest amplification methods is strand displacement amplification (SDA). It was first proposed by Walker et. al., in 1992 not long after the invention of PCR⁷. SDA is a nucleic acid amplification method that uses polymerase and endonuclease to generate new DNA. Ideally SDA (or any isothermal amplification technique) can be performed by using a hot water bath and avoids any costly instrument (**Figure 1.1D**). SDA takes advantage of two very efficient enzymes, a nicking endonuclease and a displacing polymerase (such as Bst, from *Bacillus stearothermophilus*). Polymerization, nicking, and displacing of strands each occur at a single constant temperature. SDA can be simple linear or exponential amplification type. Based on the amplification nature of the SDA, this review highlights different SDA mechanisms that are bioanalytically important including basic linear SDA, as well as advances in exponential SDA or exponential amplification reaction (EXPAR)⁸, some recent advanced SDA such as RNA based SDA-RNA aptamer involved cascade transcription amplification(RACTA)⁹, PEN tool kit^{10,11} and CRISPR/Cas based SDA. These different SDA-based techniques will reveal the diverse assay design and recent progress of this strong amplification method. In particular, the review addresses different common signal reporting techniques for SDA and how different sources of undesired non-specific

amplification are overcome. Finally, the existing literature of the application of SDA to detect different biomolecules are also discussed.

1.2 Linear SDA:

Linear SDA amplifies target DNA in a linear fashion by using nick endo nuclease and strand displacing DNA polymerase. Joneja and Huang et al., describe such an SDA reaction¹².

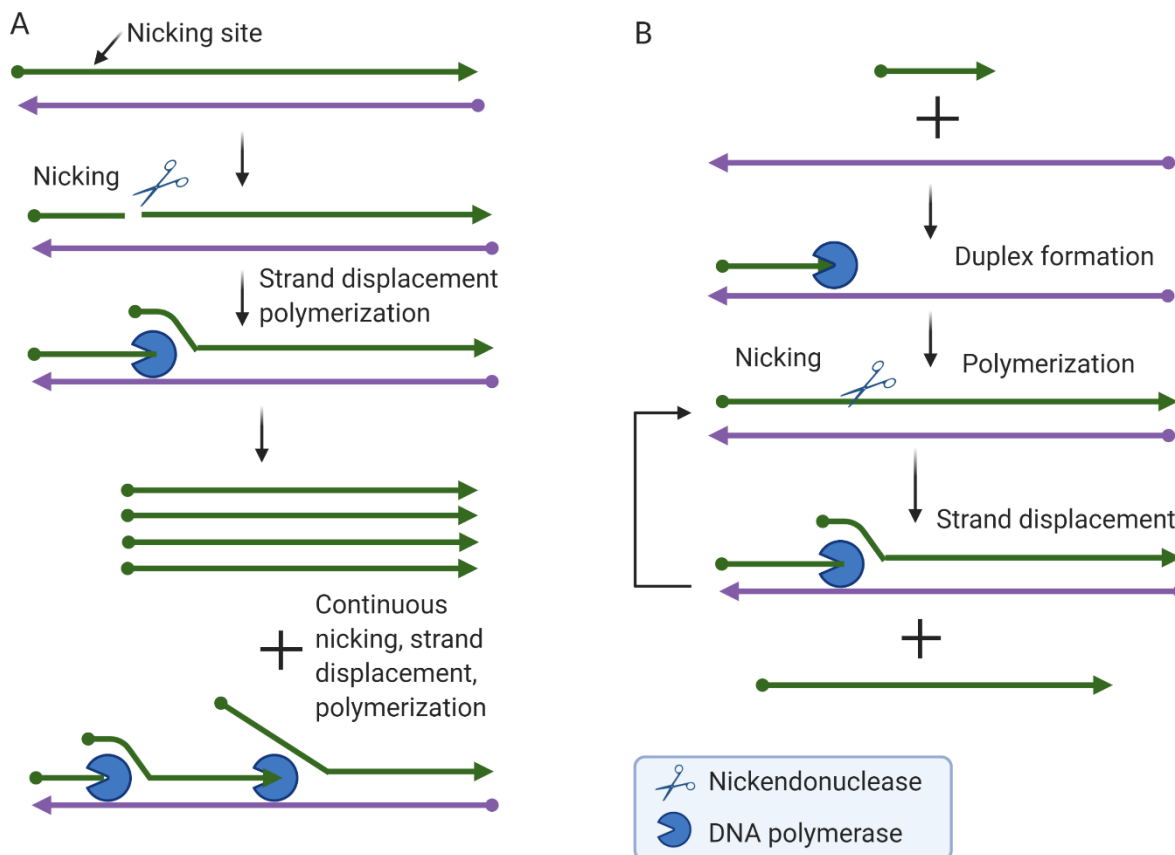


Figure 1.2. Schematic of SDA using two different template A) Linear SDA using dsDNA Template B) Linear SDA using ssDNA Template.

Figure 1.2A shows the principle of linear SDA to amplify a dsDNA target by a nicking enzyme mediated process. This process requires the presence of specific short sequence on the target. For that a ligation process is performed beforehand where the target is ligated with a “duplex adapter” which contain the nicking site. Therefore, the nicking site, that contain 7 bases in a specific order, in one strand of a dsDNA target is recognized by the nicking enzymes with endonuclease properties which cleave phosphodiester bond. The cleaved short strand acts as

primer for the subsequent DNA polymerase binding and extending the strand from 3' end. The polymerase possesses strand displacement activity which resulted in displacing the downstream strand to generate ssDNA product and newly formed double strand nicking site for the next round of polymerization. Thus, a compatible pair of nicking endonuclease and DNA polymerase ensure repetitive cycles of nicking, polymerizing and strand displacing to realize linear SDA of target DNA. One disadvantage, though, of this method is that it requires separate ligation process with T4 ligase enzyme to introduce nicking site.

SDA can give linear amplification using ssDNA template too¹³. The template is designed to have complementary binding domain along with nick recognition site. The primer activated amplification occurred with the presence of selected enzymes; nick endonuclease and DNA polymerase and dNTPs. The amplified ssDNA product can be readout using a convenient fluorescence dye. The amplification cycle continues until the reagents are exhausted (**Figure 1.2B**). Using correct nicking endonuclease is crucial for any kind of SDA efficiency. Operating temperature, specific sequence, best combination with Bst polymerase is needed to consider for the selection of best nick endonuclease. Nicking endonuclease is a special type of restriction enzyme. While both operate on a specific sequence pattern, unlike restriction endonuclease, nick endonuclease cleaves only one strand in a duplex DNA. There are naturally occurring endonuclease found and extracted from microbes as well as commercially available engineered nicking endonuclease by protein engineering.

Some commercially available nicking endonuclease and their nicking site are given below:

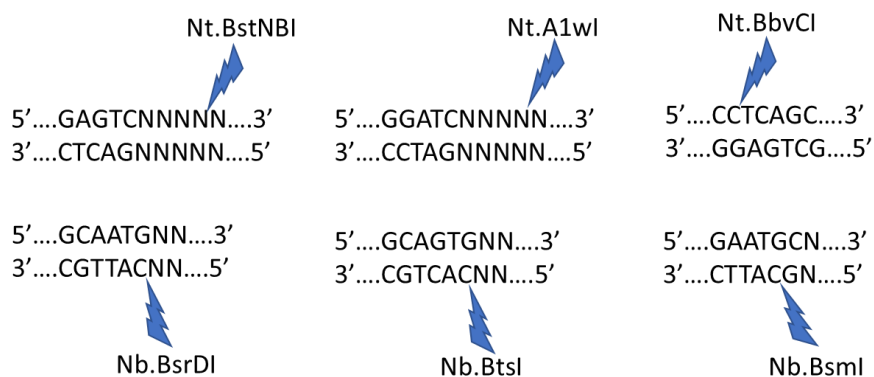


Figure 1.3. Six common nicking endonuclease used in SDA¹⁴.

At their optimum temperature, nicking endonuclease cleaves top or bottom strand at highly specific location of the sequence. Thus, name Nt comes for nick top and Nb for nick bottom (**Figure 1.3**).

1.3 Exponential amplification reaction (EXPAR)

EXPAR is the exponential version of SDA. It is a chain reaction version of linear SDA and uses the same pair of enzymes. The template is designed in a different way. It is designed in such a way that each product of the linear SDA can serve as the primer of a parallel cycle to generate more of the products¹³. EXPAR, first proposed by J.V. Ness et al., in 2003, is a very sensitive and highly efficient amplification¹³. Upon triggering by a specific target oligonucleotide, an amplification of $> 10^6$ -fold can be achieved within minutes. The key difference between linear SDA and the EXPAR is in the template used. EXPAR template is designed to have two complementary primer binding domains separated by a complementary sequence of the nicking site in the middle. The EXPAR template and the primer sequence, which can match the target analyte, along with deoxynucleotide triphosphates (dNTPs), and two enzymes in an appropriate buffer accomplish the exponential amplification reaction. EXPAR starts with the primer binding to the template. This primer/template duplex then serves as the readily available initiation site for polymerization by the enzyme DNA polymerase. The enzyme uses dNTPs to extend the existing primer on the template in the direction of 3' end of the primer to make a full duplex of extended primer/EXPAR template where the top strand is the extended primer strand (**Figure 1.4**).

The top strand in the duplex contains a nick recognition site for nicking endonuclease such as Nt. BstNBI. The nicking site is four bases downstream of the recognition sequence, GAGTC. For any other nick endonuclease to be used, the EXPAR template must be redesigned for a different recognition site. Nt.BstNBI cleaves the top strand at its specific location. The nearby DNA polymerase, with its aggressive strand displacement activity, finds the cleavage site, binds, and restarts the polymerization while simultaneously releasing the previous product. The released partial top strand has the same sequence as the original primer. It readily binds to another EXPAR template (each has two binding sites). This positive type of feedback loop

repeats until some reagent is exhausted. The EXPAR template is used in excess in the reaction system on order to create conditions for a rapid chain reaction.

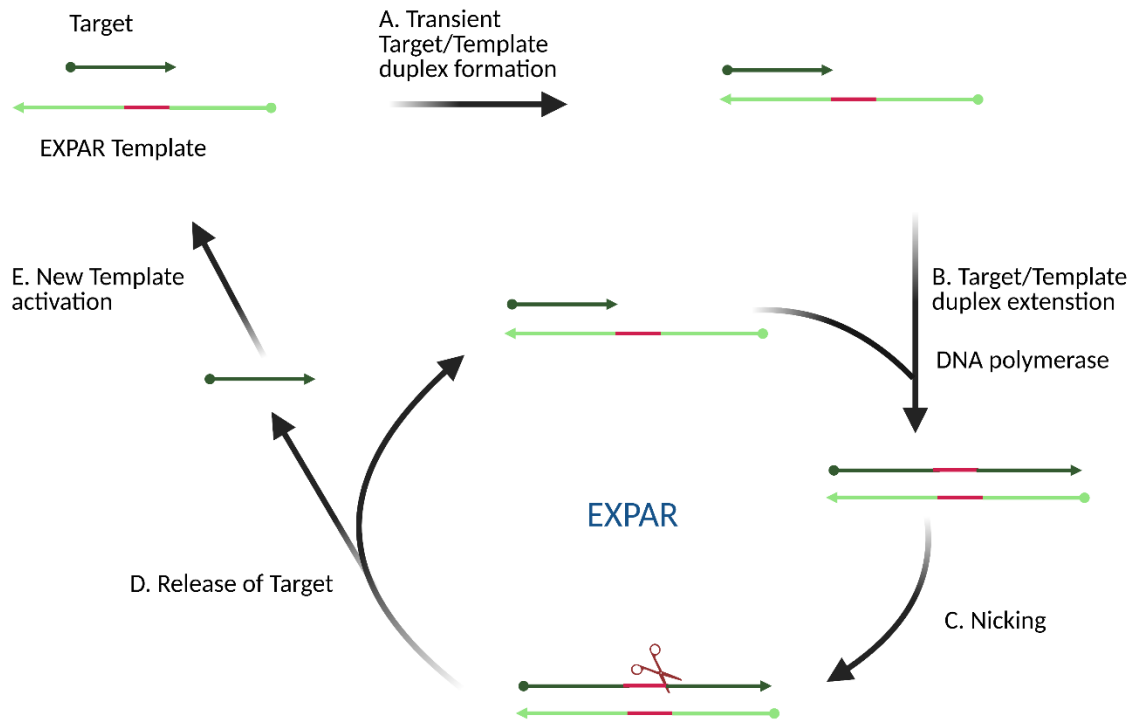


Figure 1.4. Schematic of a typical EXPAR: (A) Target binds to the complementary sequence at the 3'-end of the EXPAR template to form a transient duplex; (B) The target is extended by the DNA polymerase using the EXPAR template, forming EXPAR template/extended primer duplex with a nicking enzyme recognition site on the newly extended top strand; (C) Nicking endonuclease cuts the extended top strand at the site specific position; (D) The "nicked" target strand is released from the EXPAR template. The remaining-cleaved duplex form of the EXPAR template continues the linear amplification cycle, through the cycle of primer extension, nicking, and release; (E) the newly formed target oligonucleotide products activate additional EXPAR templates, giving rise to exponential amplification.

The high concentration of the template causes problems for the amplification system. The amount of EXPAR template must be optimized. Very high concentration of template may cause non-specific binding. This can result in non-specific amplification even in the absence of primer or target analyte. Careful template design can help overcome this limitation. Success of EXPAR detection greatly depends on the template design. EXPAR template design should be free of secondary structure to avoid self-priming based polymerization which can result in non-specific background amplification. Nevertheless, like every other amplification technique, EXPAR also suffers from non-specific amplification which can lead to false positive results.

Therefore, the challenge in designing an EXPAR amplification should be to minimize the background signal from the non-specific product and to achieve highest sensitivity as much as possible.

For that it is important to know the characteristics of non-specific background that occur in EXPAR. The duration of the experiment is closely related to the non-specific background signal. Non-specific amplification at the beginning of the reaction has larger negative effects on the experiment and needs to be addressed in the assay design. To address this concern, a combination of different treatment is often necessary. Sometimes one measure is helpful for one specific EXPAR assay while the same measure may not work in another assay. For instance, chemical modification at the 3' end of the template with a phosphate group can prevent self-priming of template and subsequent extension activity of polymerase enzyme^{13,15}. Other groups reported no significant effect of 3' end chemical modification on non-specific amplification¹⁶. In the same report, Niemz and co-workers investigated the non-specific background in EXPAR in a comprehensive way using various approaches. They investigated template design, optimized reaction parameters (e.g., time, temperature, reagent composition), chemical modification, and reagent purity (among others). DNA polymerase is a hyperactive enzyme that can generate signal even without template given enough time. Therefore, it is very important to optimize the assay time of EXPAR in order to reduce non-specific based amplification that might occur after the assay reached a certain time point. A recent report on non-specific amplification explored template-template interaction in EXPAR. This interaction was found to be the main source of non-specific amplification¹⁷. In another report, Niemz and coworkers found that the template sequence has a significant effect on the non-specific amplification⁸. Niemz et. al. measured the performance of a large number of sequences. Purine rich template sequences generated more background, likely because polymerase has higher binding affinity to purine than pyrimidine bases. Although EXPAR operates at a single temperature, appropriate temperature of the assay is important for the overall efficiency of the assay. Temperature should be high enough for the highest reaction rate and low enough so that primer effectively bind to the template

to begin with. In summary, if non-specific amplification is kept to a minimum, an EXPAR reaction can be a great way to detect a nucleic acid target.

1.4 PEN toolbox:

Developed as “PEN toolbox (polymerase/exonuclease/nickase)” by Yannick Rondelez and co-workers is also similar to SDA and EXPAR. Non-specific amplification is minimized with the addition of one more enzyme, an exonuclease¹⁰. Exonuclease is used to deactivate all the product strand and to maintain the dynamic nature of the system. Interestingly, this dynamic molecular toolbox is designed to have amplification isothermally with simultaneous absorption of non-specific products from the system¹¹. Unlike EXPAR, here a set of four templates was used instead of two. A conversion template, autocatalytic or amplification template, pseudo template, and reporting template, were used for four different modules to detect miRNA (**Figure 1.5**). This is contrary to what is normally reported previously that too many templates might contribute to the non-specific amplification. They addressed this issue by phosphate group modification at the 3' end of each template.

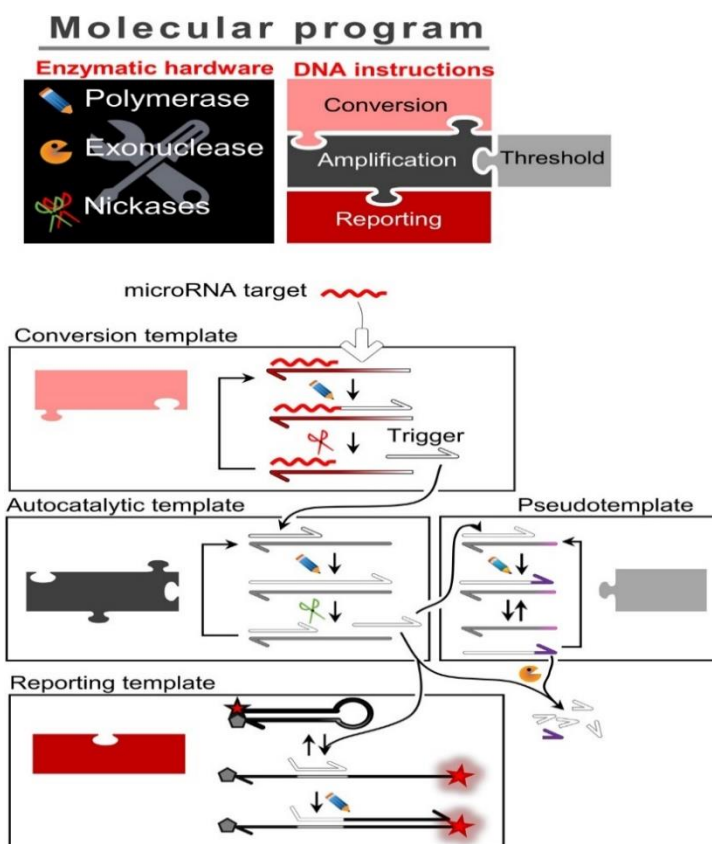


Figure 1.5. PEN toolbox molecular program for the detection of microRNA. A four-template based amplification using three types of enzymes (polymerase, exonuclease, and endonuclease): The conversion template converts the target microRNA to a short DNA sequence; The autocatalytic template acts as amplification template to amplify input DNA strand, pseudo template is used to suppress the non-specific amplification; the reporting template reports the amplification of the system in fluorescence readout mode. (Reproduced with permission from¹¹)

The use of four templates is possible by careful design. The conversion template is optional. It generates DNA oligonucleotide output from target miRNA without any reverse transcriptase enzyme. This can be omitted in case of a DNA based target. For enzymatic exponential amplification, the design of the amplification template contains two repeating domains that are complementary to the converted DNA sequence generated by the conversion template (similar to EXPAR, above). The output DNA strand acts as a signal strand. To ensure background free amplification, the amplification template and pseudo template work in a cooperative way by establishing an “amplification threshold”. If undesired reactions occur in the absence of target oligonucleotide, the pseudo template works as a “sink” to deactivate them until a certain limit is reached. Above this limit, the “sink effect” is saturated. This serves

as an immediate permission for the amplification template to start the amplification cycle. The importance of using the pseudo template is demonstrated. The limit of detection of the assay is reported to be 1 fM. However, in absence of the pseudo template (the non-specific background threshold), the limit of detection was degraded to 3.7 pM. This clearly indicates the negative effects of non-specific amplification in absence of pseudo template. To suppress non-specific background amplification, the amount of amplification template was optimized. The ratio of concentration of amplification template/pseudo template was about 3 to establish the “amplification threshold”. This PEN tool has the potential for use as a detection platform for any short nucleic acid-based target by only redesigning the templates. The PEN toolbox has been further developed and demonstrated for practical applications in several recent publications^{10,18,19}.

1.5 RACTA (RNA aptamer involved cascade transcription amplification)

Another advanced version of SDA designed to detect miRNA is called RNA aptamer involved cascade transcription amplification (RACTA)⁹. This involves three enzymes: Bst DNA polymerase, nicking endonuclease, and T7 RNA polymerase. The reaction also uses two templates for two different purposes: 1. an amplification module and 2. a label-free signal generation module based on a light up RNA aptamer (**Figure 1.6**).

This SDA process is based on the formation of RNA-DNA-RNA. It starts with the miRNA binding to a template, and subsequent extension by DNA polymerase, specific nicking by nick endonuclease and displacing of trigger DNA input for transcriptional amplification. The trigger DNA initiates transcription amplification. While the first module of SDA amplification cycle is a conventional SDA, the interesting part is how the label free signal reporting is integrated in the transcriptional amplification. This signal generation cycle starts with the activation of a second template designed specifically to generate the RNA aptamer, “spinach.” T7 RNA polymerase is recruited to generate the RNA aptamer.

The “spinach” aptamer is a single stranded RNA that has unique binding affinity to its target²⁰. Since its advent three decades ago^{21,22}, aptamer technology has gone through many developmental phases from advanced selection process to many diverse applications^{23–27}.

RACTA uses the spinach aptamer^{28,29}, an RNA aptamer that can generate fluorescence when it binds to a small molecule DFHBI ((Z)-4-(3,5-difluoro-4-hydroxybenzylidene)-1,2-dimethyl-1H-imidazol-5(4H)-one). This light-up phenomenon is used for label-free signal reporting. However, this sensitive method of miRNA detection uses two different temperatures for two amplification cycle which seems discouraging for an isothermal technique.

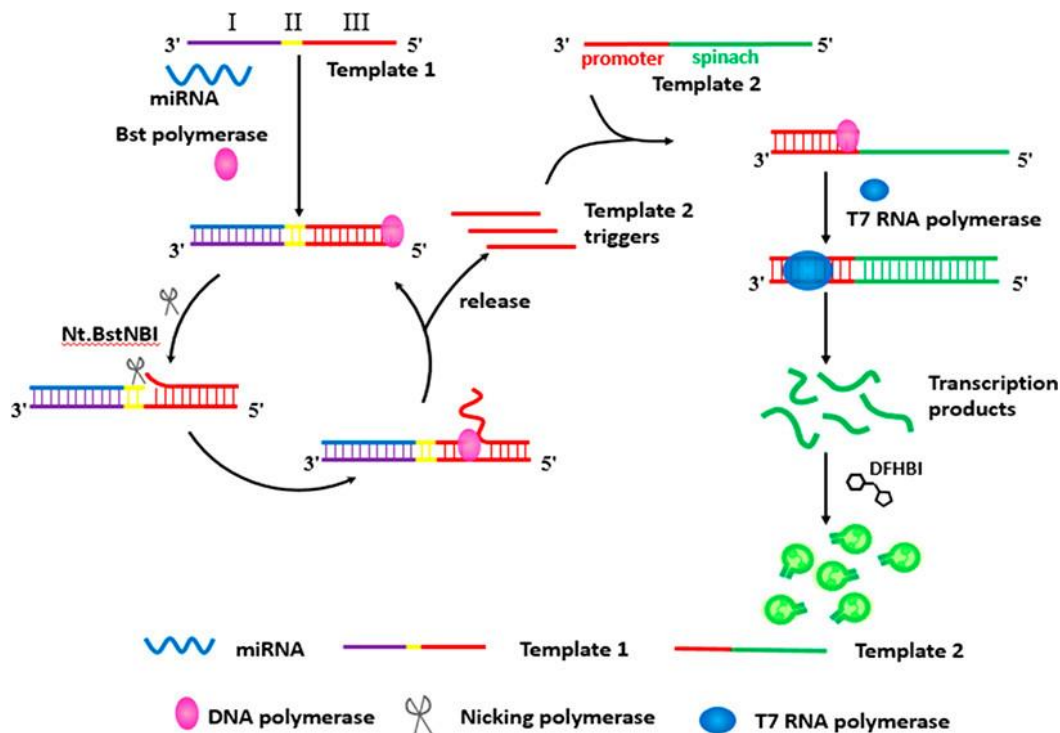


Figure 1.6. Schematic of SDA based RNA aptamer involved cascade transcription amplification (RACTA). RACTA involves two templates for two modules. Amplification module: Template 1 contains three complementary sites- target miRNA binding site, nick site, input strand site for downstream amplification cycle. Signal reporting module- Template 2 contains two complementary sites- trigger binding promoter site and reporter generating spinach site (reprinted with permission from⁹ Copyright © 2019, American Chemical Society).

The heavy enzymatic dependency can be minimized by modifying the scheme. Instead of RNA aptamer-based signal reporting, a suitable DNA light up aptamer can be developed and used to generate label free signal to avoid the use of T7 RNA polymerase in the second amplification stage. Nevertheless, this different approach of SDA has great potential as a biosensor.

1.6 CRISPR/Cas based SDA

Clustered regularly interspaced short repeats (CRISPR) is a recently discovered gene editing tool. CRISPR occurs in bacterial cells and is part of the adaptive immune system in bacteria.

Bacteria use the CRISPR system to defend against viruses. Although the CRISPR concept was known for decades³⁰, its use as a gene manipulating tool occurred only about 10 years ago³¹. Since then, it has gone through remarkable development. It has been used as a gene editing tool in many species from bacteria³¹ to humans³². This molecular technique is seeing new applications from gene editing to diagnostics^{33,34}. The underlying principle of CRISPR relies on two main components, a Cas enzyme and specifically designed short RNA molecules. Both the Cas enzyme and RNA form an effector complex. RNA guides the Cas enzyme to recognize a specific target complementary DNA, hence known as “short guide RNA” (sgRNA). The Cas enzyme then cleaves the target DNA. The effector complex is very specific to the sequence encoded by the sgRNA³⁵, and cleaves only at a precise location in a genome.

Isothermal amplification was combined with a CRISPR/Cas system for sensitive target detection in a real-world application^{33,36}. One such report was published which leveraged the CRISPR technology to initiate exponential amplification based on a system like SDA³⁷. This is outlined in **Figure 1.7**.

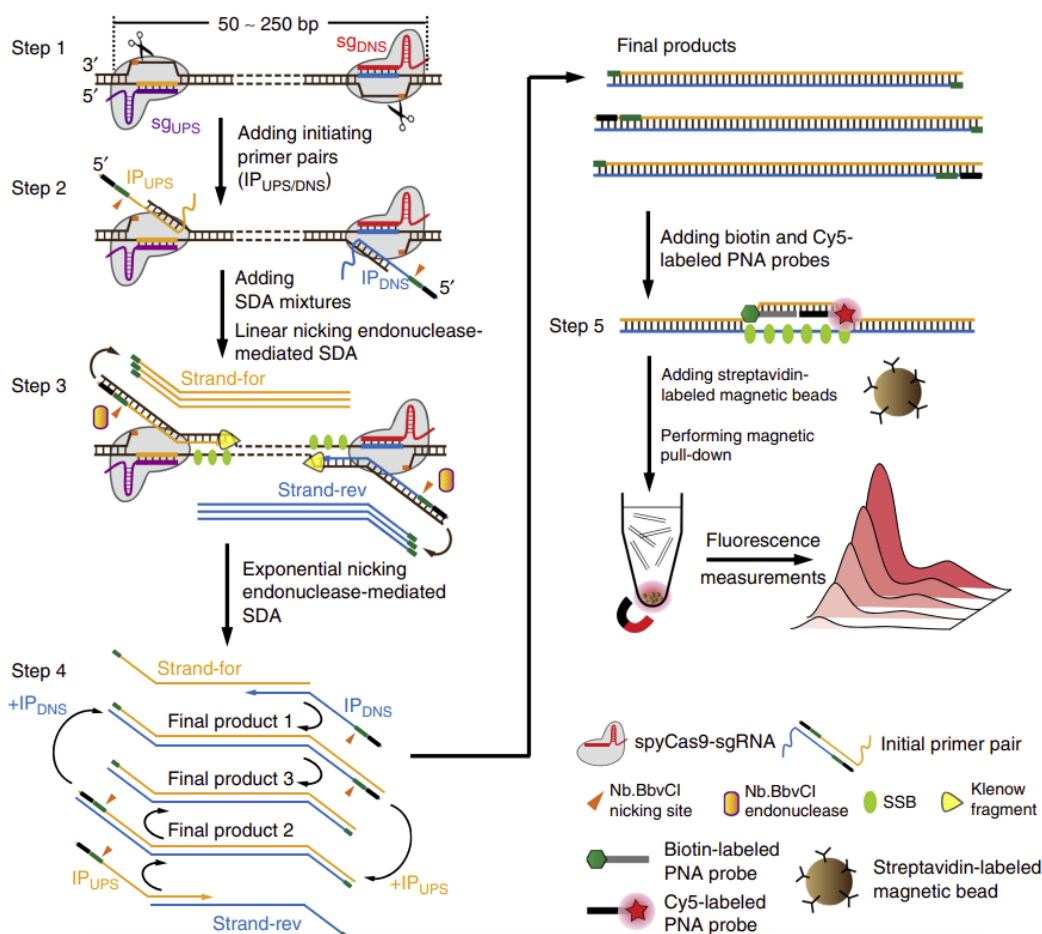


Figure 1.7. Schematic reaction mechanism of CRISPR powered SDA. **Step 1, Target recognition:** Ribonucleoprotein complexes, a pair of Cas9 enzyme guided by guide RNA (sgRNA) specifically recognize two ends of the target dsDNA resulting in two, specific nicks. **Step 2, Primer binding:** Two initiating (IP) primers hybridize with the nicked strands. **Step 3, Linear SDA starts:** SDA mixture (Klenow Fragment (KF) polymerase ($3' \rightarrow 5'$ exo⁻), Nb.BbvCI nikase, and single-stranded DNA binding protein (SSB), dNTPs) drives linear SDA from two primer binding sites resulted in the displacement of single strands. **Step 4, Exponential SDA starts:** Upon reannealing with the primers, the displaced strands of step 3 generate exponential SDA. **Step 5, Signal readout:** the end products are reported based on fluorescence measurement by a biotin and cy5 labeled PNA probes in cooperation with streptavidin coated magnetic beads. (Figure reprinted with permission³⁷)

The first step in this SDA-based method is the formation of a DNA-Cas9-sgRNA complex. This complex triggers subsequent SDA reactions. In this CRISPR-SDA method, several steps were involved for two basic functions in the reaction design. First, CRISPR initiated exponential SDA amplification. Second, a fluorescence-based signal detection (see **Figure 1.7** for an outline of the process). In brief, the double stranded target DNA is recognized by the ribonucleoprotein complex, Cas9/sgRNA, which cleaves the DNA. This allows a primer to hybridize to the cleaved

DNA strands. This results in linear SDA (using polymerase and other SDA components as noted above). The specific design of the primer sets allows the initial SDA products to reanneal and to generate new, active SDA substrates. This results in exponential SDA. The products are detected by capture on microspheres with PNA. The microspheres are interrogated for fluorescence. This is an interesting method which can reportedly achieve attomolar sensitivity. However, the design of the primers, sgRNA, and PNA probes all require careful consideration in relation to the specific target sequence and operating temperature. The operating temperature, 37 °C, is an ideal temperature for physiological conditions. However, this might also negatively affect the signal generation. Non-specific background amplification might occur at this low temperature by (e.g.) primer dimer formation rather than the desired primer target binding. This must be carefully excluded in the design.

1.7 SDA signal reporting method

SDA (and any efficient nucleic acid amplification method) needs sensitive and convenient signal reporting. This gives an analytical signal when amplification occurs and allows the analyst to detect a target. One of the most traditional ways of analyzing the products of SDA is gel electrophoresis. This classical method is applied post-amplification at the experimental endpoint. There are now real-time readout modes as well. Different physical principles can be employed to generate a signal from SDA. These methods can be based on fluorescence, electrochemistry, or colorimetry.

1.7.1 Fluorescence based reporting method

The most used and convenient SDA reporting system is based on fluorescence. In this method, light is emitted by the SDA product. We highlight four representative approaches: 1. dye based; 2. hybridization probe based; 3. carbon nano dot based and 4. Label-free light-up probe-based signal reporting. Dye based fluorescence readout employs intercalating dyes and other dyes that bind nonspecifically to DNA. Different commercially available fluorescence dyes are used in SDA and most other nucleic acid-based amplification systems. Some small

molecule dyes bind the dsDNA structure and fluoresce when excited with short-wavelength light (**Figure 1.8A**). In their free state, they generate much lower levels of fluorescence. As amplification progresses, more products accumulate. The dye binds this product and becomes fluorescent (**Figure 1.8B**). Hence the amount of amplification products is proportional to fluorescence generated from the dye/DNA products. Both linear SDA¹² and EXPAR⁸ used fluorescence dye SYBR green I to report their amplification products. These were both used to generate signal when specifically excited by a micro RNA (miRNA)^{38,39}. SYBR green II binds preferentially to single-stranded DNA (ssDNA) and can also be used to detect the SDA or LAMP products⁴⁰. Although low cost, the disadvantages with fluorescent dye are that they indiscriminately bind to any DNA. Such dyes will report amplified target products, non-specific products, or primer-dimers. Hence quantitative information derived from fluorogenic dyes is often unreliable.

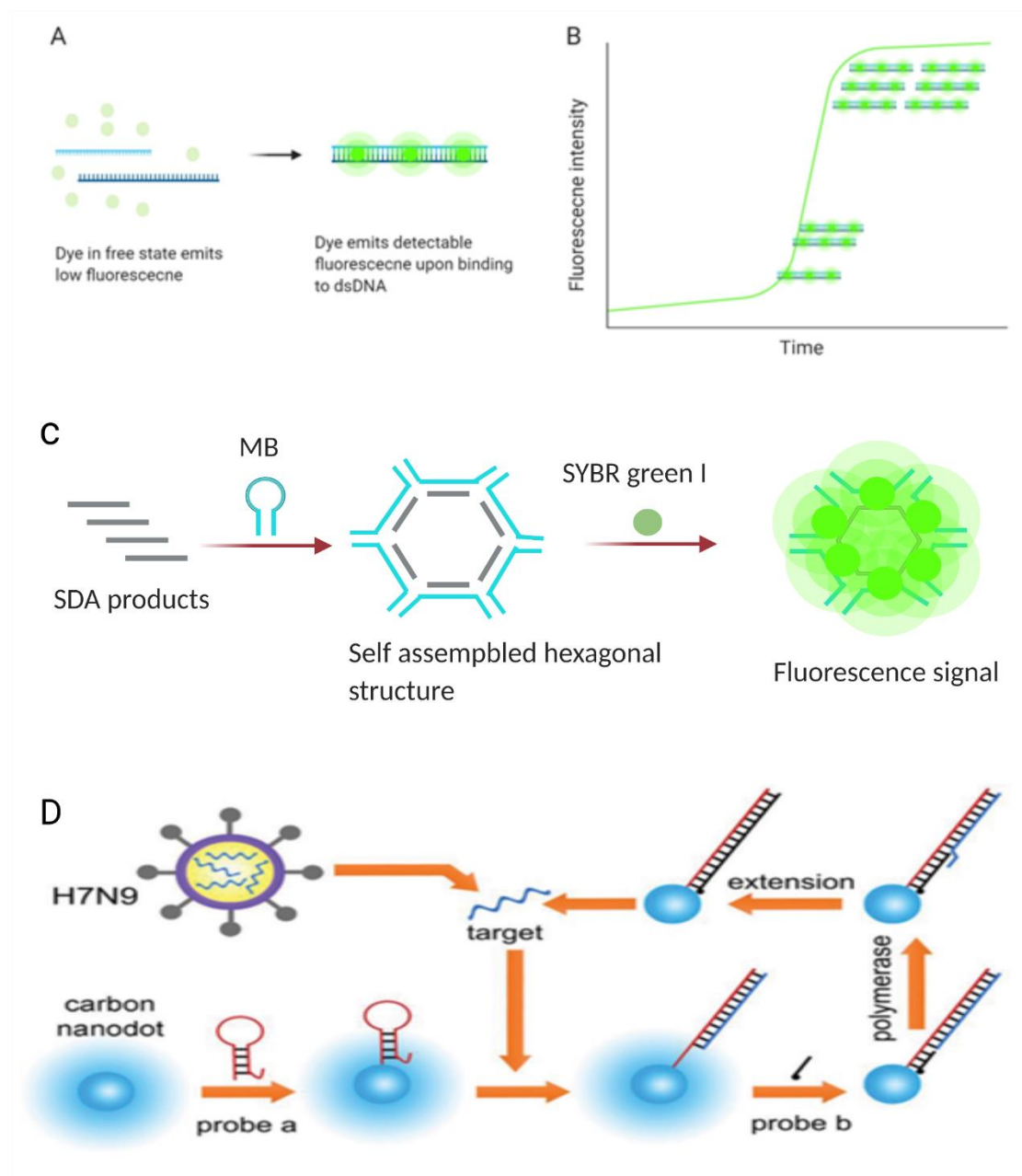


Figure 1.8. Schematic of intercalating dyes generating fluorescence when interacting with DNA. A) Dye generates fluorescence only after binding to dsDNA. B) Fluorescence intensity increases as a function of time after the amount of dsDNA increases due to a DNA amplification reaction. C) Label-free hairpin-based SDA detection⁴¹. D) Schematic shows carbon dot-based SDA detection. Reprinted from ref.⁴².

To reduce the non-specific background signal from the non-specific binding of intercalating dyes, fluorogenic hybridization probes can also be used to report DNA amplification. Such probes can report many types of amplification including PCR and SDA. They have the

advantage of sequence specificity. They bind based on base-pair interactions. Aside from this common factor, probe-based detection is diverse.

The most common probe-based detection method uses a self-hybridized “hairpin” nucleic acid probe (sometimes called a “molecular beacon”). The use of this probe structure was first reported by Kramer and co-workers⁴³. Traditionally, the specific signal reporting by hairpin probe is achieved by labelling the two ends of the probe with a quencher and fluorophore group. In its free state the probe is non-fluorescent because of the proximity of the two groups involved in fluorescence resonance energy transfer (FRET). The opening of the molecular beacon/hairpin probe and the disruption of its stem-loop structure activates the probe to report fluorescence signal. This conformational change only occurs upon binding with a specific strand.

This photophysical principle is used in the PEN toolbox system of SDA (**Figure 1.5**). In the PEN toolbox system, the reporter template is designed to have hairpin structure and is labelled with fluorophore and quencher group at both ends of the template. When SDA products are produced, they bind to the reporter template probe to disrupt the hairpin conformation and as a result the fluorophore and quencher separate and generate fluorescence.

SDA is a versatile approach, and there are many variations on the hairpin reporter. One example is a label-free hairpin probes lacking the fluorophore or quencher. Unlabeled hairpins acted as a secondary detection probe and generated the signal through rearrangement and interaction with a small molecule dye.

The label free hairpin-based reporting system generates the self-assembled nanostructure detection probe⁴¹. This detection method has been reported using aptamer(ssDNA/RNA) sequence. The method takes advantage of a high specificity aptamer and a self-assembling probe sequence. Rongfeng Cai and co-workers developed an SDA method to detect food borne bacteria in milk. Their target specific SDA generates ssDNA products which in the presence of a hairpin probe form a signal reporting complex. The hairpin probe is unlabeled and specifically designed to interact with the products. Together SDA products and hairpin probe self-assembled to form a hexagonal signal reporting complex. The hexagonal complex

has double stranded secondary structure which in presence of SYBR green I generates fluorescence signal (**Figure 1.8C**). In their optimized experiment, the researchers were able to obtain a linear range over several orders of magnitude in concentration of the analyte plus a limit of detection of 1.7 CFU/mL.

Recently, carbon dots acted as fluorophores instead of non-specific DNA-binding dyes^{42,44}. This class of semiconductor nanoparticles have potential application in biosensing for their facile synthesis with good biocompatibility and stability⁴⁵. In one example, researchers detected a DNA virus in a simulated biological sample using the fluorescence of carbon dots (carbon quantum dots). This “signal off” approach used a hairpin probe to initiate SDA⁴². A hairpin probe was designed to attach carbon dots through amino group modification. Hairpin was designed to recognize the target and a quencher labeled ssDNA probe. In the presence of target viral DNA, the hairpin structure is opened which then binds with ssDNA probe. As a result, a complex ternary structure of target, hairpin attached carbon dots, and ssDNA probe is formed. The presence of quencher group in the ssDNA probe decreases the overall fluorescence of this complex. The presence of polymerase enzyme extends the ssDNA probe on the hairpin template to make duplex attached carbon dots by displacing the target DNA sequence (**Figure 1.8D**). This process repeats for many cycles and results in a large drop in fluorescence. This proof of principle study needs validation with clinical samples.

Light-up probes can also be used to detect the SDA reaction. This approach is often called a label free detection system because no covalently attached fluorophores are needed. Instead, a dye in solution is induced to fluoresce through non-covalent interactions. In the presence of certain DNA structures, these small molecules generate enhanced fluorescence by forming a DNA-dye complex^{46–48}.

There are several reports on light-up sensors that use the small molecule Zn/protoporphyrin IX (ZnPPIX)^{46,49,50}. Perhaps the most widely used dye in biosensing application is thioflavin T⁵¹ (ThT). ThT interacts with guanine-rich oligonucleotides and becomes fluorescent^{52–54}. To detect an SDA reaction with ThT, the SDA template is designed to produce a G-quadruplex (G4) structured product. In the presence of ThT, G4 generates much higher fluorescence. This

fluorogenic property is used to detect biomolecule in a label free fashion⁵⁵. More specific detection is possible using an aptamer-based approach. Instead of generating G-quadruplex as SDA product, a DNA aptamer is produced. This aptamer can bind with its light-up target (i.e., ThT or another specific dye) and generate characteristic fluorescence. RNA based spinach aptamer can light up the DFHBI dye in the RACTA method discussed earlier⁹. A DNA based ThT aptamer has also been published which can light up ThT for a label-free SDA reaction⁵⁶. However, the template sequence must be designed carefully to minimize non-specific amplification. Template sequences used in light-up sensors are constrained by an aptamer generating domain. This may limit the target sequence to avoid target-aptamer interactions.

1.7.2 Colorimetric detection

Colorimetric detection is very popular. The reaction can be monitored with a color change. The experimenter can see the results without any instruments. Several colorimetric detection methods using gold nanoparticles (AuNPs) have been reported for SDA biosensors. The disaggregation of AuNPs causes a color change from blue to red. The optical properties of AuNPs are incorporated in two different ways to detect SDA. AuNPs serves as a reaction platform in the amplification process, or they can induce color change by interacting with the SDA products at the end of each amplification cycle.

The first kind of example was reported by Ye and co-workers⁵⁷. They used a specific nucleic acid probe to detect miRNA sensitively using AuNPs. As shown in **Figure 1.9A**, the probe was designed to attach directly on the surface of AuNPs through phosphorothioate modification at its 5' ends while the other ends were designed to bind the target in the amplification process. This attachment of the probe prevented aggregation of the AuNPs. The probe-conjugated AuNPs served as the seed for target-initiated exponential reaction. The many cycles of polymerization and cleavage of the strands by EXPAR enzymes resulted in the detachment of the conjugated probe from AuNPs. Amplification produced unconjugated AuNPs that aggregated in the presence of salt and changed color.

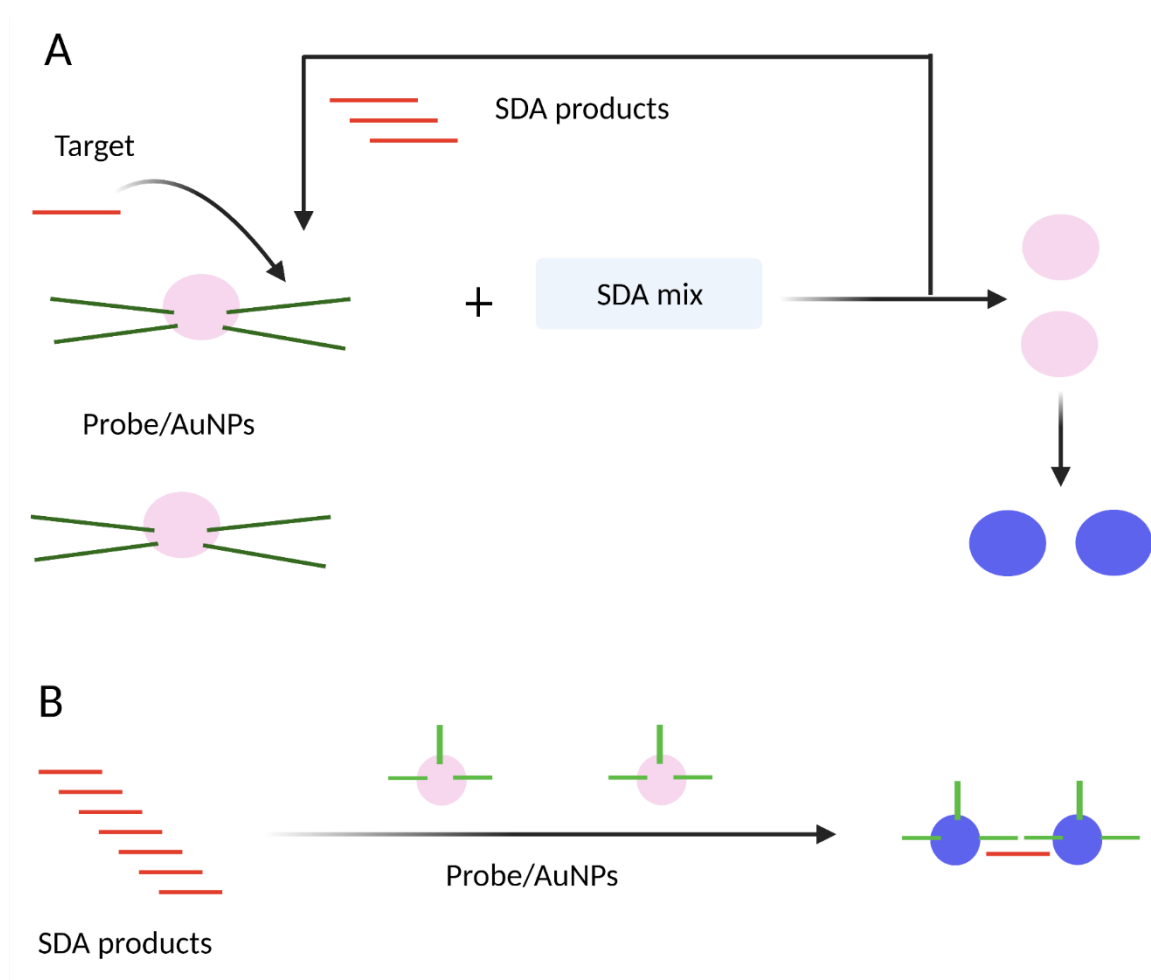


Figure 1.9. Schematic shows calorimetric-based SDA detection. A) Target initiated SDA on Probe/AuNPs platform. B) SDA products induced Probe/AuNPs aggregation.

The second kind of colorimetric detection is to generate a signal when the AuNPs interact with the SDA products. Target-initiated SDA or EXPAR produces DNA products that act as linkers. The linkers hybridize to DNA functionalized AuNPs. If a linker bridges two AuNPs, it can bring them together. This aggregates them and causes a change in color. Zhang et. al used AuNPs conjugated with thiol modified DNA probes for colorimetric detection of a protein⁵⁸. In this technique, AuNPs were separated from each other in the absence of an EXPAR reaction and the solution was red. Once target initiated EXPAR occurs, the products of the reaction then act as a bridge between oligonucleotide conjugated AuNPs to bring them into proximity. The upstream reaction template is designed in such a way that the oligonucleotide products hybridize with the oligonucleotide probes conjugated on the AuNPs. Once the AuNPs were

aggregated, the solution turned blue. Similar techniques were also reported by Niemz and coworkers^{59,60}. In all cases, the EXPAR product acted as bridge between two DNA functionalized AuNPs to bring them together (**Figure 1.9B**).

There are two common sources of non-specific signal. Firstly, DNA on the AuNPs may interact in the absence of target. Secondly, AuNPs may aggregate due to changes in environment or experimental conditions.

In order to produce a strong signal, probe DNA density needs to be high on AuNPs. However, if the DNA density is too high, it can suppress the DNA-DNA interactions by crowding and inhibit color generation. This strategy requires the probe to be stripped off the surface of the AuNPs. Also highly monodisperse AuNPs is required for reliable detection of target. Otherwise, non-specific signal can occur.

While high density of DNA on AuNPs might be a challenge for the first mechanism it can be good for the second mechanism. -a high density of DNA on AuNPs can trigger large aggregates and sensitive detection with a linker DNA.

Probe DNA needs to be designed carefully relative to target sequence. Otherwise, probe induced self-aggregation can occur.

Second, experimental conditions can generate undesired signal. For example, high salt concentration required for typical SDA reaction can cause non-specific signal generation as salt concentration also allows aggregation of AuNPs⁶¹. Also, Mg^{2+} cation is crucial for efficient enzymatic SDA circuits. Mg^{2+} is also a potential source of non-specific signal in colorimetric based detection. Mg^{2+} needs to be optimized as it causes self-aggregation of AuNP^{62,63}. Temperature can also affect DNA/AuNPs: stable conjugation under wide range of temperatures is important to efficient enzymatic operation. Thermal stability of DNA/AuNPs in a wide range of temperature is important for efficient enzymatic SDA and low non-specific signal.

Other colorimetric detection mechanisms for SDA involved the formation of G-quadruplex/hemin DNAzyme, a catalytic DNA complex^{64,65}. A G-quadruplex (G4) oligonucleotide is generated by an EXPAR reaction with a specially designed template. Hemin in the reaction buffer can

bind to G4 structures. This G4/hemin complex possesses peroxidase-like properties that can catalyze a chromogenic reaction and produce a color change⁶⁶. G4/hemin is a versatile signal reporter which has been used with electrochemical mode also. This is discussed in the following sections.

1.7.3 Electrochemical detection

Electrochemical detection is economical and avoids the complexity of optical instruments. The success of the blood glucose meter shows that electrochemical biosensors can be mass produced and widely adopted.. An electrochemical readout method for an SDA reaction will require some way to generate or immobilize electrochemically active molecules by SDA. One option is to use SDA to generate a G4/hemin complex and measure its peroxidase activity on an electrochemically active substrate⁶⁷⁻⁶⁹. This DNA based catalyst has found many diverse applications in biosensing⁷⁰⁻⁷².

We will consider two recent examples: each relied on the formation of the DNAzyme structure. The EXPAR-based miRNA detection started with a smartly designed duplex probe immobilized on the Au electrode surface⁷³. This immobilized duplex DNA served two roles in the system. First, it triggered exponential amplification upon target interaction. Second, it was converted into a DNAzyme at the electrode surface for detection. This dual function of the duplex probe lies with its specially designed two strand components. One sequence is complementary with the target sequence (denoted "capture DNA") while the other has a G4 forming sequence (denoted "reporter DNA"). Both were fixed on the electrode surface. The target competed with the capture DNA to bind the surface. When the target did bind, it disrupted the structure of the probe. This left the single strand reporter DNA fixed on the electrode surface. The reporter DNA strand adopted a G4 structure and captured hemin. The G4/hemin complex had peroxidase like catalytic activity. The electrochemical reduction of hemin was catalyzed by G4 in presence of K^+ , thereby generating electrochemical response (**Figure 1.10A**). Meanwhile, the target and capture DNA together were a substrate for EXPAR

amplification with the action of polymerase and nicking endonuclease enzymes. The result of this mechanism was a limit of detection of the target miRNA in fM range.

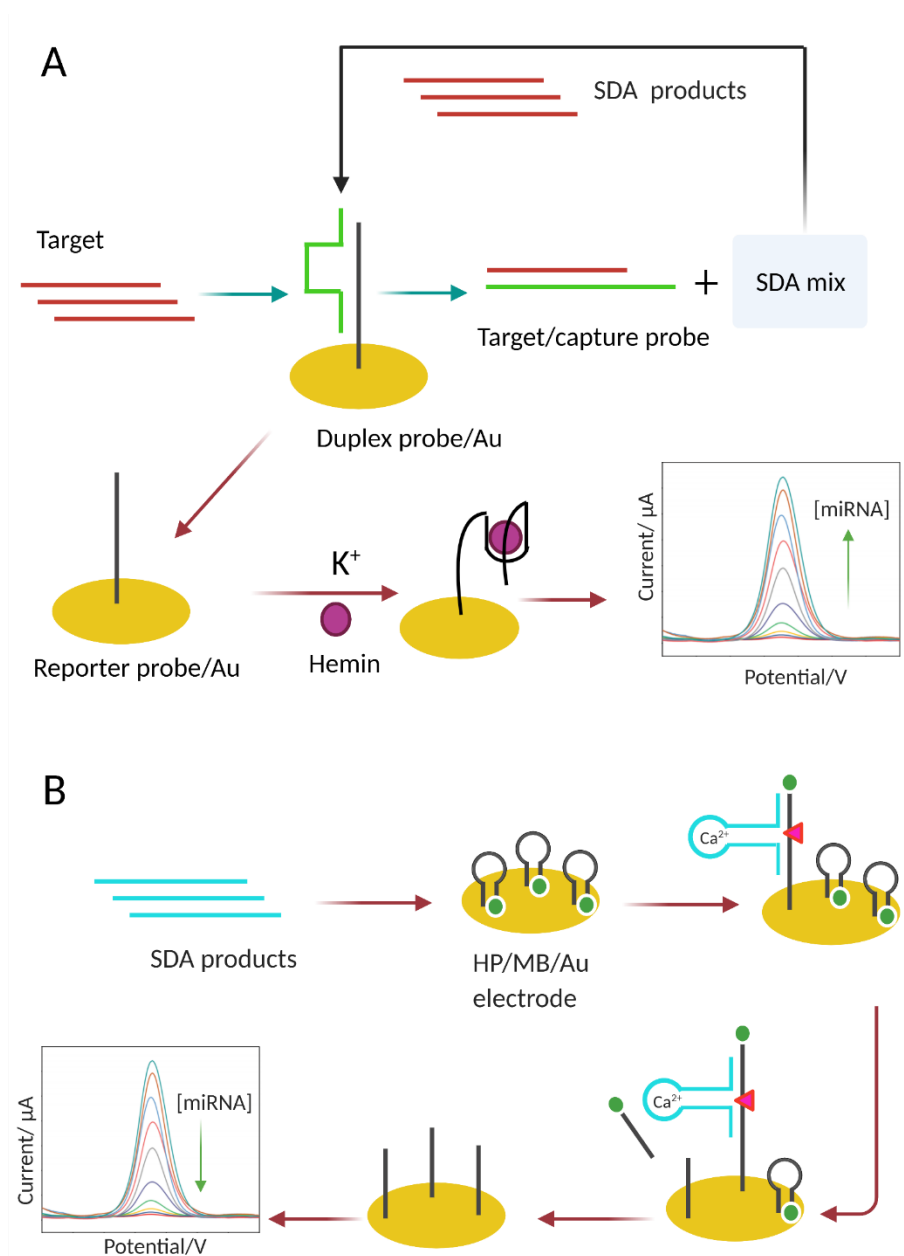


Figure 1.10. Schematic shows electrochemical-based SDA/EXPAR detection. A) SDA with dual function duplex probe for electrochemical readout of G4 catalyzed redox reaction of hemin. B) SDA products interacts with methylene blue (MB) labeled hairpin probe (HP) immobilized on Au electrode.

A probe lacking G4 structure can also act as a DNAzyme⁷⁴. Yang et. al reported an electrochemical method with a redox-active dye, methylene blue (MB). They achieved detection of miRNA with a slightly different approach. They immobilized a MB-modified

hairpin DNA probe on a gold electrode surface. This hairpin structure of the probe allowed the MB group to be positioned very close to the electrode surface. This allowed for rapid charge transfer⁷⁵. The response current is a function of the proximity of the MB molecules to the gold electrode. Without any target present, maximum current was obtained. When SDA was initiated by target, it generated DNA strands that hybridized with the MB-hairpin probe. The SDA product and the hairpin probe formed a specific, self-cleaving DNAzyme structure in presence of Ca^{2+} . This newly formed structure cleaved itself and removed the MB group from the surface (**Figure 1.10B**). Thus, with increasing target concentration, current response is decreased. The limit of detection (LOD) was reported to be 2.3×10^{-17} M. However, the electrochemical readout mode may find some challenges towards rapid experimentation. The electrode preparation and immobilization of the functional probe can be a tedious process. Duplex probe design can be challenging for versatile targets (**Figure 1.10A**). Competitive binding of the capture probe between target and reporter probe would be such that the capture probe readily binds to the target. The main source of the non-specific signal is non-specific adsorption of hemin into the surface of the Au electrode.

1.8 Analyte/target of SDA

SDA is a versatile detection tool of different class of analytes ranging from biomolecules to microorganism to small molecules, metal ions. The simple and versatile mechanism of SDA enables easy and sensitive detection of different analytes (**Figure 1.11**). As discussed earlier, there is report of genomic DNA amplification by SDA^{12,37}. Joneja et al., also showed fluorescence-based amplification of long DNA sequence of 5000 nucleotides. However, these are enzyme heavy processes and uses more than one temperature for different stages of the study. Since SDA efficiency depends on the synchronous action of both polymerase and nick endonuclease enzymes, longer DNA can pose challenges for nick endonuclease to nick in the desired site with precision. Multiple nicks on the undesired sites also invites polymerase enzymes to act upon to extend randomly. This can lead to non-specific amplification of the

target. However, SDA is most useful in detecting single-strand, short nucleic acid sequence. The popular use of this kind is detection of miRNA, short sequence of non-coding RNA of 20-24 nucleotides. Different miRNA has been attributed as related factor for different diseases⁷⁶, especially cancers⁷⁷. Hence easy, simple, and early detection of miRNA is very important. A significant number of studies has been done to detect different physiologically important miRNAs via different SDA methods^{57,73,74,78-80}. Recent authors of this article also developed an SDA-based simple and label-free approach to detect miR-215 sensitively⁵⁶. The light-up aptamer-based can be performed at room temperature to detect both DNA and RNA using only two enzymes. Guanine rich sequence binds to a dye named thioflavin T to light up the dye. This property of fluorescence enhancement was used in the study. However, this approach is constrained by rational template design for less guanine-based target to avoid possible non-specific signal generation.

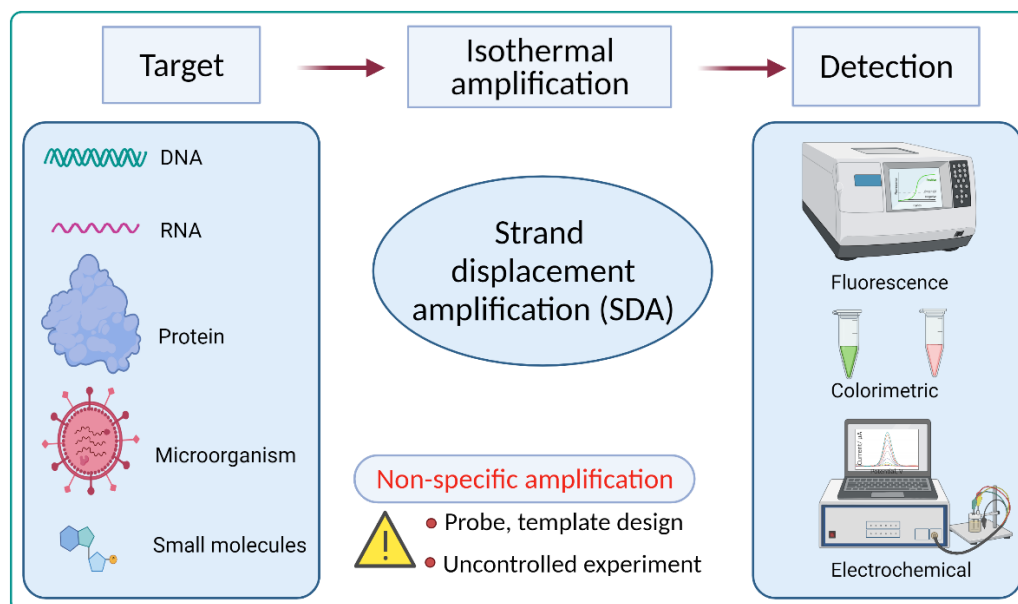


Figure 1.11: Schematic shows versatile SDA targets detection via different readout modes

Apart from nucleic acid, protein and other biomolecules can also be detected by SDA^{49,58,81,82}. However, detection of protein by nucleic acid amplification has been an indirect method as protein cannot be amplified. Protein can be detected using its binding properties with some form of functional oligonucleotides (aptamer or other double-stranded probe). This oligonucleotide acts as intermediate recognition element. Their interaction can be converted

into a trigger oligonucleotide by proper probe design. The trigger oligonucleotides execute the downstream EXPAR. For example, Zhang et al., developed an EXPAR-based colorimetric assay for the detection of a protein, transcription factor NF- κ B p50⁵⁸. This assay leveraged protein-DNA interaction of the target and a double strand probe, which utilized the activity of Exo III enzyme. The generation of a reporter oligonucleotide from this interaction lead to subsequent EXPAR to achieve 3.8 pM limit of detection of the target transcription factor.

SDA can also detect different enzymatic function. Li et al., developed an EXPAR system in combination to CRISPR/Cas system to monitor the cleavage activity of Cas9 enzyme⁸³. This enzyme is a crucial component of CRISPR/Cas system of gene editing, hence monitoring its activity is important. Clustered regularly interspaced short palindromic repeat (CRISPR) is a single guide RNA (sgRNA) mediated system. It can be customized for specific double strand DNA (dsDNA) target cleavage by Cas9 enzyme. The dsDNA substrate was designed with a nicking site to be recognized by Nt.BstNBI nicking enzyme in the subsequent EXPAR. This study is an interesting proof of concept example of both CRISPR/Cas and EXPAR systems integrated in the same experiment to detect dsDNA target and to monitor Cas9 enzyme efficiency. However, from non-specific amplification/signal point of view, there is serious concern in detecting dsDNA with an intercalating dye like EvaGreen. This dye indiscriminately binds to any dsDNA. The authors did not use nicked generated ssDNA EXPAR product as signal reporter, instead they used the whole duplex substrate generated by polymerase. This substrate is a transient structure in the amplification cycle. Also, it is less convenient to be used as signal reporter in EXPAR because signal can be generated from the initial dsDNA target even if it was not cleaved by the Cas enzyme due to the non-specific binding of the dye.

Isothermal strand displacement amplification has been used to detect tumor cells and microorganisms such virus and bacteria. Niemz et al., reported a AuNPs assisted colorimetric detection of herpes simplex virus⁵⁹. This is a proof-of-principle study of how genomic DNA of the virus can be used to trigger a subsequent EXPAR system. A more convenient and direct approach to detect cancer cells and pathogens via strand displacement amplification system has been reported also. This approach relies on the aptamer-cell binding interaction. Two

similar studies for detecting tumor cells⁸⁴ and pathogenic bacteria has been reported using two stage EXPAR system⁶⁴. However, more rigorous study for optimization of the reaction conditions is necessary for this type of analysis. The basis of this approach solely depends on the binding interaction between aptamers and their targets and the aptamer/aptamer* complementary probe design. Optimization of aptamer sequences and modified aptamer sequences is worth investigation to reduce non-specific amplification.

Various small molecules (such as ATP⁸⁵ and cocaine⁸⁶) have been detected by isothermal amplification techniques, specially strand displacement amplification. He et al., showed that unlabeled molecular beacon can be used to initiate SDA reaction for cocaine detection. The SDA starts with the formation of molecular beacon triggered ternary complex. The dsDNA products can be detected with SYBR green I as intercalating dye. This is concerning as a potential source of non-specific amplification because the dye can be intercalated with double stranded region of reactant component such as the molecular beacon probe and other intermediate duplex in the system.

1.9 Conclusion

SDA is a versatile nucleic acid based isothermal method. It has found application in numerous bioanalytical fields. With the discovery and engineering of different enzymes, design of different probes, and fluorescence dyes, this process is going through many phases of development. One of the crucial areas is to investigate non-specific amplification, its origins, and different approaches to minimize them in SDA. There should not be any signal in the absence of analyte (i.e., reagent blank). But background is unavoidable in DNA-DNA reactions involving hyperactive enzymes, especially Bst DNA polymerase. Therefore, various approaches need to be applied in order to get very high signal over background for a highly sensitive detection. The goal is to suppress non-specific amplification and non-specific signal readout. Although related, non-specific amplification and non-specific signal readout have different

origins. The former originates primarily from the amplification process and the latter from the detection mode.

To minimize non-specific amplification, the design of oligonucleotides such as template, primer, and other probes should be carefully done. For instance, in experiments where primer and other DNA are required (e.g., probe DNA for downstream detection), the design should be such that competitive binding is avoided. The template needs to be designed to omit self-hybridization specially in the 3' end. Also, the GC content in the primer need to be optimized as this determines the operating temperature. Operating temperature also cannot exceed the active range for the polymerase and nicking enzymes to be used. Bst polymerase is a hyperactive enzyme (even at the low end of its active temperature range). This causes non-specific amplification. It is often useful to assemble reaction the mixture in an ice bath. Bst polymerase should be exposed to the minimum time with dNTPs and template. Therefore, it is advisable to assemble the other reaction components in separate vials. Extensive optimization of time, temperature, enzyme concentration, oligonucleotide concentrations, and buffer composition are crucial for minimization of non-specific amplification.

A suitable detection mode can also help to decrease the nonspecific detection. For fluorescence, it is better to avoid non-specific intercalating dye. Detection probes like covalently labeled molecular beacons or labeled hairpin probes can be used for specific signal reporting. CRISPR based collateral cleavage of the reporter probe, or peptide nucleic acid probe can give higher detection specificity. However, this can be costly for low resource settings and may add complexity to the SDA process (which already contains two enzymes and their buffer components). Additionally, it necessitates high purity DNA which must be maintained carefully. Specific detection probes also add constraints to the reaction conditions. The amplification temperature now needs to comply with the temperature needed for molecular beacon FRET activity (i.e., below the melt transition of the hairpin structure). It needs to be opened from its native hairpin structure at the same operating temperature. These constraints are not prohibitive. As this review has shown, the use of SDA and other, similar isothermal amplification is widespread. Scores of labs have successfully built analytical

techniques using SDA. Nonspecific amplification can be overcome with good reaction conditions and DNA sequence designs. The detection limits for these techniques approach single molecule levels. It seems likely that diagnostics and practical applications are on the horizon.

1.10 Reference

1. Questions and Answers | E. coli | CDC. <https://www.cdc.gov/ecoli/general/index.html> (2019).
2. Lisby, G. Application of nucleic acid amplification in clinical microbiology. *Mol. Biotechnol.* **12**, 75–99 (1999).
3. Chen, H.-L. *et al.* Nucleic acid amplification-based methods for microRNA detection. *Anal. Methods* **7**, 2258–2263 (2015).
4. Mullis, K. B. The Unusual Origin of the Polymerase Chain Reaction. *Sci. Am.* **262**, 56–65 (1990).
5. Powledge, T. M. The polymerase chain reaction. *Adv. Physiol. Educ.* **28**, 44–50 (2004).
6. Valones, M. A. A. *et al.* Principles and applications of polymerase chain reaction in medical diagnostic fields: a review. *Braz. J. Microbiol.* **40**, 1–11 (2009).
7. Walker, G. T. *et al.* Strand displacement amplification—an isothermal, in vitro DNA amplification technique. *Nucleic Acids Res.* **20**, 1691–1696 (1992).
8. Qian, J. *et al.* Sequence dependence of isothermal DNA amplification via EXPAR. *Nucleic Acids Res.* **40**, e87 (2012).
9. Zhou, M., Teng, X., Li, Y., Deng, R. & Li, J. Cascade Transcription Amplification of RNA Aptamer for Ultrasensitive MicroRNA Detection. *Anal. Chem.* **91**, 5295–5302 (2019).
10. Baccouche, A., Montagne, K., Padirac, A., Fujii, T. & Rondelez, Y. Dynamic DNA-toolbox reaction circuits: A walkthrough. *Methods* **67**, 234–249 (2014).
11. Gines, G. *et al.* Isothermal digital detection of microRNAs using background-free molecular circuit. *Sci. Adv.* **6**, eaay5952 (2020).
12. Joneja, A. & Huang, X. Linear nicking endonuclease-mediated strand displacement DNA amplification. *Anal. Biochem.* **414**, 58–69 (2011).

13. Ness, J. V., Ness, L. K. V. & Galas, D. J. Isothermal reactions for the amplification of oligonucleotides. *Proc. Natl. Acad. Sci.* **100**, 4504–4509 (2003).
14. Biolabs, N. E. Nicking Endonucleases | NEB. <https://www.neb.com/products/restriction-endonucleases/hf-nicking-master-mix-time-saver-other/nicking-endonucleases/nicking-endonucleases>.
15. Dames, S., Margraf, R. L., Pattison, D. C., Wittwer, C. T. & Voelkerding, K. V. Characterization of Aberrant Melting Peaks in Unlabeled Probe Assays. *J. Mol. Diagn.* **9**, 290–296 (2007).
16. Tan, E. *et al.* Specific versus Nonspecific Isothermal DNA Amplification through Thermophilic Polymerase and Nicking Enzyme Activities. *Biochemistry* **47**, 9987–9999 (2008).
17. Reid, M. S., Paliwoda, R. E., Zhang, H. & Le, X. C. Reduction of Background Generated from Template-Template Hybridizations in the Exponential Amplification Reaction. *Anal. Chem.* **90**, 11033–11039 (2018).
18. Montagne, K., Plasson, R., Sakai, Y., Fujii, T. & Rondelez, Y. Programming an in vitro DNA oscillator using a molecular networking strategy. *Mol. Syst. Biol.* **7**, 466 (2011).
19. Padirac, A., Fujii, T. & Rondelez, Y. Bottom-up construction of in vitro switchable memories. *Proc. Natl. Acad. Sci.* **109**, E3212–E3220 (2012).
20. Cho, E. J., Lee, J.-W. & Ellington, A. D. Applications of Aptamers as Sensors. *Annu. Rev. Anal. Chem.* **2**, 241–264 (2009).
21. Ellington, A. D. & Szostak, J. W. In vitro selection of RNA molecules that bind specific ligands. *Nature* **346**, 818–822 (1990).
22. Tuerk, C. & Gold, L. Systematic evolution of ligands by exponential enrichment: RNA ligands to bacteriophage T4 DNA polymerase. *Science* **249**, 505–510 (1990).
23. Sefah, K., Shangguan, D., Xiong, X., O'Donoghue, M. B. & Tan, W. Development of DNA aptamers using Cell-SELEX. *Nat. Protoc.* **5**, 1169–1185 (2010).
24. Blind, M. & Blank, M. Aptamer Selection Technology and Recent Advances. *Mol. Ther. - Nucleic Acids* **4**, e223 (2015).

25. Iliuk, A. B., Hu, L. & Tao, W. A. Aptamer in Bioanalytical Applications. *Anal. Chem.* **83**, 4440–4452 (2011).
26. Mazaafrianto, D. N., Maeki, M., Ishida, A., Tani, H. & Tokeshi, M. Recent Microdevice-Based Aptamer Sensors. *Micromachines* **9**, (2018).
27. Wu, Y., Midinov, B. & White, R. J. Electrochemical Aptamer-Based Sensor for Real-Time Monitoring of Insulin. *ACS Sens.* **4**, 498–503 (2019).
28. Paige, J. S., Wu, K. Y. & Jaffrey, S. R. RNA Mimics of Green Fluorescent Protein. *Science* **333**, 642–646 (2011).
29. Huang, H. *et al.* A G-Quadruplex-Containing RNA Activates Fluorescence in a GFP-Like Fluorophore. *Nat. Chem. Biol.* **10**, 686–691 (2014).
30. Lander, E. S. The Heroes of CRISPR. *Cell* **164**, 18–28 (2016).
31. Jinek, M. *et al.* A Programmable Dual-RNA-Guided DNA Endonuclease in Adaptive Bacterial Immunity. *Science* **337**, 816–821 (2012).
32. Cong, L. *et al.* Multiplex Genome Engineering Using CRISPR/Cas Systems. *Science* **339**, 819–823 (2013).
33. Broughton, J. P. *et al.* CRISPR–Cas12-based detection of SARS-CoV-2. *Nat. Biotechnol.* **38**, 870–874 (2020).
34. Zhang, Y. *et al.* Rapid Molecular Detection of SARS-CoV-2 (COVID-19) Virus RNA Using Colorimetric LAMP. <http://medrxiv.org/lookup/doi/10.1101/2020.02.26.20028373> (2020) doi:10.1101/2020.02.26.20028373.
35. Jore, M. M. *et al.* Structural basis for CRISPR RNA-guided DNA recognition by Cascade. *Nat. Struct. Mol. Biol.* **18**, 529–536 (2011).
36. Kellner, M. J., Koob, J. G., Gootenberg, J. S., Abudayyeh, O. O. & Zhang, F. SHERLOCK: nucleic acid detection with CRISPR nucleases. *Nat. Protoc.* **14**, 2986–3012 (2019).
37. Zhou, W. *et al.* A CRISPR–Cas9-triggered strand displacement amplification method for ultrasensitive DNA detection. *Nat. Commun.* **9**, 5012 (2018).
38. Shi, C., Liu, Q., Ma, C. & Zhong, W. Exponential Strand-Displacement Amplification for Detection of MicroRNAs. *Anal. Chem.* **86**, 336–339 (2014).

39. Jia, H., Li, Z., Liu, C. & Cheng, Y. Ultrasensitive Detection of microRNAs by Exponential Isothermal Amplification. *Angew. Chem. Int. Ed.* **49**, 5498–5501 (2010).
40. Zhou, Y. *et al.* Fluorometric determination of microRNA based on strand displacement amplification and rolling circle amplification. *Microchim. Acta* **184**, 4359–4365 (2017).
41. Cai, R., Yin, F., Chen, H., Tian, Y. & Zhou, N. A fluorescent aptasensor for *Staphylococcus aureus* based on strand displacement amplification and self-assembled DNA hexagonal structure. *Microchim. Acta* **187**, 304 (2020).
42. Yang, D. *et al.* Carbon Nanodot–Based Fluorescent Method for Virus DNA Analysis with Isothermal Strand Displacement Amplification. *Part. Part. Syst. Charact.* **36**, 1900273 (2019).
43. Tyagi, S. & Kramer, F. R. Molecular Beacons: Probes that Fluoresce upon Hybridization. *Nat. Biotechnol.* **14**, 303–308 (1996).
44. Luo, J., Shen, X., Li, B., Li, X. & Zhou, X. Signal amplification by strand displacement in a carbon dot based fluorometric assay for ATP. *Microchim. Acta* **185**, 392 (2018).
45. Xu, Q. *et al.* Preparation of highly photoluminescent sulfur-doped carbon dots for Fe(iii) detection. *J. Mater. Chem. A* **3**, 542–546 (2015).
46. Zhang, Z., Sharon, E., Freeman, R., Liu, X. & Willner, I. Fluorescence Detection of DNA, Adenosine-5'-Triphosphate (ATP), and Telomerase Activity by Zinc(II)-Protoporphyrin IX/G-Quadruplex Labels. *Anal. Chem.* **84**, 4789–4797 (2012).
47. González-Moreno, R. *et al.* Attachment of Protoporphyrin Dyes to Nanostructured ZnO Surfaces: Characterization by Near Edge X-ray Absorption Fine Structure Spectroscopy. *J. Phys. Chem. C* **115**, 18195–18201 (2011).
48. Gao, T., Luo, Y., Li, W., Cao, Y. & Pei, R. Progress in the isolation of aptamers to light-up the dyes and the applications. *Analyst* **145**, 701–718 (2020).
49. Wang, L., Zhang, Y. & Zhang, C. A target-triggered exponential amplification-based DNazyme biosensor for ultrasensitive detection of folate receptors. *Chem. Commun.* **50**, 15393–15396 (2014).

50. Xue, Q. *et al.* Highly sensitive fluorescence assay of DNA methyltransferase activity by methylation-sensitive cleavage-based primer generation exponential isothermal amplification-induced G-quadruplex formation. *Biosens. Bioelectron.* **66**, 547–553 (2015).
51. Damase, T. R., ISLAM, M. M., Shipley, M. & Allen, P. B. Thioflavin T as a noncovalent reporter for a label-free, non-enzymatic, catalytic DNA amplifier. *Methods Appl. Fluoresc.* (2020) doi:10.1088/2050-6120/aba357.
52. Mohanty, J. *et al.* Thioflavin T as an Efficient Inducer and Selective Fluorescent Sensor for the Human Telomeric G-Quadruplex DNA. *J. Am. Chem. Soc.* **135**, 367–376 (2013).
53. Renaud de la Faverie, A., Guédin, A., Bedrat, A., Yatsunyk, L. A. & Mergny, J.-L. Thioflavin T as a fluorescence light-up probe for G4 formation. *Nucleic Acids Res.* **42**, e65–e65 (2014).
54. Zhou, H. *et al.* Stable and Label-Free Fluorescent Probe Based on G-triplex DNA and Thioflavin T. *Anal. Chem.* **90**, 3220–3226 (2018).
55. Du, Y.-C., Zhu, L.-N. & Kong, D.-M. Label-free thioflavin T/G-quadruplex-based real-time strand displacement amplification for biosensing applications. *Biosens. Bioelectron.* **86**, 811–817 (2016).
56. Islam, M. M., Ghielmetti, V. M. & Allen, P. B. Graphene oxide assisted light-up aptamer selection against Thioflavin T for label-free detection of microRNA. *Sci. Rep.* **11**, 4291 (2021).
57. Li, R.-D., Yin, B.-C. & Ye, B.-C. Ultrasensitive, colorimetric detection of microRNAs based on isothermal exponential amplification reaction-assisted gold nanoparticle amplification. *Biosens. Bioelectron.* **86**, 1011–1016 (2016).
58. Zhang, Y., Hu, J. & Zhang, C. Sensitive Detection of Transcription Factors by Isothermal Exponential Amplification-Based Colorimetric Assay. *Anal. Chem.* **84**, 9544–9549 (2012).
59. Tan, E., Erwin, B., Dames, S., Voelkerding, K. & Niemz, A. Isothermal DNA Amplification with Gold Nanosphere-Based Visual Colorimetric Readout for Herpes Simplex Virus Detection. *Clin. Chem.* **53**, 2017–2020 (2007).

60. Tan, E. *et al.* Isothermal DNA Amplification Coupled with DNA Nanosphere-Based Colorimetric Detection. *Anal. Chem.* **77**, 7984–7992 (2005).
61. Liu, B. & Liu, J. Methods for preparing DNA-functionalized gold nanoparticles, a key reagent of bioanalytical chemistry. *Anal. Methods* **9**, 2633–2643 (2017).
62. Liu, J. & Lu, Y. A Colorimetric Lead Biosensor Using DNAzyme-Directed Assembly of Gold Nanoparticles. *J. Am. Chem. Soc.* **125**, 6642–6643 (2003).
63. Zhou, W., Wang, F., Ding, J. & Liu, J. Tandem Phosphorothioate Modifications for DNA Adsorption Strength and Polarity Control on Gold Nanoparticles. *ACS Appl. Mater. Interfaces* **6**, 14795–14800 (2014).
64. Qiu, T. *et al.* Label-free, homogeneous, and ultrasensitive detection of pathogenic bacteria based on target-triggered isothermally exponential amplification. *RSC Adv.* **6**, 62031–62037 (2016).
65. Nie, J., Zhang, D.-W., Tie, C., Zhou, Y.-L. & Zhang, X.-X. G-quadruplex based two-stage isothermal exponential amplification reaction for label-free DNA colorimetric detection. *Biosens. Bioelectron.* **56**, 237–242 (2014).
66. Li, W. *et al.* Insight into G-quadruplex-hemin DNAzyme/RNAzyme: adjacent adenine as the intramolecular species for remarkable enhancement of enzymatic activity. *Nucleic Acids Res.* **44**, 7373–7384 (2016).
67. Chang, T. *et al.* Activity Enhancement of G-Quadruplex/Hemin DNAzyme by Flanking d(CCC). *Chem. – Eur. J.* **22**, 4015–4021 (2016).
68. Cao, Y. *et al.* Investigation and improvement of catalytic activity of G-quadruplex/hemin DNAzymes using designed terminal G-tetrads with deoxyadenosine caps. *Chem. Sci.* **11**, 6896–6906 (2020).
69. Pelossof, G., Tel-Vered, R. & Willner, I. Amplified Surface Plasmon Resonance and Electrochemical Detection of Pb²⁺ Ions Using the Pb²⁺-Dependent DNAzyme and Hemin/G-Quadruplex as a Label. *Anal. Chem.* **84**, 3703–3709 (2012).

70. Wang, Z.-H., Lu, C.-Y., Liu, J., Xu, J.-J. & Chen, H.-Y. An improved G-quadruplex DNAzyme for dual-functional electrochemical biosensing of adenosines and hydrogen peroxide from cancer cells. *Chem. Commun.* **50**, 1178–1180 (2014).
71. Sun, D., Lu, J., Chen, Z., Yu, Y. & Mo, M. A repeatable assembling and disassembling electrochemical aptamer cytosensor for ultrasensitive and highly selective detection of human liver cancer cells. *Anal. Chim. Acta* **885**, 166–173 (2015).
72. Li, D., Shlyahovsky, B., Elbaz, J. & Willner, I. Amplified Analysis of Low-Molecular-Weight Substrates or Proteins by the Self-Assembly of DNAzyme–Aptamer Conjugates. *J. Am. Chem. Soc.* **129**, 5804–5805 (2007).
73. Yu, Y. *et al.* Ultrasensitive Electrochemical Detection of MicroRNA Based on an Arched Probe Mediated Isothermal Exponential Amplification. *Anal. Chem.* **86**, 8200–8205 (2014).
74. Yang, D., Cheng, W., Chen, X., Tang, Y. & Miao, P. Ultrasensitive electrochemical detection of miRNA based on DNA strand displacement polymerization and Ca²⁺-dependent DNAzyme cleavage. *Analyst* **143**, 5352–5357 (2018).
75. Farjami, E., Clima, L., Gothelf, K. V. & Ferapontova, E. E. DNA interactions with a Methylene Blue redox indicator depend on the DNA length and are sequence specific. *Analyst* **135**, 1443–1448 (2010).
76. Liu, N. & Olson, E. N. MicroRNA regulatory networks in cardiovascular development. *Dev. Cell* **18**, 510–525 (2010).
77. Calin, G. A. & Croce, C. M. MicroRNA signatures in human cancers. *Nat. Rev. Cancer* **6**, 857–866 (2006).
78. Yin, B.-C., Liu, Y.-Q. & Ye, B.-C. Sensitive Detection of MicroRNA in Complex Biological Samples via Enzymatic Signal Amplification Using DNA Polymerase Coupled with Nicking Endonuclease. *Anal. Chem.* **85**, 11487–11493 (2013).
79. Zhang, Y. & Zhang, C. Sensitive Detection of microRNA with Isothermal Amplification and a Single-Quantum-Dot-Based Nanosensor. *Anal. Chem.* **84**, 224–231 (2012).

80. Attomolar Ultrasensitive MicroRNA Detection by DNA-Scaffolded Silver-Nanocluster Probe Based on Isothermal Amplification | Analytical Chemistry. <https://pubs.acs.org/doi/10.1021/ac300483f>.
81. Zhang, H. *et al.* AuNPs colorimetric sensor for detecting platelet-derived growth factor-BB based on isothermal target-triggering strand displacement amplification. *Sens. Actuators B Chem.* **207**, 748–755 (2015).
82. Xie, S., Chai, Y., Yuan, Y., Bai, L. & Yuan, R. A novel electrochemical aptasensor for highly sensitive detection of thrombin based on the autonomous assembly of hemin/G-quadruplex horseradish peroxidase-mimicking DNAzyme nanowires. *Anal. Chim. Acta* **832**, 51–57 (2014).
83. Zhang, K., Deng, R., Li, Y., Zhang, L. & Li, J. Cas9 cleavage assay for pre-screening of sgRNAs using nicking triggered isothermal amplification. *Chem. Sci.* **7**, 4951–4957 (2016).
84. Tang, W. *et al.* Sensitive detection of tumor cells based on aptamer recognition and isothermal exponential amplification. *RSC Adv.* **6**, 89888–89894 (2016).
85. Wang, X. *et al.* Four-stage signal amplification for trace ATP detection using allosteric probe-conjugated strand displacement and CRISPR/Cpf1 trans-cleavage (ASD-Cpf1). *Sens. Actuators B Chem.* **323**, 128653 (2020).
86. He, J.-L. *et al.* Fluorescence Aptameric Sensor for Strand Displacement Amplification Detection of Cocaine. *Anal. Chem.* **82**, 1358–1364 (2010).

CHAPTER 2: Towards label-free, non-enzymatic, and isothermal detection of DNA-DNA reactions: Application of Thioflavin T as light up dye

Md Mamunul Islam, Peter B. Allen*

*Correspondence to: pballen@uidaho.edu.

University of Idaho, Dept. of Chemistry, 001 Renfrew Hall, 875 Perimeter Dr, Moscow, ID 83844-2343

(Part of this work has been published in the journal of Methods and Applications of fluorescence of IOPscience under the title of "Thioflavin T as a noncovalent reporter for a label-free, non-enzymatic, catalytic DNA amplifier")

KEYWORDS: Thioflavin T, label-free DNA circuits, G-rich sequence, entropy-driven amplifier reaction

DNA-DNA reactions can be monitored with a label-free fluorogenic reaction. Thioflavin T (ThT) can be used as light up dye in presence of Guanosine-rich (G-rich) DNA oligonucleotides. In its free state thioflavin T (ThT) has negligible fluorescence, however, upon binding to G-rich sequences, it generates high fluorescence. This fluorogenic property can be used in reporting DNA-DNA reaction without any modification of the DNA strands. We demonstrated the feasibility of such label-free reporting system. For this purpose, we used a novel DNA sequence that derived from a G-quadruplex sequence. We denote this oligonucleotide ThTSignal. We use ThTSignal as a label-free reporter for monitoring of several, both simple and complex, designed DNA-DNA reactions (DNA circuits). The DNA circuits is designed to perform in absence of any enzyme and in isothermal system. This approach has potential of developing label-free, low-cost, and highly sensitive detection of target DNA.

2.1 Introduction

At its chemical structure, a DNA (deoxyribo nucleic acid) molecule is formed by four repetitive bases; adenine, guanine, thymine, and cytosine on a backbone made up of pentose sugar and phosphate group¹. Naturally occurred DNA is an integral part of any organism in their

structural unit cell. This natural DNA, in its double stranded form, perform many physiological functions in any organism². However, DNA is not only found in organisms; it can also be synthesized in laboratory. However, unlike natural DNA, DNA is synthesized as single stranded molecule (ssDNA)^{3,4}. ssDNA can be synthesized with precise sequence order of four bases, modified with different functional groups as needed. In terms of application, a whole new field in chemistry named “DNA nanotechnology” has been evolved over the last two decades⁵. This new field deals with DNA-DNA reactions. DNA-DNA reactions can be designed based on fundamental non-covalent base pairing between adenine and thymine and guanine and cytosine⁶. This complementarity property between bases of two ssDNA can be used to make synthetic double stranded DNA (dsDNA). The designed DNA-DNA reactions can be used to detect target DNA which can be accomplished without any enzyme⁷, and in an isothermal setting thus offers low-cost method of detection. The simplest form of DNA-DNA reactions are strand displacement reactions⁸.

A single-stranded DNA (ssDNA) oligonucleotide can interact with a partially double-stranded DNA (formed between a shorter single strand and its complementary longer single strand) complex to produce a more stable complex and a new ssDNA oligonucleotide output. The output from one strand displacement reaction can be the input of a second strand displacement reaction. In this way, strand displacement reactions can be “wired” together into reaction networks called DNA circuits⁹. The DNA circuit field is growing rapidly and is finding application in DNA-based biosensors. Diverse DNA based platforms¹⁰⁻¹² help to evolve DNA circuits in both conventional^{13,14} and microfluidic research^{15,16}. Designed DNA-DNA reactions need to be monitored to report the reaction output and to extrapolate quantitative information for detection assay. There are a few reporting techniques each with own pros and cons. They are optical, electrochemical, coloremetric¹⁷ but the most common reporting techniques is fluorescence-based.

Fluorescence is sensitive, biocompatible, and non-destructive technique. Moreover, researchers can select a wide range of fluorescent dyes compatible with their detection instrument. Commercially readily available fluorescent dyes can be conjugated during DNA

synthesis. The most common fluorescence-based reporting technique in the DNA circuit (DNA-DNA reactions) is to design DNA strands with covalently attached quenchers and fluorophores such that fluorescence is activated by the DNA reactions^{18,19}. However, such modification of DNA is expensive. For instance, a DNA strand with 20 bases cost only \$10. Modification of the same DNA with fluorophore and quencher groups can increase the cost up to several hundreds. Modification of DNA may introduce purity considerations. Degradation or synthesis impurities reduce the analytical performance of the sensors by adding non-specific background. To avoid the modification of DNA and to keep the cost at a minimum, label-free monitoring has been introduced. Label-free approach does not require covalently modified DNA strands to report reaction output of a DNA-DNA reaction.

Small molecules, low-cost fluorescence dyes are used in label-free detection²⁰. In the absence of the DNA, dyes are not fluorescent. These dyes interact with specific DNA structures and bind in a non-covalent way to generate fluorescence. Thus, they are known as light-up dyes or fluorogenic dyes. Both dsDNA and ssDNA can interact with light-up dyes. SYBR green, a cyanine-based dye, is widely used as a light-up dye for dsDNA monitoring. This dye binds to the groove area of the double helical DNA structure. The problem with this dye is that it can generate fluorescence in the presence of any dsDNA, which is not desired for a detection system.

Like dsDNA, ssDNA can also interact with fluorogenic dyes. ssDNA has a polyanionic backbone stemming from negatively charged phosphate groups. Cationic dyes interact with the polyanionic ssDNA by non-covalent electrostatic force. Such a cationic dye is thioflavin T (ThT) also known as Basic Yellow 1. It consists of a benzothiazole ring and a benzyl ring connected by a C-C bond²¹. ThT has been shown to interact with guanine-rich DNA sequences G-Quadruplexes, a structure formed from stacked tetramers of hydrogen-bonded guanosine bases^{22,23}, including DNA oligonucleotides with the sequence of telomeric DNA²⁴. ThT has also been widely used in protein study. It has a convenient spectrum with excitation and emission wavelengths of ~440 nm and ~500 nm, respectively. It is easily soluble in water and commercially available.

We have developed a label-free, isothermal method to monitor non-enzymatic DNA-DNA reactions. This label-free technique uses Thioflavin-T (ThT) dye and a guanosine-rich novel DNA oligonucleotide (denoted ThTSignal) that interacts with the dye and induces fluorescence. Previously, an aptamer selected against ThT has been published²⁵, but ThTSignal is more than ten times brighter in the buffer used for DNA circuits. Other light-up aptamers such as the dimethylindole red (DIR) aptamer might also be adapted²⁶. A recent review covers a host of light-up aptamers that might be considered²⁷. However, the convenient spectral properties and availability of ThT make it an attractive option. We present the application of this fluorogenic ThT detection scheme to a complex, catalytic DNA circuit, the entropy-driven amplifier (EDA). The EDA is a catalytic, enzyme-free DNA circuit that produces many output molecules for each input molecule²⁸. We developed a new label-free analytical approach to monitor DNA circuits. This technique is not subject to the purity and cost requirements of covalent fluorophores.

2.2 Methods

2.2.1 Materials

DNA oligonucleotides (standard desalting purification unless stated otherwise in the text) were purchased from Integrated DNA Technologies, IDT (Coralville, IA, USA). All DNA sequences are shown in **Table 1**. Potassium chloride was obtained from Avantor Performance Materials, PA, USA. All reagents used were of analytical grade. Nuclease-free water was purchased from Thermo Scientific (Waltham, MA, USA). ThT was purchased from Acros Organics, NJ, USA. Ethylenediaminetetraacetic acid (EDTA) and sodium chloride (NaCl) were purchased from EMD Chemicals, Gibbstown, Germany. For microplate reader fluorescence intensity measurements, samples were loaded in 384 well black plates with clear bottoms (Corning ME, USA).

2.2.2 ThT fluorescence sensitivity with PW17Ext and ThTSignal oligonucleotide

Ten samples of PW17Ext and ThTSignal oligonucleotide (standard desalted) (5 μ M, 4 μ M, 2 μ M, 1 μ M, 0.5 μ M, 0.4 μ M, 0.25 μ M, 0.2 μ M, 0.1 μ M and 0.05 μ M) were made in tris buffer (20 mM Tris, 50 mM NaCl, 10 mM EDTA, pH 7.6) with or without potassium chloride (10 mM)

containing 5 μM ThT. A digital photograph was acquired under blue light with an amber filter (FastGene Blue LED Gel Illuminator, Bulldog Bio, Portsmouth, NH). The fluorescence intensity (of 20 μl of each sample) was measured in the plate reader (SpectraMax iD3) in triplicate with an excitation wavelength of 440 nm and an emission wavelength of 510 nm.

2.2.3 Binding Curve

ThT and DNA were combined, and fluorescence was measured to determine the binding dissociation constant (K_d) between ThT and ThTSignal. DNA oligonucleotide was added to the appropriate final concentration, as noted in the graph (Figure S2). The final concentration of ThT was 1 μM of ThT. The increase in fluorescence was taken as proportional to the ThTSignal-ThT complex concentration. A single binding equilibrium was assumed ($\text{ThT} + \text{ThTSignal} \rightleftharpoons \text{Complex}$), and a nonlinear fit was conducted using Excel's Solver function.

2.2.4 Melt Curve Analysis of the PW17Ext and ThTSignal oligonucleotides

An Open qPCR (Chai Biotechnologies, Santa Clara, CA) was used to monitor fluorescence as a function of temperature (i.e., melt curve analysis or thermofluorimetry). HPLC purified PW17Ext and ThTSignal oligonucleotides were prepared at 2 μM in the tris buffer as above with or without potassium chloride (10 mM) containing 5 μM ThT. Thermofluorimetric analysis of both oligonucleotides was carried out in duplicate under two conditions: with and without 10 mM potassium chloride. UV melt curve analysis of desalted oligonucleotides was performed using Varian Cary 100 Bio UV-Vis Spectrophotometer without ThT in the solution using 1 μM of both ThTSignal and PW17Ext at 295nm.

2.2.5 Circular Dichroism and PAGE Analysis of PW17Ext and ThTSignal

PW17Ext and ThTSignal samples were prepared at 10 μM in Tris buffer (20 mM Tris, 50 mM NaCl, 10 mM EDTA, pH 7.6) with or without potassium chloride (10 mM). As controls, an arbitrary ssDNA, dsDNA, and blank were also made using the same buffer. All DNA strands were annealed before CD measurement by a Jasco 720 Circular Dichroism Spectrophotometer (Jasco, Inc., Easton, Maryland, USA).

Both native and denaturing 10% PAGE analysis of ThTSignal and PW17Ext were carried out at various concentrations (0.5, 2, 5, 10, 20 μM). The gel was post stained in 1X SYBR Gold Nucleic Acid Gel Stain (ThermoFisher) for one hour. We imaged the gel with a FastGene illuminator and an Olympus PEN PL-2 digital camera.

2.2.6 One-step strand (OSD) reaction with ThT detection

The one-step strand displacement reaction was initiated by mixing the Spine-ThTSignal complex (0.5 μM) and Fuel (0.5 μM) in the presence of 5 μM of ThT in tris buffer (20 mM Tris, 50 mM NaCl, 10 mM EDTA, pH 7.6). The reaction time was 3 hours. Kinetic fluorescence intensity was collected as above.

2.2.7 Effect of ThT dye on the rate of the OSD reaction

Several (18) OSD reactions consisting of Spine-ThTSignal complex (1 μM) and Fuel (1 μM) in tris buffer (20 mM Tris, 50 mM NaCl, 10 mM EDTA, pH 7.6) were carried out in triplicate fashion. These reactions were designed to be carried out for 18 different times period (0, 8, 12, 18, 24, 30, 48, 62, 90, 120, 150, 180, 210, 240, 270, 300, 330, and for 360 min) in 6 hours duration. After completion of these OSD reactions for their assigned time period, 5 μM of ThT was added, and fluorescence endpoint measurements were taken.

A six-hour kinetic experiment of the One-step Strand Displacement (OSD) reaction (Spine-ThTSignal complex, 1 μM and Fuel, 1 μM) was carried out in triplicate measurement in the presence of 5 μM of ThT.

2.2.8 Comparison of OSD reaction between ThT and Fluor-Quencher detection system

A kinetic fluorescence experiment of One-step Strand Displacement (OSD) reaction (Qspine-FluorSignal complex, 1 μM and Fuel, 1 μM) was carried out in the presence of tris buffer (20 mM Tris, 50 mM NaCl, 10 mM EDTA, pH 7.6) in triplicate measurement.

A kinetic fluorescence experiment of the One-step Strand Displacement (OSD) reaction (Spine-ThTSignal complex, 1 μM and Fuel, 1 μM) was carried out in triplicate measurement in the presence of 5 μM of ThT. Both reactions were carried out for 2.5 hour.

2.2.9 Entropy Driven Amplifier with ThT readout

The entropy-driven amplifier (EDA) circuit reaction was initiated by mixing HPLC purified components: Spine-ThTSignal-Block complex with 0%, 20%, 30%, 60%, 80% and 100% (1 μ M) Catalyst in the presence of Fuel (1 μ M) and 5 μ M of ThT in tris buffer (20 mM Tris, 50 mM NaCl, 10 mM EDTA pH 7.6). Fluorescence data were acquired over a period of 20 hours, at 30 °C, with an excitation wavelength of 440 nm and an emission wavelength of 510 nm with triplicate experiments. As negative controls, three mutant catalysts strands (non-specific DNA denoted “mutCatalyst”) were included in the place of the EDA catalyst. Other controls were assembled at 1 μ M concentration of the following oligonucleotides: Spine-ThTSignal-Block complex + Fuel (leakage control), Spine-ThTSignal-Block complex, Catalyst, mutCatalyst 1, mutCatalyst 2, mutCatalyst 3, Spine, ThTSignal, Block, and Fuel also in triplicate. For sequences of the oligonucleotides, see **Table 1**. The EDA reaction of the Fluorosignal-Quencher system was also carried out in the same manner.

The EDA circuit reaction was also analyzed by 10% native PAGE (including 10 mM Mg^{2+}). EDA circuit reactions were carried out for 10 hours at 30 °C before PAGE analysis. We ran this reaction for an extended time to ensure a measurable product. EDA circuit reactions and controls were assembled as follows: Lane 1, Spine at 1 μ M. Lane 2, Fuel at 1 μ M. Lane 3, Block at 1 μ M. Lane 4, ThTSignal-Spine at 1 μ M. Lane 5, Spine-ThTSignal, and Fuel (OSD control at 1 μ M). Lane 6, Spine-ThTSignal-Block complex at 1 μ M. Lane 7, Spine-Fuel control at 1 μ M, lane 8, ThTSignal at 1 μ M. Leakage control: lane 9, Spine-ThTSignal-Block complex at 1 μ M, and Fuel at 1 μ M. Lane 10, Spine-ThTSignal-Block complex at 1 μ M and Catalyst at 1 μ M. Experimental: lane 11 and 12, 100% Catalyst: Spine-ThTSignal-Block complex at 1 μ M, Fuel at 1 μ M, Catalyst at 1 μ M. Lane 13, Experimental: 50% Catalyst: Spine-ThTSignal-Block complex at 1 μ M, Fuel at 1 μ M, and Catalyst at 0.5 μ M. Lane 14, Positive control: ThTSignal 10 μ M, and lane 15, ladder. The electrophoresis was carried out in a refrigerator (4 °C) for 22 hours at 80 V in 1X Sodium Borate buffer (5 mM sodium borate, 10 mM $MgSO_4$, pH 8). The gel was stained first in 3X GelRed (Biotium, CA, USA) for 30 minutes and then in 20 μ M ThT for 30 minutes. A digital fluorescence photograph was taken under blue illumination with an amber filter after

each staining.

A one-step strand displacement (OSD) reaction and EDA reaction with necessary controls were performed in triplicate to compare kinetics between the ThT system and a standard fluorophore/quencher pair system. The reaction was assembled as described above. The comparison between OSD reaction and EDA reaction was carried out at room temperature and at 30 °C, respectively. The DNA oligonucleotides used in the OSD, and EDA reactions were HPLC purified and were purchased from Integrated DNA Technologies, IDT (Coralville, IA, USA).

2.3 Results and Discussion

2.3.1 Discovery of a new fluorogenic oligonucleotide for ThT

We found a new fluorogenic oligonucleotide (denoted “ThTSignal”). ThTSignal was designed to be a non-fluorescent oligonucleotide containing one-half of PW17. **Figure 2.1** shows the comparison of two ThT reporter oligonucleotides; ThTSignal and PW17Ext DNA. ThTSignal has a G-score²⁹ of 21, while PW17 has a G-score of 41 and is a known G-Quadruplex³⁰⁻³². The PW17 sequence is underlined in **Figure 2.1A**. We attempted to truncate the ThTSignal oligonucleotide sequence but found that the full ThTSignal sequence of 27 nucleotides was necessary to generate the highest fluorescence (**Figure 2.1B**). Seven fragments of the whole ThTSignal were compared against the entire sequence. The full-length ThTSignal oligonucleotide was substantially brighter than even the existing aptamer selected against ThT²⁵ by more than a factor of 10 (**Figure 2.1B, Supplementary Figure 2.S1A-B**). It should be noted that this comparison was conducted in a high salt buffer appropriate for DNA circuits, not the buffer in which the aptamer was selected.

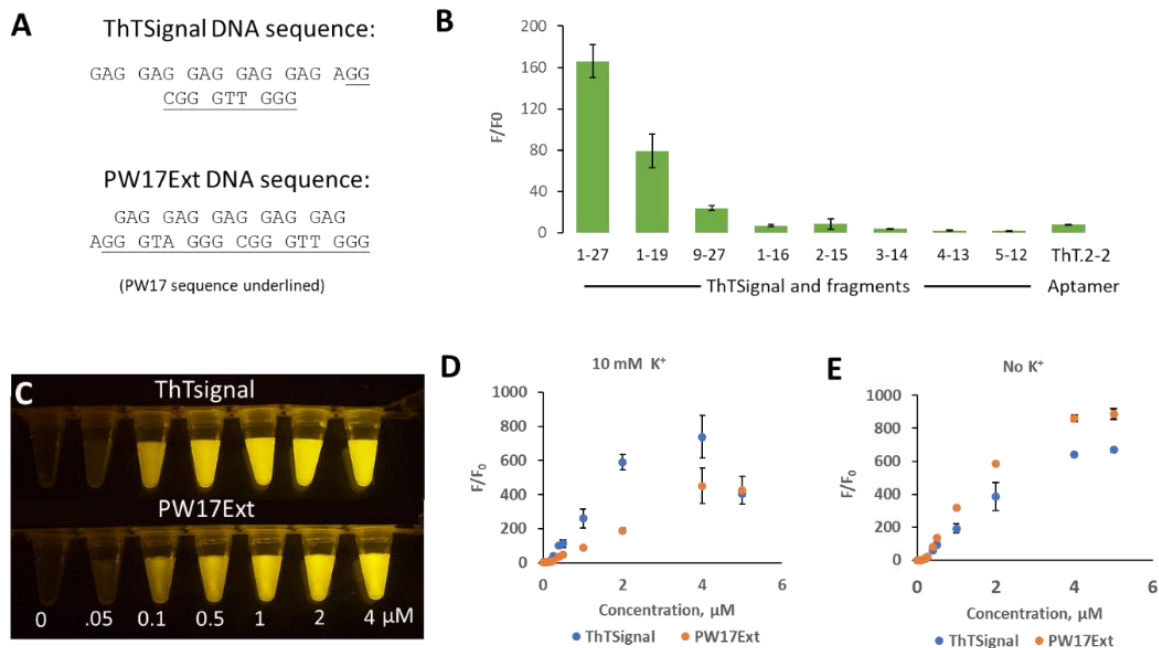


Figure 2.1. ThT fluorescence-activated by DNA. (A) ThTSignal and PW17Ext sequences with highlighted guanosine triplets. (B) Fluorescence enhancement comparison between ThTSignal and shortened versions of ThTSignal (names indicate the selected bases from the full sequence), and Aptamer ThT.2-2 (C) Fluorescence emission of 5 μ M ThT upon excitation with a blue transilluminator in the presence of the indicated concentrations of PW17Ext or ThTSignal DNA. (D) Fluorescence measurement of PW17Ext and ThTSignal upon excitation with a wavelength of 440 nm as a function of DNA concentration in the presence of 10 mM KCl. (E) Fluorescence measurement of PW17Ext and ThTSignal in the absence of potassium (The fluorescence is given as a fluorescence enhancement relative to ThT alone. Error bars represent the standard deviation of triplicate measurements).

2.3.2 Spectroscopic and PAGE analysis of ThT reporter oligonucleotides

We studied the interaction of PW17Ext and ThTSignal oligonucleotides with ThT to determine appropriate conditions for use as a reporter of DNA circuit activity. ThTSignal has several desirable features, including intense fluorescence in the presence of ThT, consistent brightness in the presence/absence of potassium ions, and an easily denatured structure. Our ThTSignal molecule was derived from PW17 and may share some structural features with PW17Ext.

ThTSignal is similarly bright compared to PW17Ext. We explored the possibility that buffers containing potassium could affect the performance of the reporter. Buffers containing sodium and potassium cations are important for DNA circuit function. We compared the fluorescence

generated by both guanosine-rich oligonucleotides at equivalent concentrations (see **Figure 2.1C**).

ThTSignal has more consistent fluorescence than PW17Ext in the presence (**Figure 2.1D**) and absence (**Figure 2.1E**) of potassium ions. Both ThTSignal and PW17Ext show higher fluorescence in the absence of potassium. The dependence on potassium is much larger for PW17Ext. Without potassium, PW17Ext showed a slightly higher fluorescence intensity than ThTSignal at high DNA concentrations ($>1\mu\text{M}$) and similar fluorescence at lower concentrations ($<1\mu\text{M}$). We hypothesized that the higher fluorescence of PW17Ext might be due to tighter binding of ThT to PW17Ext. We performed binding assays of ThT with the two oligonucleotides in the absence of potassium. We found that the dissociation constant for ThTSignal was $800\text{ nM} \pm 300\text{ nM}$, and the dissociation constant for PW17Ext was $300\text{ nM} \pm 200\text{ nM}$ (see **Supplementary Figure 2.S2**). Both ThTSignal and PW17Ext have a similar percentage of bound dye at high ThT concentration and low DNA concentration.

ThTSignal structure melts at lower temperatures and thus forms a less stable structure than PW17Ext (a critical feature for our applications). We confirmed that ThTSignal was a weaker structure than PW17Ext by thermophotometry and UV/Vis melt experiments. In the absence of potassium, ThTSignal loses fluorescence at a lower temperature ($41\text{ }^\circ\text{C}$) compared with PW17Ext ($57\text{ }^\circ\text{C}$), as shown in **Supplementary Figure 2.S3A-B**. The addition of potassium increases the temperature at which ThTSignal loses fluorescence, but the melt transition is broad with several local maxima. (**Figure 2.S3C**). Potassium strongly affects the concentration at which PW17Ext loses fluorescence, producing a complex system with a peak at $70\text{ }^\circ\text{C}$ (**Figure 2.S3D**). Some DNA structures are stabilized in the presence of potassium²⁴, and PW17Ext may adopt an alternate structure in the presence of potassium that does not strongly enhance the fluorescence of ThT. This reflects the large and negative change in total fluorescence for PW17Ext in response to the addition of potassium.

We also performed UV melt curves following protocols from the literature²⁵. The results are shown in **Supplementary Figure 2.S4**. ThTSignal showed a lower melt transition than

PW17Ext. Without potassium, ThTSignal showed a melt transition at $\sim 40^{\circ}\text{C}$, which is consistent with a weak structure (also consistent with the loss of fluorescence at $\sim 41^{\circ}\text{C}$). PW17Ext without potassium showed a melt transition at $\sim 51^{\circ}\text{C}$, indicating a stronger structure. With potassium, ThTsignal did not show a melt transition under UV. PW17Ext showed an increased melt temperature of 65°C , indicating that its structure in the presence of potassium is more stable.

ThTSignal shows peaks in circular dichroism (CD) similar to PW17Ext (see **Figure 2.2A**), suggesting some structural similarity. However, the signal from ThTSignal is less intense than the PW17Ext. We suspect it may arise from intermolecular interactions. At the recommended concentrations of oligonucleotides for the CD experiments ($10\ \mu\text{M}$), the formation of intermolecular structures may be favored. Using PAGE analysis (see **Figure 2.2B-D**), we confirmed that multiple stable species form at high concentrations. These may be multimers or folded monomolecular species. We feel multimers are more likely as the ratio of the concentrations of two monomolecular folded states should not be affected by the concentration. The ratio does seem to change as a function of concentration: the ratio of high mobility to low mobility band fluorescence intensity ranged from 1 to 5 in the ThTSignal case and from 2 to 5 in the PW17Ext case (as measured with ImageJ; see **Supplementary Figure 2.S5**). Slower migrating bands appeared when ThTSignal was $2\ \mu\text{M}$ or higher (see **Figure 2.2B**). Slower migrating bands formed at a concentration as low as $0.5\ \mu\text{M}$ for PW17Ext (see **Figure 2C**). We confirmed that these larger structures were denaturable. Denaturing PAGE analysis with $7\ \text{M}$ urea eliminated the slower migrating bands at all concentrations (see **Figure 2.2D**). ThT binding to ThTSignal is used as a reporter at low concentrations of oligonucleotide ($100\text{-}1000\ \text{nM}$), where the slower migrating bands are not observed for ThTSignal.

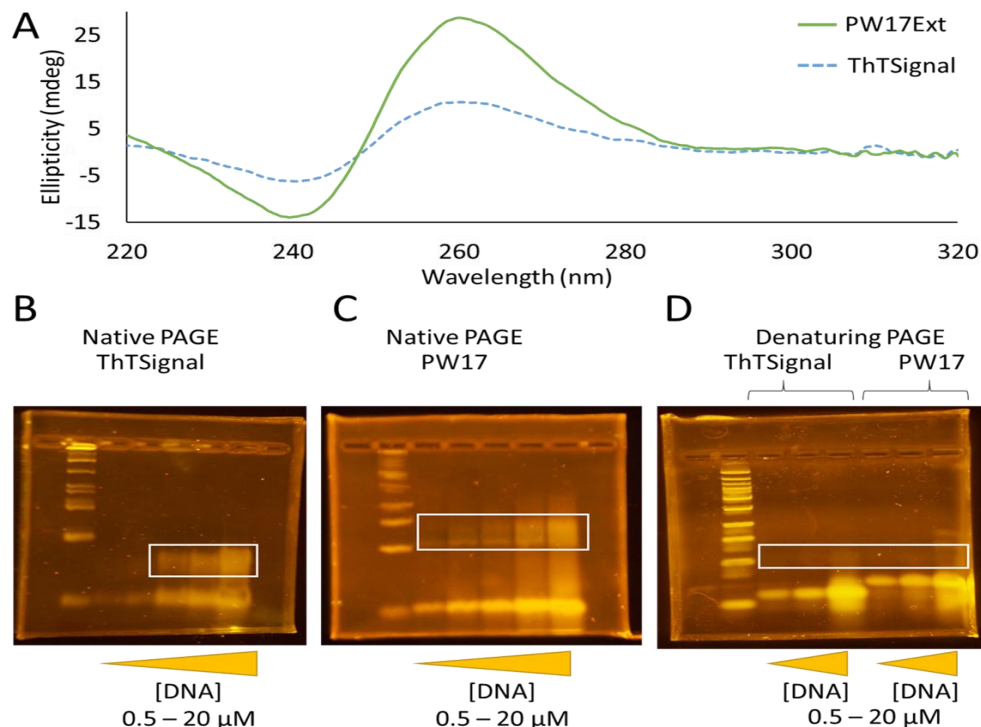


Figure 2.2. Structural analysis of ThTSIGNAL and PW17Ext using Circular dichroism (CD) and PAGE. (A) Background subtracted CD spectra from 220 nm-300 nm for both ThTSIGNAL (dashed) and PW17Ext (solid). (B) Native PAGE analysis (no urea, 10% w/w polyacrylamide) of ThTSIGNAL. The white box indicates slow migrating bands. (C) Native PAGE analysis (no urea, 10% w/w polyacrylamide) of PW17Ext. The white box indicates slow migrating bands. (D) Denaturing PAGE analysis (7M urea, 10% w/w polyacrylamide) of both ThTSIGNAL and PW17Ext. The white box indicates the region where we do not see significant slow migrating species.

Although assigning a precise structure is beyond the scope of this work, all lines of evidence (UV melt, fluorescence melt, and CD spectra) suggest the ThTSIGNAL is structured at low temperatures in the absence of potassium, binds ThT, and is easily denatured. The lower stability of the ThTSIGNAL structure relative to PW17Ext is an advantage: we must be able to easily and selectively denature the interaction between ThTSIGNAL and ThT. ThTSIGNAL is also shorter than PW17Ext. We used ThTSIGNAL without potassium for the remainder of this work.

2.3.3 A simple DNA-DNA reaction show fluorogenic activity with ThT

We used our novel ThTSIGNAL oligonucleotide to monitor different label-free DNA circuit reactions. We designed a simple DNA-DNA reaction that activated ThT fluorescence at first. **Figure 2.3A** shows the abstraction of ThTSIGNAL oligonucleotides which is necessary for clearly represent DNA-DNA reaction system. Conventionally, the 5' of any DNA is indicated by the left

end of the sequence and 3' by the right end. The sequence of the whole strand is further simplified by dividing them into several arbitrary domain which are indicated numerically. For instance, the ThTSignal contains 1-2-3 arbitrary domain (from left to right). **Figure 2.23B** shows the schematic of a simple A one-step strand displacement (OSD) reaction. The reaction includes a duplex DNA (Spine/Signal) and a displacer DNA named as Fuel. Strand displacement reactions have been used previously to generate reporter complexes^{26,27}.

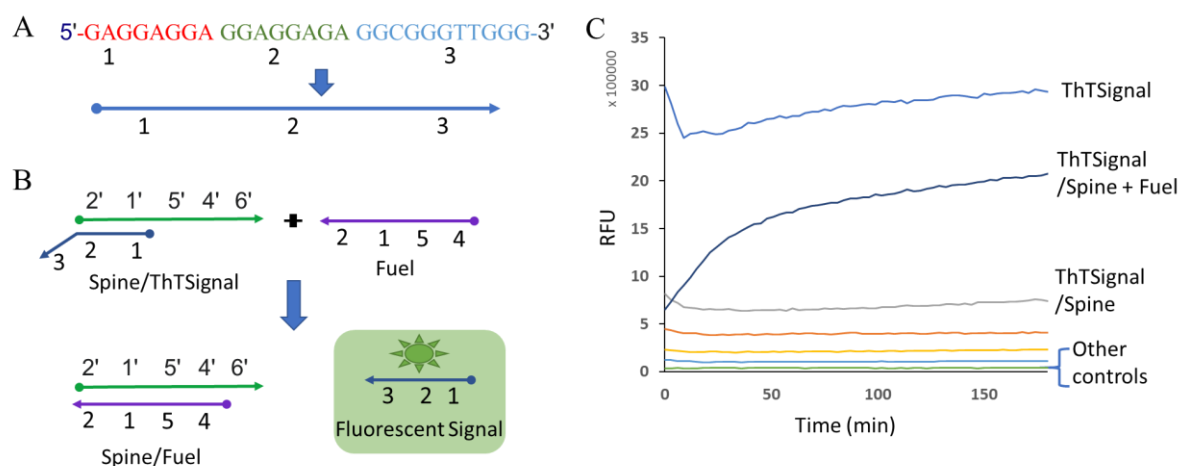


Figure 2.3. A simple reaction shows fluorogenic activity (RFU) as a function of time with ThT. (A) Base abstraction of ThTSignal. (B) Schematic of one-step strand displacement reaction. (C) Label-free fluorescence measurement of a one-step strand displacement reaction. Overlapping “other controls” include Spine, Fuel, Fuel/Spine, ThT. Oligos were at 0.5 μM in the presence of 5 μM of ThT.

We made the duplex DNA of Spine/Signal from individual strands of Spine and ThTSignal. A stoichiometric quantity of Spine and ThTSignal were added to a solution, the solution was heated in a thermocycler to 80 °C for three minutes followed by slow cooling at 0.1 °C per second to room temperature. The Fuel strand is designed in such a way that can form more stable duplex with Spine strand by displacing the ThTSignal from the Spine/Signal duplex. The displaced ThTSignal oligonucleotide, which then interacted with ThT. This basic reaction can be used as the final detection step in the design of other, more complex DNA circuits. **Figure 2.3C** shows the results of this simple reaction. Each individual strand (noted as other controls) and the Spine/Signal duplex cannot generate measurable fluorescence with ThT. Only in the presence of Fuel strand the fluorescence is increased. We show the average of triplicate experiments. The strand displacement reaction produced 1.8 times the fluorescence of the

sum of the reactants within 3 hours.

The presence of ThT does not affect the rate of strand displacement reactions. We determined this by running a strand displacement reaction in the presence of ThT and compared to a control in which ThT was added at the endpoint of multiple experimental samples at a range of times (see **Figure 2.4A**). We found no significant difference in the reaction rate.

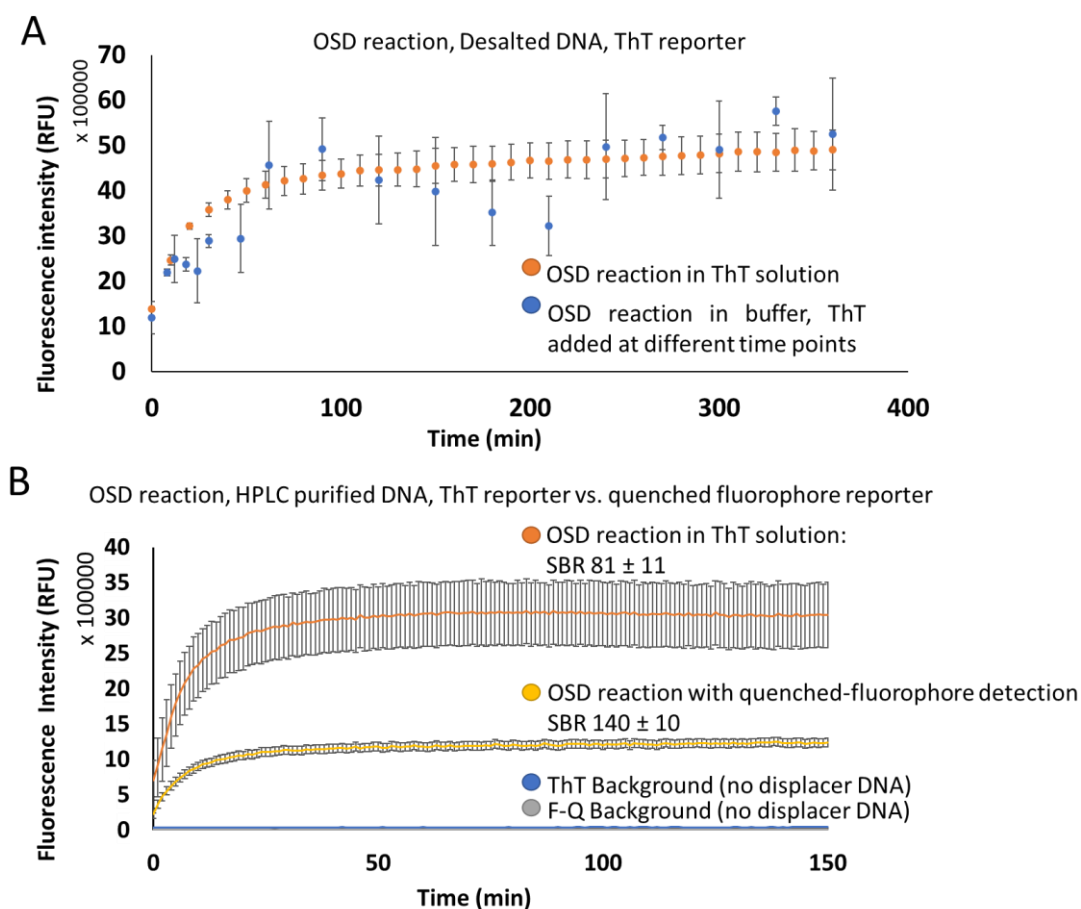


Figure 2.4. ThT effect on reaction kinetics. (A) Effect of ThT dye on the rate of the One-step Strand Displacement (OSD) reaction. Graph shows fluorescence as a function of time in two conditions: (orange) where ThT is present in the reaction and (blue) where ThT was added at the specified reaction time. (B) Effect of ThT dye on the rate of the OSD reaction. Graph shows fluorescence as a function of time in two conditions: (orange) where ThT is present in the reaction and (yellow) where a quenched fluorophore was used instead. Blue and gray are negative controls as labeled. Error bars are the standard deviation of triplicate reactions.

The kinetics of the OSD reaction with the ThT reporter are similar to the quenched fluorophore reporter system (see **Figure 2.4B**, both using HPLC-purified DNA for a fair comparison). The

signal to background ratio (SBR) in the ThT reporter system ($SBR\ 81 \pm 11$) is not as high as a traditional quenched fluorophore reporter system ($SBR\ 140 \pm 10$). However, the ThT reporter system has the advantage of being less expensive and less vulnerable to background caused by the degradation of the fluorophore or quencher strand.

The OSD reaction was not as fast as some published reactions, and we attribute this fact to the G-rich sequences and to the impure, desalted DNA used for this experiment. The result when we used HPLC purified DNA was still slower than some published OSD reactions. G-rich sequences are prone to assume transient intermediate structures, which may account for the sluggish reaction rate. The desalted OSD reaction presented in **Figure 2.4A** has an approximate reaction time of ~15 minutes to half-max at 25 °C. The desalted OSD reaction time in Figure 4C is ~20 minutes at 25 °C. Both use desalted DNA and both are relatively quick single-stage reactions. Using HPLC-purified DNA at 25 °C reduces reaction time to 6 minutes with either ThT or conventional quenched fluorophore detection (**Figure 2.4B**), increasing the apparent reaction rate by a factor of 3-5. The advantage of the ThT system is that it does not require purification or chemical modification. With application-specific optimization, one or more of the three strategies above may be advantageous for testing DNA circuit designs. The encouraging performance of the simple OSD reaction motivates us to build a more controlled, complex catalytic DNA circuit, the entropy-driven amplifier (EDA).

2.3.4 Entropy Driven Amplifier with ThT readout

We demonstrate the ThT reporter technique for the label-free detection of a complex, multi-step DNA circuit. **Figure 2.5A** illustrates the mechanism of the entropy-driven amplifier (EDA) circuit with ThT detection. The EDA contains two strand displacement reactions. A complex of three oligonucleotides sequestered the ThTSignal oligonucleotide in a dsDNA complex (denoted "Spine-ThTSignal-Block"). An oligonucleotide, "Block," prevented further activity until the addition of an oligonucleotide denoted "Catalyst." The first strand displacement occurred when Catalyst displaced Block. In the second strand displacement reaction, an oligonucleotide denoted "Fuel" displaced both ThTSignal and Catalyst. The

displaced ThTSignal light up ThT by enhancing its native fluorescence. The oligonucleotide Catalyst was regenerated so that it could bind to another Spine-ThTSignal-Block complex and repeat the reaction and continue its catalytic activity. With the customizable design of the components, the EDA circuit could be redesigned to perform with any target sequence of DNA or RNA (i.e., the Catalyst sequence is entirely separate from the ThTSignal sequence). In future we wish to explore of this design to detect disease related miRNA sequences. The EDA with ThT reporter is an example of label-free, low-cost, DNA circuit-based detection for nucleic acid analytes.

Using polyacrylamide gel electrophoresis (PAGE) with HPLC purified oligonucleotides, we analyzed the EDA product with the ThT reporter. **Figure 2.5B** shows the PAGE results (false-color image). The PAGE image was taken after double staining procedure. Firstly, GelRed, a non-specific intercalating dye was used to stain the gel. Then ThT dye was used to stain the gel again. As a result, two different colors blue and yellow generated. The fluorescence after staining with GelRed generates blue color while fluorescence after staining the same gel with ThT generates yellow color. This distinct yellow color band indicates that ThT dye can potentially be used to gel staining purpose for specific ssDNA. Most commercial dye such as GelRed only can stain dsDNA non-specifically and cannot stain ssDNA. Most single-stranded component controls in lanes 1-4 did not stain with either dye. These lanes are omitted for clarity. Component images of the full gel with all lanes are included in **Supplementary Information** (see **Supplementary Figure 2.S6**).

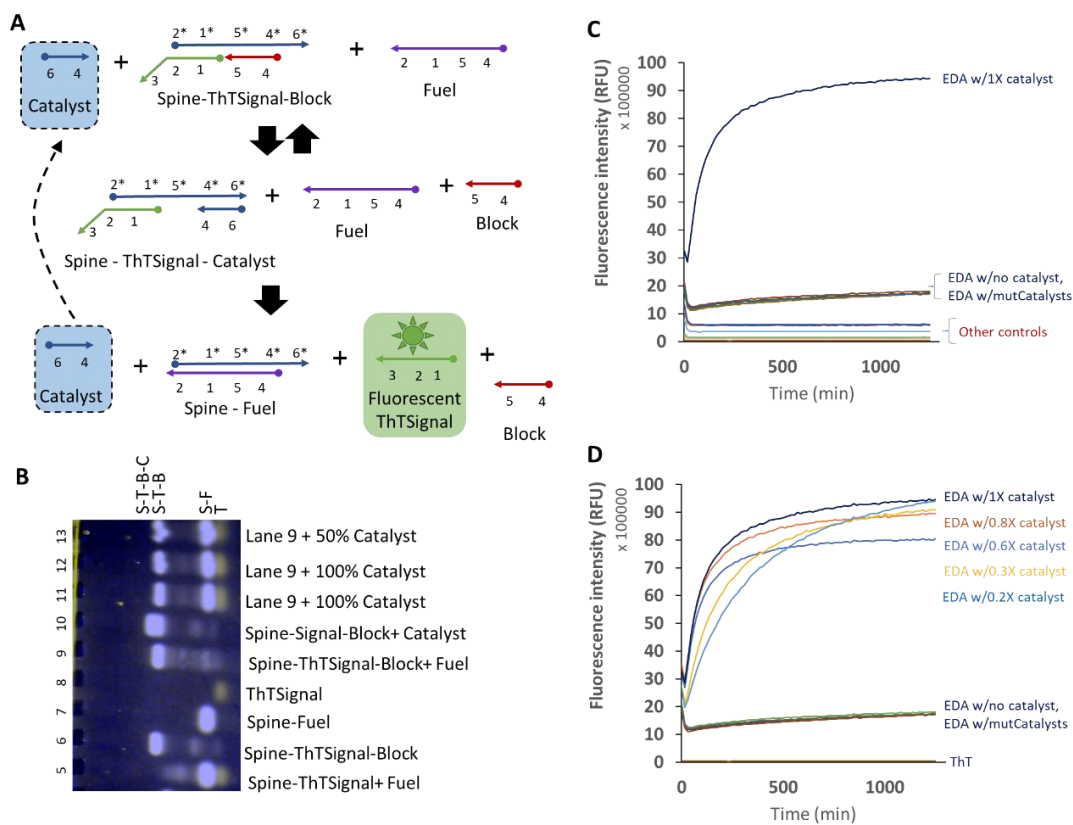


Figure 2.5. Entropy Driven Amplifier with ThT reporting system. (A) Schematic of the entropy-driven amplifier system. (B) PAGE analysis of the EDA system. (C) Fluorescence readout of EDA reaction. Overlapping “other controls” include Spine-ThTSIGNAL-Block, Spine-ThTSIGNAL-Block + Catalyst, Fuel, Catalyst, Spine, mutCatalyst 1, mutCatalyst 2, mutCatalyst 3, Block, and ThT. (D) Comparison of EDA with various concentrations of Catalyst as labeled.

In the presence of Fuel and Catalyst, ThTSIGNAL oligonucleotide appears as a new band, which clearly indicated that the EDA reaction happens. The reaction proceeded in all cases for 10 hours (based on the time course data over 20 hours, we determined that acceptable reaction progress occurs within 10 hours) at 30 °C. The electrophoresis was performed at 4 °C for 22 hours with running buffer containing 10 mM magnesium sulfate. This was necessary to maintain the DNA in the designed multi-strand complexes and active, folded conformations. Higher voltages (and shorter migration times) reduced diffusional band-broadening but caused the complexes to dissociate due to Joule heating. Fluorescence was measured as a function of time at 30 °C **Figure 2.5C**). We collected fluorescence intensity at the appropriate wavelengths for ThT over 20 hours. Only with the presence of Catalyst, the EDA is able to

generate ThTSignal. This reporter product then binds to ThT to light it up. In **Figure 2.5C**, only 1 μM Catalyst is shown. We also performed the reaction with 800, 600, 300, and 200 nM, as shown in **Figure 2.5D**. It is found that only sub-stoichiometric quantity of Catalyst is enough to produce a complete reaction. The result shows the catalytic activity of the system.

The data in **Figure 2.5C-D** were obtained using HPLC purified oligonucleotides for increased reaction performance. We also compare the performance of this label-free cost-effective EDA with modified and high-cost EDA system. The rates of the EDA reactions with the ThTSignal reporter and the fluorophore-quencher reporter were similar (see **Supplementary Figure 2.57**) Label-free is less expensive than the equivalent fluorophore quencher system. Including modified oligonucleotides increases the cost by a factor of 6 or more (depending on the desired fluorophore, discounts, vendor pricing, etc.).

2.4 Conclusion

Modified nucleic acids with different fluorophores are expensive, and any degradation of the oligonucleotides produces undesired background. To address the detection problem for DNA circuits, we demonstrated the ThT reporter technique, which can be used for label-free, enzyme-free DNA circuits. Other labs have shown that DNA with guanine-rich secondary structures can be conveniently detected with ThT²⁹. ThT binds diverse DNA (many but not all sequences, including folded structures and mismatched duplexes). In addition to PW17 and our ThTSignal reporter, other DNA sequences also activate ThT fluorescence. This includes aptamer²⁵ and several G-quadruplexes^{22,23} as well as other bulged and mismatched structures^{33,34}. Contemporary work has also approached biosensing with ThT and light-up probes³⁵. Collectively, these results suggest that many sequences are applicable. Such sequences might be similarly adapted for this or other DNA-based detection schemes. However, the choice of the reporter system is challenging, and experimental optimization is necessary.

Here we show that complex DNA circuit reactions like the EDA (which is built on coupled OSD reactions) can be detected. Our technique uses a guanosine-rich specific oligonucleotide

reporter sequence, which may slow the EDA circuit. Other target ssDNA in the system can be detected which need to be screened for interaction with ThT to reduce sources of background.

Several conclusions from our study are useful for such a project: guanosine-rich sequences, in general, can activate ThT; sequestering such sequences in dsDNA complexes in the design helps to keep background low. The mechanism by which a DNA circuit lights up the reporter must be chosen with care; the structure of the reporter DNA must not be so strong that it competes with double-stranded (inactive) structures.

We work from simple interactions that activate the reporter to complex multi-step circuits. This chapter is a proof of concept in adapting a readily available light-up dye and cognate DNA probe to several potential DNA circuits. While the sequences of DNA probes to recognize other dyes will differ, the overall strategy for developing a reporter should be similar. Researchers should compare multiple options for denaturing and re-naturing the active DNA sequence. The array of output reactions makes the ThT reporter compatible with many possible DNA circuits or other DNA reactions. We hope to explore the production of ThT reporters by other means in future work. For example, ThTSignal could also be generated by enzymatic means (e.g., by strand displacement amplification³⁶, rolling circle amplification³⁷) or other non-enzymatic amplification processes such as the hairpin chain reaction³⁸. These reactions should also be amenable to detection with ThT and our reporter oligonucleotide. An advanced version of the ThT reporter technique would allow for improved performance at lower concentrations of ThT. We hope to perform *in vitro* selection of an aptamer against ThT dye with a higher fluorescence and stronger binding properties. An optimized aptamer for ThT would be a fascinating candidate for further structure-function studies.

The use of ThT to detect DNA circuit activity is less expensive than quenched fluorophore detection. It is more specific than intercalating dyes. However, it is not as specific as molecular beacons or TaqMan probes. This is a prototype of the work-up for integrating any novel light-up DNA sequence as a reporter for different non-enzymatic DNA circuits. This technique may also find use in educational settings. The low cost per design means that new researchers and

undergraduates can try DNA circuit designs with lower risk. We hope that this work reduces the barriers to entry for researchers to experiment with DNA circuits.

Table 2.1. Sequences of all DNA

Name	Sequences
PW17Ext <i>G-score: 41</i>	GAGGAGGAGGAGGAGAGGGTAGGGCGGGTTGGG <i>Underlined sequence is PW17</i>
Spine	TCTCCTCC TCCTCCTC TTTTC TGAATAAGAAGAAGAA TCTCCA
Block	TTCTTCTTCTTATTCA GAAAA
ThTSignal <i>G-score: 21</i>	GAGGAGGA GGAGGAGA GGCGGGTTGGG
Catalyst	TGGAGA TTCTTCTTCTTATTCA
Fuel	TTCTTCTTCTTATTCA GAAAA GAGGAGGA GGAGGAGA
ThTSignal 1-27	GAGGAGGA GGAGGAGA GGCGGGTTGGG
ThTSignal 9-27	GGAGGAGA GGCGGGTTGGG
ThTSignal 1-19	GAGGAGGA GGAGGAGA GGC
ThTSignal 1-16	GAGGAGGA GGAGGAGA
ThTSignal 2-15	AGGAGGA GGAGGAG
ThTSignal 3-14	GGAGGA GGAGGA
ThTSignal 4-13	GAGGA GGAGG
ThTSignal 5-12	AGGA GGAG
FluoroSignal (Fluorophore ThTSignal)	GAGGAGGA GGAGGAGA - 3' Fluorescein
Qspine (Quencher Spine)	Iowa Black 5' - TCTCCTCC TCCTCCTC TTTTC TGAATAAGAAGAAGAA TCTCCA
mutCatalyst 1	TTGAGA CCAATGAATCCATAAC
mutCatalyst 2	ATCTTC TTCTTCTTCTTATTCA
mutCatalyst 3	ATCTTC CCAATGAATCCATAAC

2.5 Supplementary Information

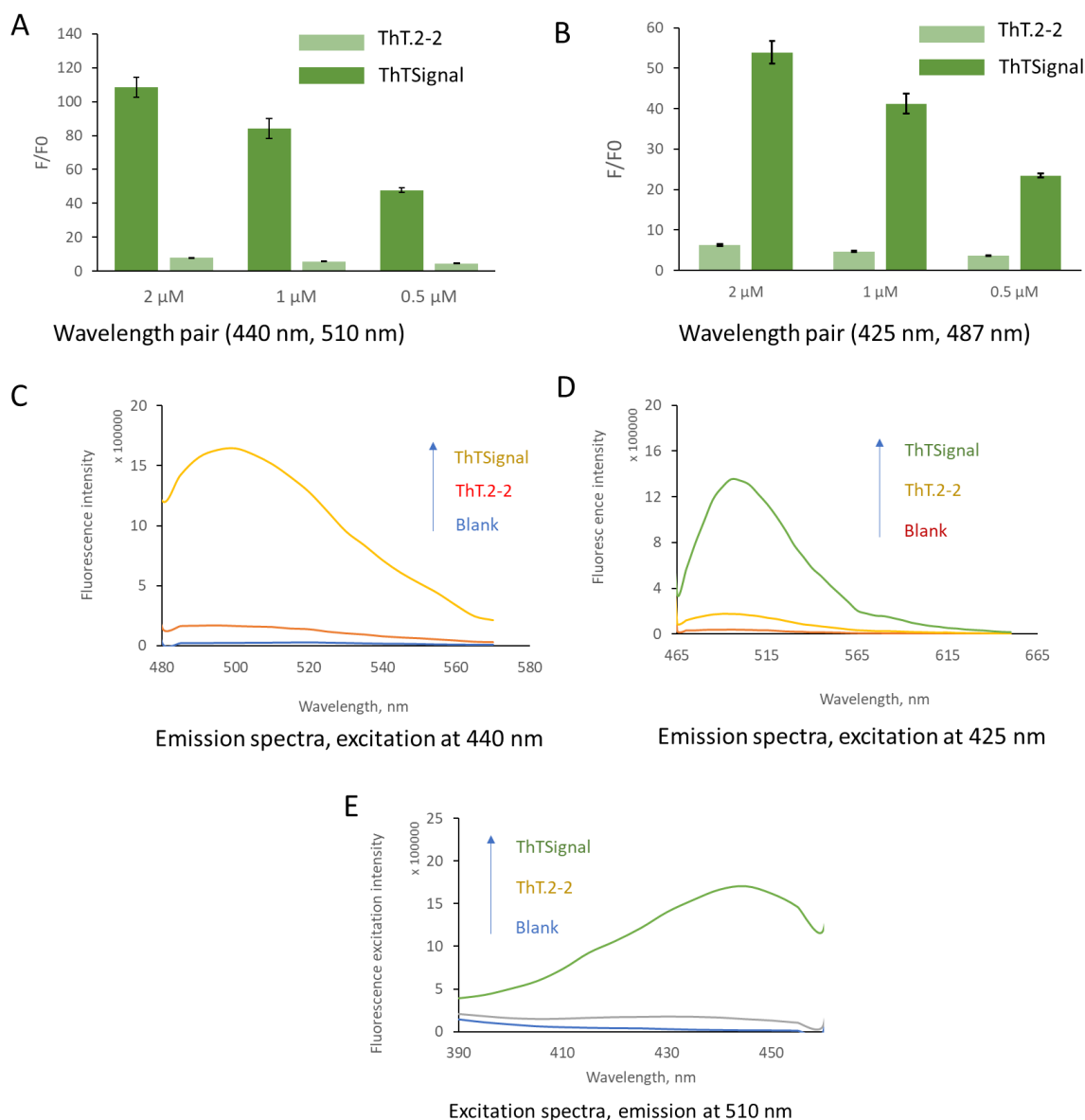


Figure 2.S1. Fluorescence comparison of ThTSignal (this work) and ThT.2-2 (Pei et al., *Anal. Methods*, 2016, 8, 8461) at several concentrations. (A) Fluorescence enhancement of ThT (F/F_0 where F_0 is ThT only) at our chosen wavelengths by ThTSignal and ThT.2-2. (B) Fluorescence enhancement of ThT at the wavelengths chosen by Pei et al. (C) Fluorescence emission spectrum of ThT with ThTSignal, ThT.2-2, and alone with excitation at 440 nm. (D) Fluorescence emission spectrum of ThT with ThTSignal, ThT.2-2, and alone with excitation at 425 nm. (E) Excitation spectrum of ThT with ThTSignal, ThT.2-2, and alone with emission [detection] at 510 nm.

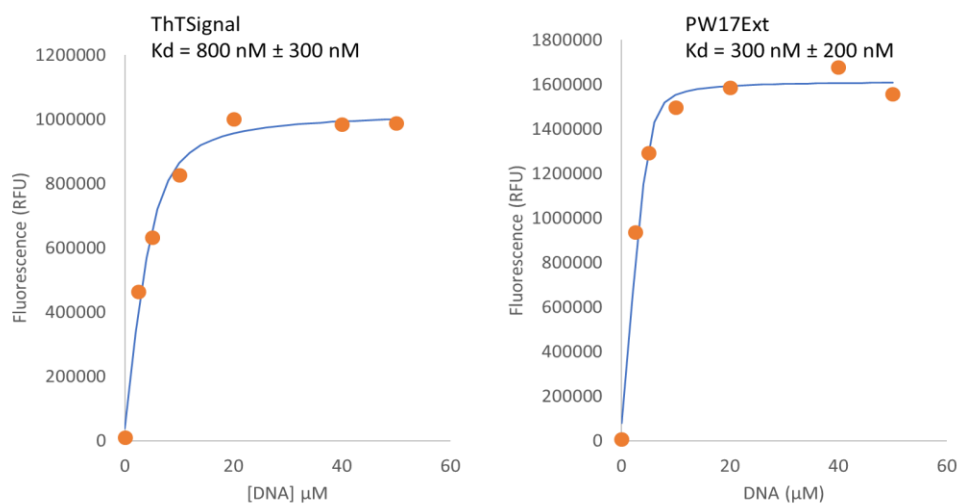


Figure 2.S2. Binding studies of ThTSignal and PW17Ext via TFA using Open Spectramax iD3 platereader. Graphs show Fluorescence (RFU) as a function of (A) ThTSignal concentration, (B) PW17Ext concentration. The blue line is the best fit binding isotherm used to determine dissociation constant (K_d) between (A)ThTSignal and ThT, (B) PW17Ext and ThT

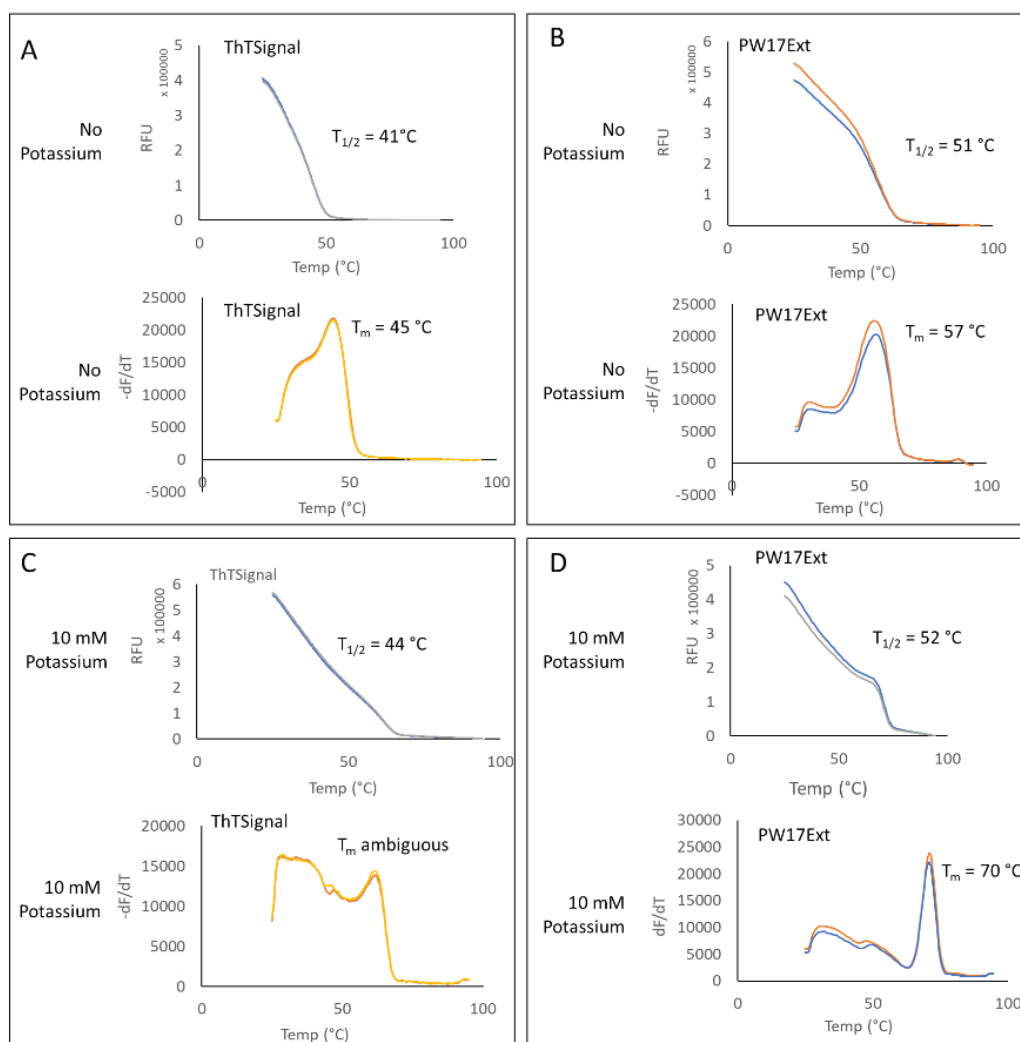


Figure 2.S3. Melt curve analysis of ThT interaction with oligonucleotides. Top graphs show the fluorescence as a function of temperature. Bottom graphs show the first derivative of fluorescence as a function of temperature. (A) Graphs show triplicate melt curves of TTTsignal in the absence of potassium. (B) Graphs show triplicate melt curves of PW17Ext in the absence of potassium. (C) Graphs show triplicate melt curves of TTTsignal in the presence of potassium and (D) Graphs show triplicate melt curves of PW17Ext in the presence of potassium. In each case, an inset show the temperature at which the fluorescence reached half its maximal value ($T_{1/2}$).

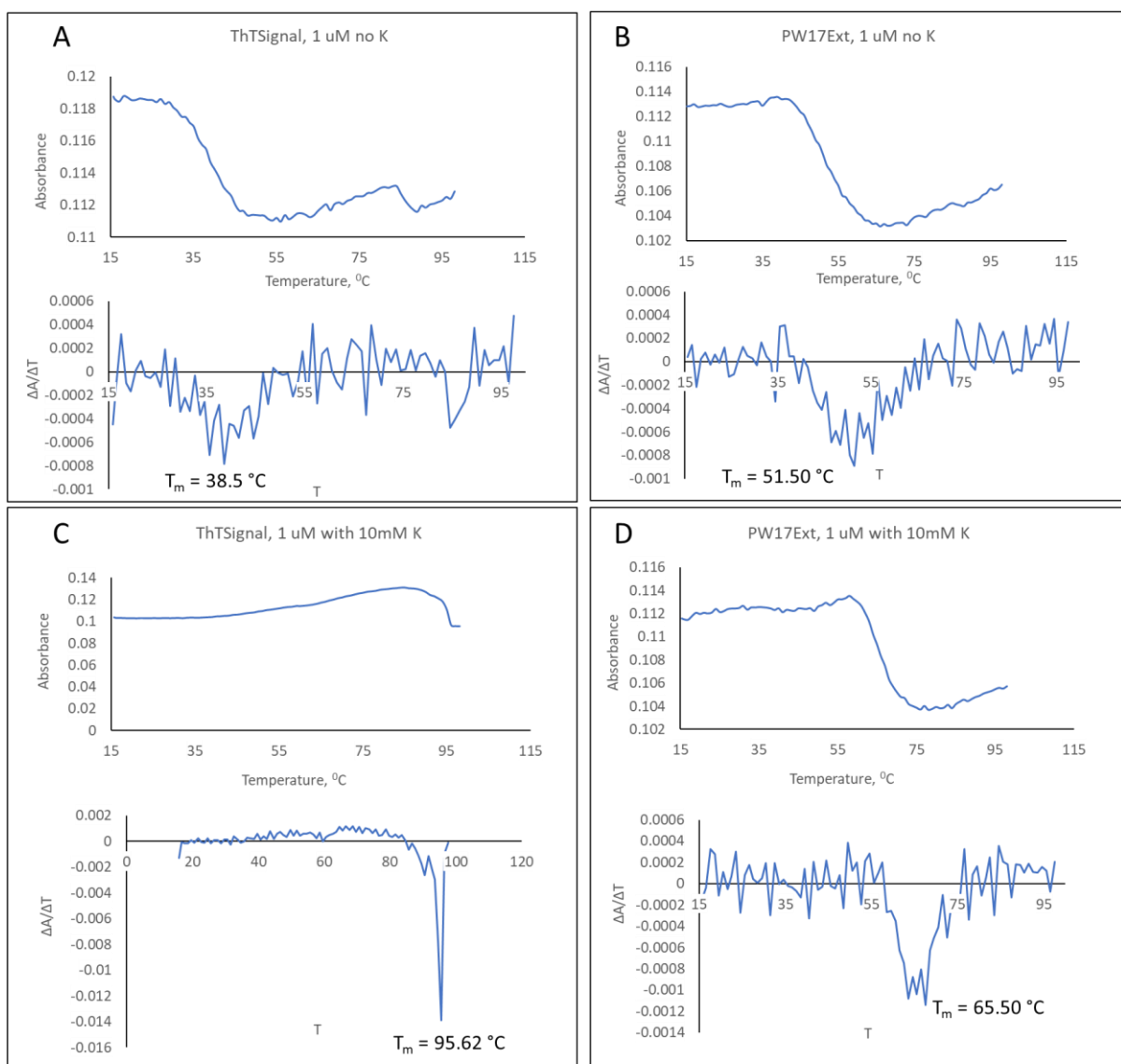


Figure 2.S4. Melt curve analysis of oligonucleotides structure with UV absorbance at 295 nm. Graphs show the absorbance as a function of temperature. (A) Graph shows melt curve of ThTsignal in the absence of potassium. (B) Graph shows melt curve of PW17Ext in the absence of potassium. (C) Graph shows melt curve of ThTsignal in the presence of potassium and (D) Graph shows melt curve of PW17Ext in the presence of potassium.

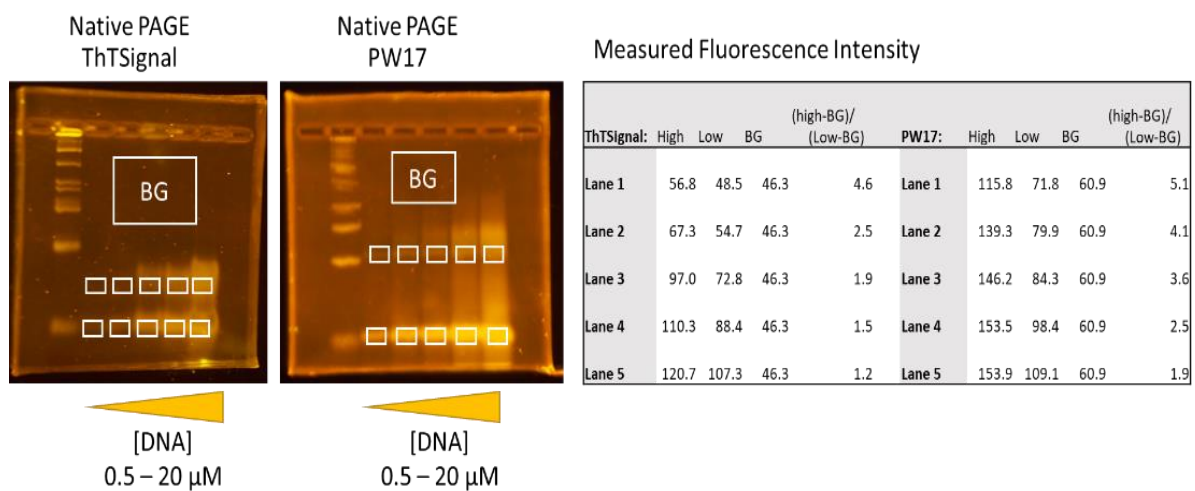


Figure 2.S5. Illustration of ImageJ analysis of ThTSignal and PW17Ext gels. Low mobility band intensity is not proportional to DNA concentration.

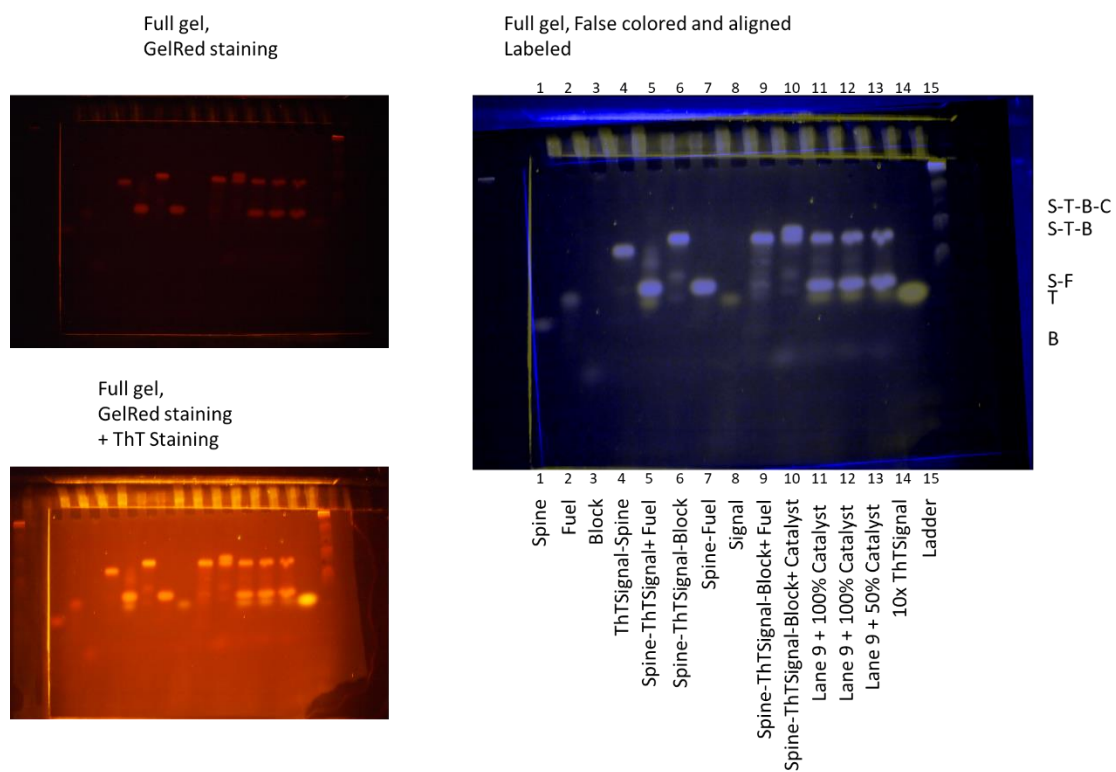
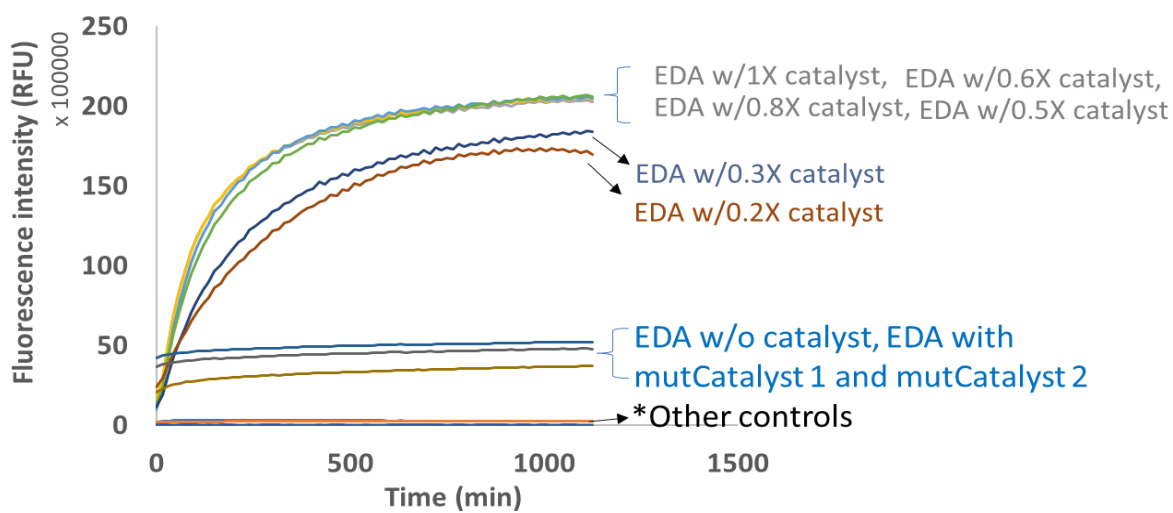


Figure 2.S6. Composite image and source image for non-denaturing PAGE analysis of the EDA circuit (Figure 4B). In the false color image (left), blue indicates the fluorescence after staining with a nonspecific intercalating dye (GelRed). Yellow color indicates fluorescence after staining the same gel with ThT. Fluorescence after staining with GelRed (center) is shown as a black-and-white fluorescence photograph. Fluorescence after staining with GelRed and ThT (right) is shown as a black-and-white fluorescence photograph.



*Other controls: FluoroSignal/Qspine/Block, FluoroSignal/Qspine/Block + Catalysts, Catalysts, Block, Spine, Fuel, Buffer, mutCatalysts1, mutCatalyst2

Figure 2.S7. Effect of reporter mechanism on DNA circuit kinetics. Reaction is equivalent to the reaction shown in Figure 5C-D, but with a fluorophore-quencher rather than ThT based detection. The reaction is very similar in kinetics.

2.6 AUTHOR INFORMATION

2.6.1 Corresponding Author

*Peter B. Allen. Email: pballen@uidaho.edu.

2.6.2 Author Contributions

P.B.A., and M.M.I conceptualized experiments. P.B.A, M.M.I, optimized, carried out experiments, and analyzed data. P.B.A, M.M.I, wrote the manuscript.

2.7 Notes

The authors declare no competing interests.

2.8 Acknowledgment

This publication was made possible by an Institutional Development Award (IDeA) from the National Institute of General Medical Sciences of the National Institutes of Health under Grant #P20GM103408. Additional support was provided by the University of Idaho ORED SEED grant. We gratefully acknowledge the University of Washington Dept. of Chemistry for the use of the Circular Dichroism spectrophotometer. We also thank Patrick Hrdlicka for the use of spectroscopic instruments for UV melt experiments.

2.9 References

1. Gomez, E. F., Venkatraman, V., Grote, J. G. & Steckl, A. J. Exploring the potential of nucleic acid bases in organic light emitting diodes. *Adv. Mater.* **27**, 7552–7562 (2015).
2. Campolongo, M. J., Tan, S. J., Xu, J., & Luo, D. (2010). DNA nanomedicine: Engineering DNA as a polymer for therapeutic and diagnostic applications. *Advanced drug delivery reviews*, *62*(6), 606–616. <https://doi.org/10.1016/j.addr.2010.03.004>
3. Veneziano, R., Shepherd, T.R., Ratanalert, S. *et al.* *In vitro* synthesis of gene-length single-stranded DNA. *Sci Rep* **8**, 6548 (2018).
4. Minev, D. et al. Rapid *in vitro* production of single-stranded DNA. *Nucleic Acids Res.* **47**, 11956–11962 (2019).

5. Kishi, J., Schaus, T., Gopalkrishnan, N. *et al.* Programmable autonomous synthesis of single-stranded DNA. *Nature Chem* **10**, 155–164 (2018).
6. R. Otero , W. Xu , M. Lukas , R. E. A. Kelly , E. Lægsgaard , I. Stensgaard , J. Kjems , L. N. Kantorovich and F. Besenbacher , *Angew. Chem., Int. Ed.*, 2008, **47** , 9673
7. Chunxia Song, Xiaohai Yang, Kemin Wang, Qing Wang, Jin Huang, Jianbo Liu, Wei Liu, Pei Liu, Label-free and non-enzymatic detection of DNA based on hybridization chain reaction amplification and dsDNA-templated copper nanoparticles, *Analytica Chimica Acta*, Volume 827, 2014, Pages 74-79.
8. Yurke, B. & Mills, A. P. Using DNA to Power Nanostructures. *Genet Program Evolvable Mach* 4, 111– 122 (2003).
9. Zhu Jinbo, Zhang Libing, Li Tao, Dong Shaojun & Wang Erkang. Enzyme-Free Unlabeled DNA Logic Circuits Based on Toehold-Mediated Strand Displacement and Split G-Quadruplex Enhanced Fluorescence. *Advanced Materials* 25, 2440–2444 (2013).
10. Shahbazi, M.-A., Bauleth-Ramos, T. & Santos, H. A. DNA Hydrogel Assemblies: Bridging Synthesis Principles to Biomedical Applications. *Advanced Therapeutics* 1, 1800042 (2018).
11. Wang, D., Hu, Y., Liu, P. & Luo, D. Bioresponsive DNA Hydrogels: Beyond the Conventional Stimuli Responsiveness. *Acc. Chem. Res.* 50, 733–739 (2017).
12. Pregibon, D. C. & Doyle, P. S. Optimization of Encoded Hydrogel Particles for Nucleic Acid Quantification. *Anal Chem* 81, 4873–4881 (2009).
13. Wang, H., Li, C., Liu, X., Zhou, X. & Wang, F. Construction of an enzyme-free concatenated DNA circuit for signal amplification and intracellular imaging. *Chem. Sci.* 9, 5842–5849 (2018).
14. Wang, J., Wang, D.-X., Ma, J.-Y., Wang, Y.-X. & Kong, D.-M. Three-dimensional DNA nanostructures to improve the hyperbranched hybridization chain reaction. *Chem. Sci.* 10, 9758–9767 (2019)

15. Islam, M. M., Loewen, A. & Allen, P. B. Simple, low-cost fabrication of acrylic based droplet microfluidics and its use to generate DNA-coated particles. *Scientific Reports* 8, 8763 (2018).
16. Allen, P. B., Arshad, S. A., Li, B., Chen, X. & Ellington, A. D. DNA circuits as amplifiers for the detection of nucleic acids on a paperfluidic platform. *Lab Chip* 12, 2951–2958 (2012)
17. Li, B., Ellington, A. D. & Chen, X. Rational, modular adaptation of enzyme-free DNA circuits to multiple detection methods. *Nucleic Acids Res* 39, e110–e110 (2011).
18. Yin, P., Choi, H. M. T., Calvert, C. R. & Pierce, N. A. Programming biomolecular self-assembly pathways. *Nature* 451, 318–322 (2008)
19. Kurata, S. et al. Fluorescent quenching-based quantitative detection of specific DNA/RNA using a BODIPY® FL-labeled probe or primer. *Nucleic Acids Res* 29, e34 (2001)
20. Guo, Y.; Xu, L.; Hong, S.; Sun, Q.; Yao, W.; Pei, R. Label-free DNA-based biosensors using structure-selective light-up dyes. *Analyst* **2016**, *141*, 6481– 6489
21. Gade Malmos K, Blancas-Mejia LM, Weber B, Buchner J, Ramirez-Alvarado M, Naiki H, Otzen D. ThT 101: a primer on the use of thioflavin T to investigate amyloid formation. *Amyloid*. 2017 Mar;24(1):1-16
22. Mohanty, J. et al. Thioflavin T as an Efficient Inducer and Selective Fluorescent Sensor for the Human Telomeric G-Quadruplex DNA. *J. Am. Chem. Soc.* 135, 367–376 (2013)
23. Renaud de la Faverie, A., Guédin, A., Bedrat, A., Yatsunyk, L. A. & Mergny, J.-L. Thioflavin T as a fluorescence light-up probe for G4 formation. *Nucleic Acids Res* 42, e65–e65 (2014)
24. Gabelica, V. et al. Multiple and Cooperative Binding of Fluorescence Light-up Probe Thioflavin T with Human Telomere DNA G-Quadruplex. *Biochemistry* 52, 5620–5628 (2013).
25. Wang, H. et al. Selection and characterization of thioflavin T aptamers for the development of light up probes. *Anal. Methods* 8, 8461–8465 (2016)

26. Wang, H. et al. Selection and characterization of dimethylindole red DNA aptamers for the development of light-up fluorescent probes. *Talanta* 168, 217–221 (2017)
27. Gao, T., Luo, Y., Li, W., Cao, Y. & Pei, R. Progress in the isolation of aptamers to light-up the dyes and the applications. *Analyst* 145, 701–718 (2020)
28. Zhang, D. Y., Turberfield, A. J., Yurke, B. & Winfree, E. Engineering entropy-driven reactions and networks catalyzed by DNA. *Science* 318, 1121–1125 (2007)
29. Kikin, O., D'Antonio, L. & Bagga, P. S. QGRS Mapper: a web-based server for predicting G-quadruplexes in nucleotide sequences. *Nucleic Acids Res* 34, W676–W682 (2006).
30. Travascio, P., Bennet, A. J., Wang, D. Y. & Sen, D. A ribozyme and a catalytic DNA with peroxidase activity: active sites versus cofactor-binding sites. *Chemistry & Biology* 6, 779–787 (1999)
31. Nandhini Saranathan and Perumal Vivekanandan. G-Quadruplexes: More Than Just a Kink in Microbial Genomes. *Trends in Microbiology*, February 2019, Vol. 27, No. 2.
32. Jochen Spiegel, Santosh Adhikari, and Shankar Balasubramanian. The Structure and Function of DNA G-Quadruplexes. *Trends in Chemistry*, February 2020, Vol. 2, No. 2
33. Zhu, J. et al. Lighting Up the Thioflavin T by Parallel-Stranded TG(GA)_n DNA Homoduplexes. *ACS Sens.* 3, 1118–1125 (2018).
34. Liu, L., Shao, Y., Peng, J., Liu, H. & Zhang, L. Selective recognition of ds-DNA cavities by a molecular rotor: switched fluorescence of thioflavin T. *Mol. BioSyst.* 9, 2512–2519 (2013).
35. Liu, Q., Jing, S., Liu, M., Jin, Y. & Li, B. Parallel [TG(GA)₃]_n-homoduplexes/thioflavin T: an intense and stable fluorescent indicator for label-free biosensing. *Analyst* 145, 286–294 (2020)
36. Walker, G. T. et al. Strand displacement amplification--an isothermal, in vitro DNA amplification technique. *Nucleic Acids Res.* 20, 1691–1696 (1992)
37. Ali, M. M. et al. Rolling circle amplification: a versatile tool for chemical biology, materials science and medicine. *Chem Soc Rev* 43, 3324–3341 (2014)

38. Dirks, R. M. & Pierce, N. A. Triggered amplification by hybridization chain reaction. Proc. Natl. Acad. Sci. U.S.A. 101, 15275–15278 (2004)

CHAPTER 3: Graphene oxide assisted light-up aptamer selection against Thioflavin T for label-free detection of microRNA

Md Mamunul Islam, Victoria Michele Ghielmetti, Peter B. Allen*

*pballen@uidaho.edu

University of Idaho, Dept. of Chemistry, 001 Renfrew Hall, 875 Perimeter Dr, Moscow, ID 83844-2343

Published in: Scientific Reports, Volume 11, Article number: 4291 (2021).

Published by: Nature

We selected an aptamer against a fluorogenic dye called Thioflavin T (ThT). Aptamers are single-stranded DNA that can bind a specific target. We selected our ThT aptamer using graphene oxide assisted SELEX and a low-cost Open qPCR instrument. We optimized, minimized, and characterized the best aptamer candidate against ThT. This aptamer, the dye, and the enzymatic strand displacement amplifier (SDA) were used in a label-free approach to detect the microRNA miR-215 in saliva and serum. The aptamer confers higher specificity than intercalating dyes but without expensive covalently modified DNA probes. This isothermal, low-cost, one-step, simple method can detect both DNA and RNA. The target, miR-215, was detected with a limit of detection of 2.6 nM.

3.1 Introduction

We developed an aptamer to report the activity of an isothermal, enzymatic amplification reaction called Strand Displacement Amplification (SDA). The aptamer binds a commercially available small molecule dye called Thioflavin T (ThT). ThT is known to be a light-up probe in the presence of many DNA structures including several G-quadruplexes (G4)^{1,2}, G-triplex³, bulged, and mismatched structures^{4,5}. Due to its easy availability, water solubility, and convenient excitation and emission wavelength, ThT has been used in many biosensing

applications (e.g., monitoring RNA metabolism⁶, RNA G-quadruplexes⁷, catalytic DNA amplifier⁸, and CRISPR/Cas9n system⁹).

We selected a new aptamer using graphene oxide (GO) assisted SELEX, or GO-SELEX^{10,11} (systematic evolution of ligands by exponential enrichment), a process that selects DNA based on its ability to change from single-stranded to higher structured upon addition of a target molecule (i.e., ThT). G4 structures bind to ThT and induce fluorescence, but structures like G4 are not ideal reporters for reactions like SDA. The G4/ThT complex has a high melting temperature. These stable structures can interfere with desired enzymatic and non-enzymatic reactions. It is also known that G4 can bind with other species in solution (e.g., metal ions¹², hemin¹³) which could make for less predictable behaviour in the system. We sought an easily denatured, dynamic reporter system that would respond only to a specific analyte.

We obtained such an aptamer with GO-SELEX. GO-SELEX was especially well-suited to this application because we could select against strongly structured DNA. GO selectively binds to ssDNA. After binding, the GO-associated ssDNA can be separated by centrifugation. We used this property to collect the bound, unstructured DNA (in the pellet) or the unbound, structured DNA (in the supernatant). We applied successive rounds of negative and positive selection. We performed negative selection by removing the supernatant containing the structured DNA in the absence of ThT (retaining the ssDNA on the GO pellet). For positive selection, we added the ThT to the mix and collected the structured DNA (retaining the supernatant). We recovered sequence data with next-generation sequencing. After evaluation and minimization, we characterized a DNA aptamer that binds to ThT and induces fluorescence, but that has no predicted structure by NuPACK¹⁴ and a G-score¹⁵ of 10 which is below the range of scores for a typical G4 structure¹⁶. The aptamer sequence has a G4Hscore¹⁷ of 0.833 which is lower than 95% of sampled G4 structures¹⁸. To date, there is only one other group who have selected an aptamer of this type¹⁹. However, our aptamer generates three times more intense fluorescence when it binds to ThT.

We applied our new aptamer to detect a strand displacement amplification (SDA) reaction. SDA is an isothermal enzymatic amplification that uses a displacing polymerase and a nicking

endonuclease to make many single-stranded copies of a template oligonucleotide²⁰. Briefly, a template DNA molecule is designed with a nicking endonuclease recognition site. The nicking endonuclease generates a break in the phosphodiester backbone of one strand. The strand displacing polymerase recognizes the 3' end of the nicked strand and initiates polymerization. The polymerization process displaces the existing ssDNA into a solution. The process then repeats. SDA based detection has been previously reported as a detector of nucleic acids like miRNA²¹.

SDA can be reported by many reporters. SDA has previously been detected with dyes like SYBR Green II²². Such dyes are nonspecific and interact with any amplicon, including undesired side products. Molecular beacons²³ can report SDA and are specific, but molecular beacons introduce high cost and high sensitivity to degradation. Degraded molecular beacons will spontaneously de-quench and generate background fluorescence. We used SDA to produce many copies of our aptamer. These SDA-generated aptamers induced fluorescence of Thioflavin-T (ThT). The aptamer yields a specific signal for the desired SDA product without the additional expense or purity requirements associated with dye-modified oligonucleotides. We optimized the reaction conditions for SDA with ThT aptamer detection. This allowed us to detect miRNA-215 (short oligonucleotide sequence of 21 bases) at low nanomolar concentrations. It has an important regulatory role for tumor suppressor gene p53²⁴. The biological importance of miR-215 has been reported as a very important agent in different cellular processes²⁴⁻²⁷. miR-215 is an important "biomarker" for colon cancer that has been reported previously^{25,26,28}. Irregular expression of *miR-215* was reported to be related to other cancers too. Levels of miR-215 are related to myeloid leukemia²⁴, neuroblastoma²⁹, and breast cancer³⁰. Therefore, it is very important to develop a sensitive detection method of miR-215. RT-PCR is currently used as a quantification of miR-215. However, RT-PCR is limited to its non-isothermal nature in many places. SDA, a simple, isothermal method, which does not require reverse transcriptase enzyme to detect miRNA. In this study, we have developed an SDA method to detect miR-215. This method has several advantages. It is label-free, low cost, simple, room temperature, and isothermal (no thermocycling needed). We propose that

this method can be used for the myriad polymerase-endonuclease-systems for more specific detection. Such systems have been demonstrated as linear amplifiers³¹, exponential amplifiers²¹, and complex reaction networks³². This SDA demonstration is proof-of-concept showing the utility and increased specificity of the ThT/Aptamer reporter system relative to intercalating and minor groove-binding fluorescent dyes.

3.2 Methods

3.2.1 Materials

DNA and RNA oligonucleotides were purchased from Integrated DNA Technologies, IDT (Coralville, IA, USA). Nuclease-free water and SYBR Green II were purchased from Thermo Scientific (Waltham, MA, USA). Sodium chloride (NaCl) was obtained from EMD Chemicals, Gibbstown, Germany. Tris base (molecular grade) was purchased from Promega Corporation (Madison WI, USA). Sodium tetraborate decahydrate was purchased from Sigma-Aldrich (St. Louis, MO, USA). ThT was purchased from Arcos Organics, NJ, USA. Graphene oxide was purchased from ACS material (Pasadena, CA, USA). Ethanol was purchased from AAPER Alcohol & Chemical Company (Shelbyville, KY, USA). Sodium acetate and butanol were purchased from Fisher Scientific (NJ, USA). PCR master mix was purchased from Thermo Scientific (Waltham, MA, USA). Gel loading dye, *Bst* 2.0 DNA Polymerase, dNTPs Solution Mix, Nt.BstNBI and Isothermal amplification buffer pack were purchased from New England Biolabs (Ipswich, MA, USA). Agarose was purchased from Life Technologies (Carlsbad CA, USA). Acrylamide/bis-Acrylamide was purchased from Research Product International (Mount Prospect, IL, USA). EvaGreen and GelRed were purchased from Biotium (Hayward, CA, USA). All reagents used were of analytical grade. For microplate reader measurements, samples were loaded in 384 well black plates with clear bottoms (Corning ME, USA).

3.2.2 Aptamer selection

The thioflavin T (ThT) aptamer was selected through eight rounds of positive and negative selection process. Round 1 of the selection processes began by mixing equimolar quantities of ThT and the DNA pool (E7N40 synthetic DNA pool, based on a published design³³, specified

in **Table 3.2**) in selection buffer (50 mM Tris, 150 mM NaCl, pH 7.4) and allowing it to incubate while tumbling for 1 hr. Then 5 mg/mL of graphene oxide (GO) was added to this mixture and the solution was allowed to incubate while tumbling for another 2 hrs. The GO was then removed from the solution by centrifuging the sample for 15 minutes and extracting the supernatant. The supernatant was then filtered with a 0.45 μm spin filter to remove any remaining GO particles. The supernatant was concentrated using the standard butanol concentration protocol until the supernatant had a final volume of 100 μL . The sample was then mixed with sodium acetate buffer (3M Sodium Acetate, pH 5.2), 250 μL ethanol, and 2 μL of glycogen and placed in a freezer at -20°C for 30 minutes. The solution was then centrifuged at 4°C for another 30 minutes at which point a white pellet was visible. The liquid was removed from the centrifuge tube and the pellet dried in 37°C oven for 2 hrs. The pellet was resuspended in 50 μL of water (boiled Millipore H_2O bottled in sterilized containers). This solution went through an 8-cycle PCR cycle-course by mixing the solution with 2X Taq PCR Master Mix, P1, and P2 (two primers designed for the E7N40 DNA pool specified in Table S1). A cycle was defined as 95°C for 15 seconds, 59.0°C for 15 seconds, and 69°C for 30 seconds. A portion of the amplified solution was mixed with a qPCR mixture (2X Taq PCR Master Mix, the two primers, and 20X EvaGreen) and placed in an Open qPCR (Chai Biotechnologies, Santa Clara, CA) that monitored the fluorescence of the amplified sample over time.

At the same time, three control samples of E7N40 DNA (100 nM, 10 nM, and 1 nM) and water were each mixed with the qPCR mixture and were run alongside the amplified sample. The Open qPCR was run with the same cycle settings as the 8-course PCR cycle-course. Once completed, the remaining sample was amplified using PCR with the same cycle settings. The sample was mixed with a PCR mixture consisting of 2X Taq PCR Master Mix, fluorescein modified P1 (P1-f), and acrydite modified P2 (P2-Acr) (modified primers specified in Table 2) and was run for the number of cycles determined by Open qPCR. A small portion of the PCR product was mixed with a loading dye and placed in the wells of a 1% Agarose Gel along with a ladder and a 72 base pair control sample (both also mixed with loading dye). This analysis with agarose in a sodium borate running buffer was done to verify that DNA was present in

the PCR product. The remaining PCR product was denatured in a 5% PAGE gel (7M, urea) by standard protocol. The product from the PAGE gel was concentrated using the standard butanol concentration procedure. The DNA was then precipitated out of the solution using ethanol and sodium acetate as before. This final Round 1 DNA pool was finally quantified with Open qPCR.

Round 2 was similar to Round 1 with two key differences. The first difference is that the Round 1 DNA pool was used instead of the E7N40 DNA pool at the beginning of the round. The second difference is that after the supernatant was collected from the DNA-GO complex, the supernatant was not concentrated with butanol or precipitated with ethanol and sodium acetate. The supernatant also did not go through an initial 8-cycle PCR cycle-course. After the supernatant was collected, it was then analyzed by Open qPCR and continued the Round 1 protocol from there.

In Round 3, the negative selection was introduced to the protocol. The Round 2 DNA pool was first mixed with GO and allowed to incubate at room temperature for 30 minutes. The supernatant was extracted using a centrifuge at room temperature and discarded. A sample of ThT equimolar to the original Round 2 DNA pool was added to the remaining DNA-GO complex. This solution was then allowed to incubate overnight while rotating and extra selection buffer was added to facilitate better rotation. The solution was centrifuged, and the supernatant collected. This eluted DNA was analyzed with Open qPCR and Round 3 thus followed the Round 2 protocol. Round 4 through Round 8 followed the protocol of Round 3 with no deviations.

3.2.3 ThT Aptamer characterization

Five aptamer candidates (Apt1, Apt2, Apt3, Apt4, Apt5, (sequences are given in Table 1) were selected from the Round 8 product based on their higher relative abundance. Using spectramax ID3 plate reader, the fluorescence intensity at 510 nm of these aptamer candidates was measured at 1 μ M of each oligonucleotide in the presence of 5 μ M of ThT dye in selection buffer (50 mM Tris, 150 mM NaCl, pH 7.4).

Further characterizations of the different fragments of the candidate Apt5 were carried out in the same way.

3.2.4 Circular dichroism analysis

Apt5.9-32, an arbitrary dsDNA (G-Arm /B-Br V4), ssDNA (B-Br V4), and blank samples were prepared at 10 μ M in selection buffer (50 mM Tris, 150 mM NaCl, pH 7.4). To construct dsDNA, a stoichiometric quantity of ssDNA and its reverse-complement were added to a solution. The solution was heated in a thermocycler to 80 °C for three minutes followed by slow cooling at 0.1 °C per second to room temperature. All oligonucleotides were annealed before CD measurement using a Jasco 720 Circular Dichroism Spectrophotometer (Jasco, Inc., Easton, Maryland, USA).

3.2.5 Binding assay of ThT and the Apt5.9-32

The binding assay of ThT and Apt5.9-32 was carried out by making six solutions with decreasing concentration (50 μ M, 40 μ M, 20 μ M, 10 μ M, 5 μ M, and 2.5 μ M) in a 1 μ M ThT solution in selection buffer (50 mM Tris, 150 mM NaCl, pH 7.4). A 20 μ L of each solution was put in a plate reader (SpectraMax iD3) to measure their fluorescence intensities. The fluorescence intensities were measured at an excitation wavelength of 440 nm and an emission wavelength of 510 nm. The increase in fluorescence was taken as proportional to the Apt5.9-32/ThT complex concentration. A single binding equilibrium was assumed (ThT + Apt5.9-32 \rightleftharpoons Complex). Using Excel's solver function a nonlinear fit was conducted.

3.2.6 Melt curve analysis of the Apt5.9-32

Apt5.9-32 and PW17Ext were prepared at five different concentrations (5, 2, 1, 0.5, and 0 μ M) in selection buffer as above with (10 mM) or without potassium. An Open qPCR (Chai Biotechnologies, Santa Clara, CA) was used to monitor fluorescence as a function of temperature. The analysis was carried out in triplicate.

UV melt curve analysis was performed using Varian Cary 100 Bio UV-Vis Spectrophotometer. The experiment was performed in two conditions: in selection buffer as above with no ThT, and in selection buffer with 5 μM ThT solution using 1 μM of Apt5.9-32 at 260 nm. The analysis was carried out in duplicate.

3.2.7 Strand displacement amplification optimization

SDA reactions at different temperatures in the range of 25-40 $^{\circ}\text{C}$ were performed. The SDA mix contained 0.04 U/ μL Bst polymerase, 0.192 U/ μL of nicking endonuclease, 0.240 mM dNTPs, 6 mM MgSO_4 , 1X iso thermal buffer, and 5 μM ThT was assembled in an ice bath. Pre annealed 2.2 μL Primer/Template duplex at 1 μM was added to 19.8 μL of SDA mix. The final concentration of the Primer/Template duplex was 100 nM of the SDA temperature optimization reaction. In addition to the Primer/Template duplex, five more controls such as blank, Template only, Primer only, nsTemplate only, nsSDA (Primer/nsTemplate duplex) were carried out in parallel. All oligo controls were at 100 nM final concentration. Fluorescence kinetics was carried out for 1 hr in a plate reader (SpectraMax iD3).

Bst polymerase was optimized at the optimum temperature of 25 $^{\circ}\text{C}$. Seven SDA mixes were prepared in the same way as mentioned above for the seven Bst concentration points in the range of 0.01 to 0.07 U/ μL . In addition to Primer/Template duplex at 100 nM, three more controls such as blank, Template only, and nsSDA (Primer/nsTemplate duplex) were also carried out in parallel. All oligo controls were at 100 nM final concentration.

The ratio of Bst polymerase and nicking endonuclease was optimized at 25 $^{\circ}\text{C}$ in the same way. Seven different SDA mixes were assembled in ice containing seven different ratios of [Bst]: [nicking endonuclease]. The selected ratios of [Bst]: [nicking endonuclease] were 1:0.5, 1:1, 1:2, 1:4, 1:5, 1:7, 1:10. The amount of Bst polymerase was fixed at 0.04 U/ μL while the amount of nicking endonuclease was varied as per the calculated ratio. In addition to the primer-template duplex at 100 nM, three more controls such as blank, the template only, and nsSDA (Primer/nsTemplate duplex) were also carried out in parallel. All oligo controls were at 100 nM final concentration.

The amount of dNTPs was optimized in the same way at 25 °C. Four different SDA mixes were prepared in ice bath containing 0.12 mM, 0.24 mM, 0.35 mM, and 0.50 mM dNTPs. The amount of Bst polymerase and nicking endonuclease was fixed at 0.04 U/ μ L and 0.2 U/ μ L respectively. In addition to the primer-template duplex at 100 nM, three more controls such as blank, the template only, and nsSDA (Primer/nsTemplate duplex) were also carried out in parallel. All oligo controls were at 100 nM final concentration.

Mg²⁺ was optimized by performing SDA in seven different concentrations. Seven SDA mix assemblies with varying MgSO₄ were prepared to have 2 mM, 6 mM, 8 mM, 10 mM, 15 mM, and 20 mM final concentration. The amount of Bst polymerase, nicking endonuclease and dNTPs were fixed at 0.04 U/ μ L, 0.2 U/ μ L, and 0.240 mM respectively. In addition to the primer-template duplex at 100 nM, three more controls such as blank, Template only, and nsSDA (Primer/nsTemplate duplex) were also carried out in parallel. All oligo controls were at 100 nM final concentration.

The amount of ThT dye was optimized by making SDA mix with six different concentrations in the range of 1-20 mM while other components were kept constant. The amount of Bst polymerase, nicking endonuclease, dNTPs and Mg²⁺ was fixed at 0.04 U/ μ L, 0.2 U/ μ L, 0.240 mM, and 10 mM respectively. In addition to the primer-template duplex at 100 nM, three more controls such as blank, the template only, and nsSDA (Primer/nsTemplate duplex) were also carried out in parallel. All oligo controls were at 100 nM final concentration.

In all cases, 1X iso thermal buffer (20 mM Tris-HCl, 10 mM (NH₄)₂SO₄, 50 mM KCl, 2 mM MgSO₄, 0.1% Tween-20, pH 8.8@25 °C) and 5 μ M ThT were used. Fluorescence kinetics was carried out at 25 °C for 1 hr in the plate reader (SpectraMax iD3). Each reaction at all optimizing conditions carried out in triplicate at an excitation wavelength of 440 nm and an emission wavelength of 510 nm.

3.2.8 SDA with different reporter system

Two SDA mixes with 0.4X SYBR Green II, and 10 μ M of ThT were prepared in an ice bath. Each of the two SDA mix contained Bst polymerase, nicking endonuclease, dNTPs, and Mg²⁺ at 0.04

U/ μ L, 0.2 U/ μ L, 0.240 mM, and 10 mM respectively. In addition to the primer-template duplex at 100 nM, three more controls such as blank, the template only, and nsSDA (Primer/nsTemplate duplex) were also carried out in parallel. All oligo controls were at 100 nM final concentration. In all cases, a 1X iso thermal buffer was used. Fluorescence kinetics was carried out at 25 °C for 1 hour in the plate reader (SpectraMax iD3). Each reaction at all optimizing conditions was carried out in triplicate at an excitation wavelength of 440 nm and an emission wavelength of 510 nm.

3.2.9 In-vitro detection of miR-215

Sixteen solutions of miR-215 at 0, 0.5, 1, 2, 5, 10, 20, 40, 50, 60, 80, 90, 100, 150, 200, and 250 nM were made in RNAase free water. An equal volume of SDA mix and miR-215 solutions were added to all samples to make 22 μ L total volume of each reaction. Concentration of the Template-215 in each reaction was constant at 100 nM. The final concentration of the SDA mix contained 1X iso thermal buffer, 10 mM MgSO₄, 0.240 mM dNTPs, 0.04 U/ μ L Bst polymerase, 0.2 U/ μ L nicking endonuclease, 10 μ M ThT. Fluorescence kinetics was carried out at 25 °C for 55 min in the plate reader (SpectraMax iD3). Each reaction at all assigned concentrations of miR-215 was carried out in triplicate at an excitation wavelength of 440 nm and an emission wavelength of 510 nm. Optimization of Template-215 concentration was carried out similarly.

3.2.10 SDA specificity

Nine SDA reactions were carried out *in vitro* using several targets at two concentration points of 50 and 20 nM. The SDA mixes were prepared as above. SDA in simulated biofluids of the same target oligonucleotides was also performed using 10% saliva (self-collected and prepared following protocols from the literature³⁴) and 10% fetal bovine serum. SDA in biofluids was performed using 20 nM target oligonucleotides. The template215 concentration was 100 nM in all SDA reactions. Fluorescence kinetics was carried out at 25 °C for 55 min in the plate reader (SpectraMax iD3). Each of the reactions was carried out in triplicate.

3.2.11. PAGE analysis of SDA product

The SDA was analyzed by 12% native PAGE (including 10 mM Mg²⁺). SDA circuit reactions were carried out for 50 min at 25 °C before PAGE analysis. SDA circuit reactions and controls were assembled as follows: Lane 1, low molecular weight DNA as a ladder. Lane 2, Template-215 only. Lane 3, Primer-215 only. Lane 4, Template-215/Primer-215 duplex only. Lane 5, Apt5.9-32 only. Lane 6, Template-215 + SDA mix. Lane 7, Primer-215 + SDA mix only. Lane 8, Template-215+ SDA mix+ Primer-215. The electrophoresis was carried out for 5 hours at 80 V in 1X Sodium Borate buffer (5 mM sodium borate, 10 mM MgSO₄, pH 8). The gel was stained in 1X GelRed (Biotium, CA, USA) for one hour. A digital fluorescence photograph was taken under blue illumination with an amber filter after staining.

3.3 Results and Discussion

3.3.1 *In Vitro* Selection

We performed *in vitro* selection to generate ThT aptamer according to an established protocol¹⁰. **Figure 3.1A** shows a schematic of the process. In early rounds, DNA (pool design TGCTCCGACCTTAGTCTCTG N40 GAACCGTG TAGCACAGCAGA) was mixed with ThT and then graphene oxide (GO) was added. Unstructured, single-stranded DNA bound GO and was discarded. Structured DNA was retained in the supernatant. The structured DNA included folded aptamers binding to ThT. Free DNA (supernatant above GO) was then amplified and regenerated using protocols developed in house and published elsewhere³⁵. In later rounds, a negative selection step was added: DNA was allowed to bind to GO first, and the supernatant was discarded. The DNA-coated GO was then mixed with ThT and incubated for an extended time. The DNA that became structured and eluted from the GO in the presence of ThT was retained and amplified. The *in vitro* selection procedure was repeated for 8 rounds. In our selection process, we used qPCR to optimize the number of cycles for each PCR amplification step (**Figure 3.1A**) to avoid contamination with non-specific amplicons and to increase SELEX efficiency. After the SELEX experiments, we submitted the pool to next-generation sequencing.

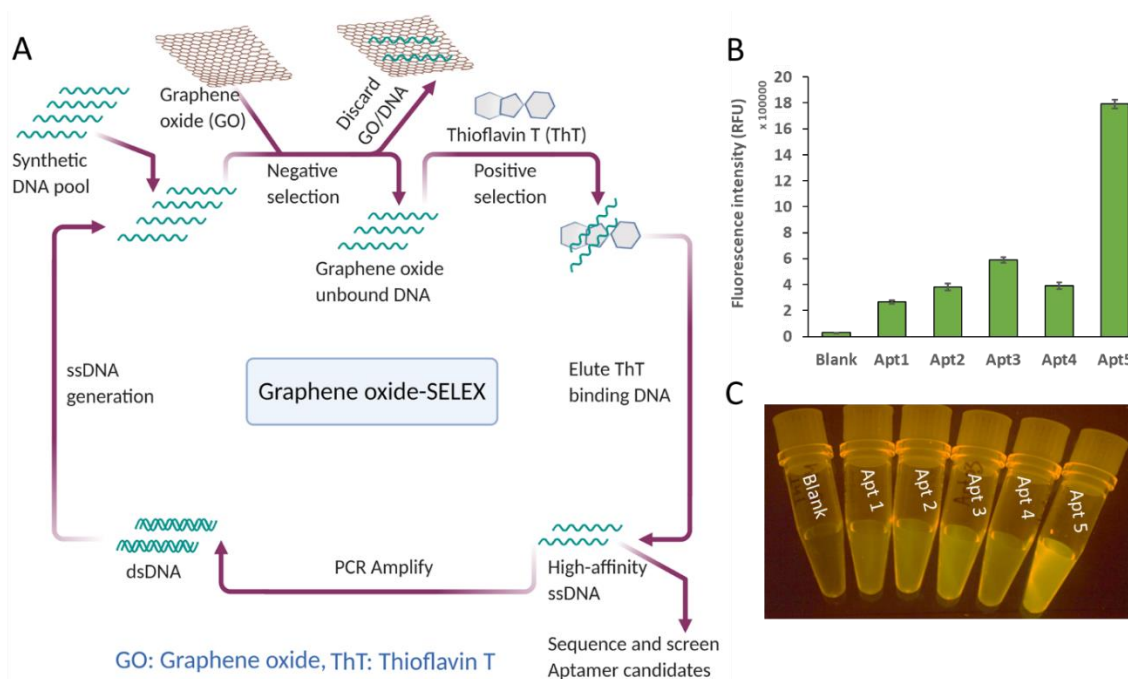


Figure 3.1. *In vitro* selection of ThT aptamer. A) Schematic shows the process of GO assisted *in vitro* selection of ThT aptamer (created with BioRender.com). B) Fluorescence intensity (RFU) of five aptamer candidates and ThT only (blank). C) An image of fluorescence generated by ThT in the absence and presence of five aptamer candidates selected in this study.

We recovered several hundred thousand reads. We ranked the recovered sequences by their abundance using in-house Python software³⁵. We counted the instances of each unique sequence in the data. Most sequences were wholly unique. However, some sequences were represented many times in the data. We took these abundant sequences to be “aptamer candidates.” We synthesized the five most abundant aptamer candidate oligonucleotides (for relative abundance see **Table 3.1**).

Table 3.1. ThT aptamer candidate sequences (1 μ M aptamer candidates and 5 μ M ThT in selection buffer).

Aptamer candidate	Abundance (reads)	Sequence (Excluding primer binding sites)	Fluorescence enhancement
Apt1	10089 (2.3%)	TCGCGTGTGCAGAGGCGAGTAGGTGGGAGATCTGTCTGGG	9X
Apt2	5771 (1.31%)	GACCGGAGGGGCATCAGCTGTCCGTGAGGTTGCCGCGAG	13X
Apt3	4028 (0.92%)	GCACGTCCAGGACGGGGGAGCGGTGCTAGTGTCTGGCAGG	20X
Apt4	4223 (0.96%)	GACCGGAGGGGCATCAGCTGTCCGTGAGGTTGCCGCGAGT	14X
Apt5	2140 (0.49%)	GCGTAGATCGAGGCTATTAGGAGGTGGGATGCGTCAGGGC	61X

We denote the aptamer candidates Apt1, Apt2, Apt3, Apt4, and Apt5. Each oligonucleotide was 40 nucleotides long (Apt2 is 39 nucleotides long) and represents only the random region of the pool (no primer binding sites). All candidates have similar guanine base content in their sequences (varying from 17 to 19 guanine bases). Each of the five oligonucleotides can enhance ThT fluorescence (see **Figure 3.1B**). ThT fluorescence was enhanced by a factor of 10 to 60 relative to the ThT dye by itself. The degree of fluorescence enhancement (relative to no-DNA control) is shown in **Figure 3.1C**. Apt5, the least abundant of the five candidates, is the most fluorescent enhancer compared to the other four candidates. Apt5 generates 60X fluorescence upon binding to ThT. Apt5 was subjected to further sequence optimization and characterization to develop a versatile reporter for the label-free strand displacement amplification (SDA) reaction.

3.3.2 Aptamer characterization and optimization

Based on the high fluorescence enhancement of Apt5, we chose it for further study. We tested the minimum portion of the aptamer that would enhance ThT fluorescence. We inspected the secondary structure of Apt5 using NUPACK (Nucleic Acid Package), a web-based nucleic acid structural analysis tool³⁴. Two hairpin structures are found in the NUPACK predicted secondary structure of Apt5 (**Figure 3.2A**). Based on the NUPACK predicted structure of Apt5, we hypothesized that the more structured region between nucleotides 20-36 might be important to the ThT-binding and fluorescence enhancing activity. To test this hypothesis, we designed truncated versions of Apt5 spanning the whole Apt5 sequence. We denote these 24 nucleotide fragments by the Apt5 subsequence as follows: Apt5.1-24, Apt5.5-28, Apt5.9-32, Apt5.13-36, and Apt5.17-40 (see **Figure 3.2B** for sequence design).

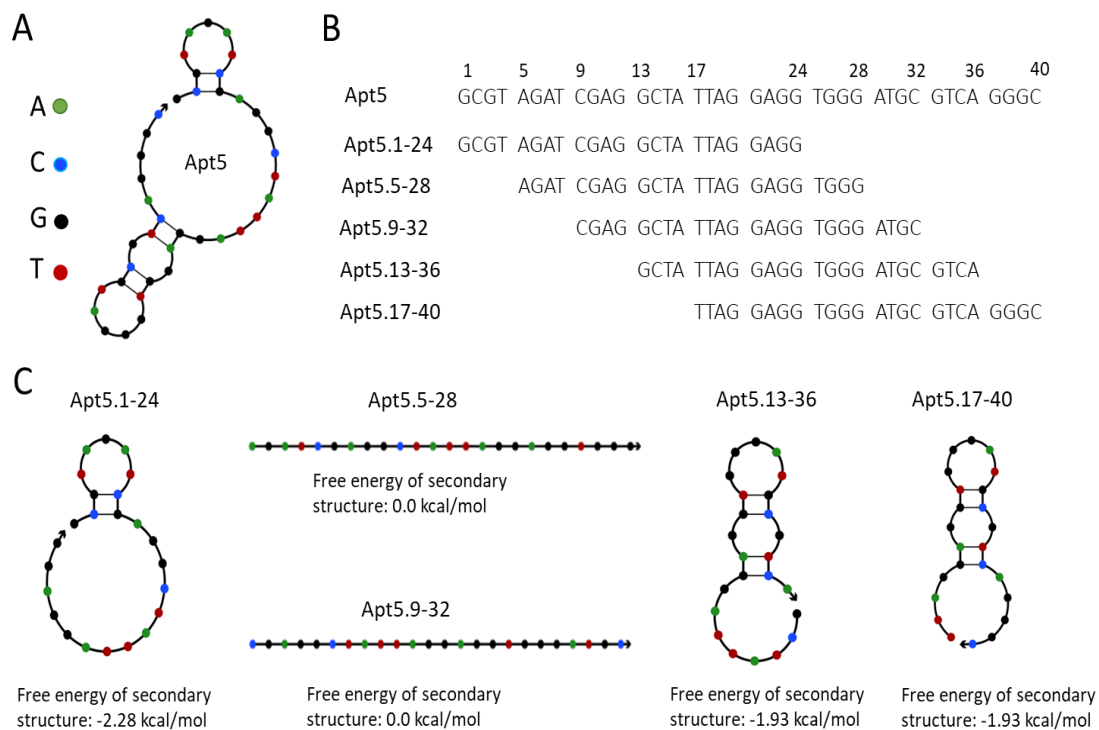


Figure 3.2. NUPACK characterization of ThT aptamer candidates. A) NUPACK predicted secondary structure of the Apt5. B) The sequence of Apt5 and its fragments. C) NUPACK predicted secondary structures of five truncated versions of Apt5.

Apt5.1-24 was designed to contain the 5' hairpin and Apt5.17-40 includes all of the 3' hairpin. NUPACK predicts no secondary structure for Apt5.5-28 or Apt5.9-32. All of the NUPACK structures of the Apt5 fragments are shown in **Figure 3.2C**.

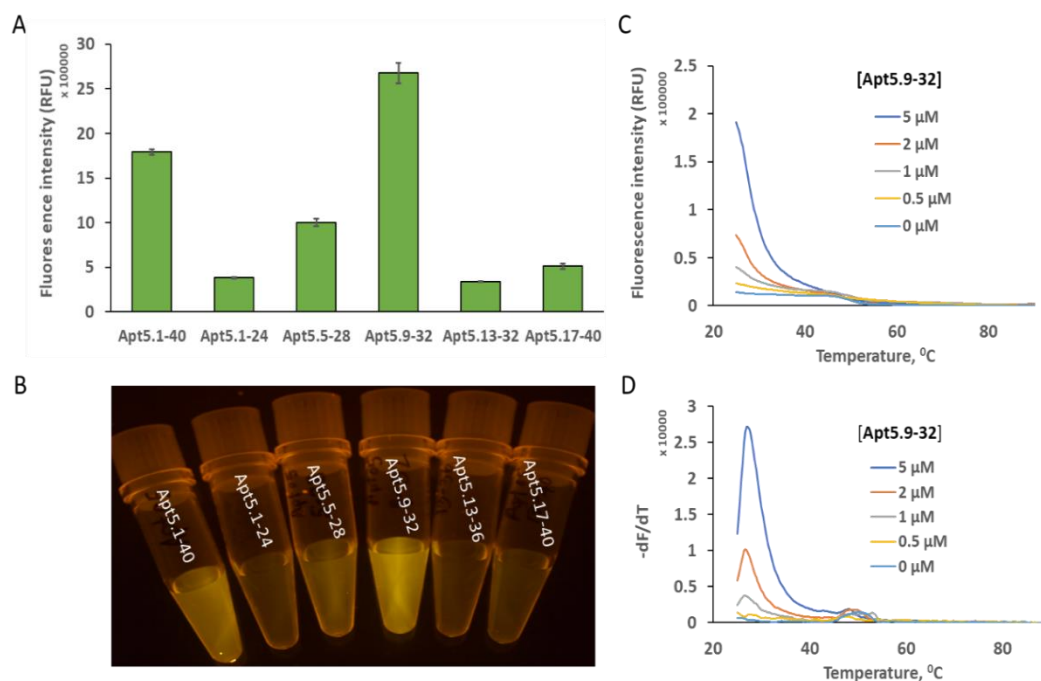


Figure 3.3. Aptamer minimization. A) Fluorescence intensity of the best aptamer candidate Apt5 and five sub-sequences of Apt 5; 1-24, 5-28, 9-32, 13-36, and 17-40 at the concentration of 1 μ M. B) Image of fluorescence generated by Apt5 and five sub-sequences of Apt 5 C) Raw fluorescence melt curve of Apt5.9-32 (fluorescence as a function of temperature) analysis. D) Negative 1st derivative plot of thermofluorometric analysis of ThT Apt5.9-32 at the indicated concentrations from 0 to 5 μ M.

We compared the ThT fluorescence enhancement of Apt5 and the five truncated versions. The NUPACK structural features did not correlate with fluorogenic activity. Of the five truncated aptamers, four were less active than the whole aptamer including all versions with predicted secondary structure (**Figure 3.3A**). However, Apt5.9-32 showed increased fluorescence (despite showing no predicted structure in NUPACK) even relative to the full-length Apt5 (see **Figure 3.3A**). Apt5.9-32 is about 50% brighter than the original Apt5. When compared to no DNA control (blank, only ThT), Apt5.9-32 is about 90X more fluorescent. **Figure 3.3B** also shows that Apt5.9-32 is visibly brighter than all other oligos. It may be that base-paired structures compete with the non-canonical structure that binds ThT. This lack of significant internal base-pairing is an advantage for our application. We require structures that can be easily denatured.

Although ThT is known to bind G-Quadruplexes², ThT Apt5.9-32 is unlikely to be a strong G-quadruplex structure. It does not display known G-quadruplex repeat patterns such as

(GGGNN)₄. As noted in the introduction, its G4Hscore (0.833) is below that of 95% of sampled G-Quadruplexes¹⁸. We also performed a melt curve analysis of Apt5.9-32. We measured fluorescence as a function of increasing temperature using an Open qPCR instrument. We used 5 μ M of ThT and four different concentrations of Apt5.9-32. Apt5.9-32 showed a $T_{1/2}$ value at 29 °C (see **Figure 3.3C**) and a peak in the negative first derivative ($-dF/dT$) at 27 °C (see **Figure 3.3D**). This is a significantly lower temperature than a typical intramolecular G-quadruplex melting. For detailed comparison see supplementary **Figure 3.S1**. Potassium does not have any effect on the thermofluorimetry of Apt5.9-32. It has the same $T_{1/2}$ and T_m values in the presence and the absence of potassium (see supplementary **Figure 3.S1 A-B**). It has been reported that G-quadruplex structures are stabilized in solutions with high potassium concentration^{12,35}. PW17Ext contains a known G-quadruplex with a G4Hscore of 1.606¹⁸, which is typical for G-Quadruplexes. Likewise, potassium shows a strong effect on PW17Ext. In the presence of potassium, PW17Ext made a more stable complex of ThT/PW17Ext. The presence of potassium increases both $T_{1/2}$ and T_m values by 11 to 19 °C respectively (see supplementary **Figure 3.S1 C-D**). While these results are circumstantial, they suggest that the interaction of ThT with Apt5.9-32 may be different from the known interaction of ThT with G-quadruplexes.

We also performed UV melt curve analysis of the Apt5.9-32. The aptamer may fold more efficiently at lower temperatures, but this is less relevant to our application. Because the polymerase is active at elevated temperatures, we performed UV melt curve analysis at room temperature and above. The results are shown in supplementary **Figure 3.S2**. The results were consistent with the fluorescence melt curve analysis of the Apt5.9-32.

We also performed CD spectroscopy of Apt5.9-32 with necessary controls including a random ssDNA, dsDNA (Supplementary **Figure 3.S3**). The negative peak of all the samples arises in the same wavelength position: 240 nm. However, the positive peak of the Apt5.9-32 is closer to that of the ssDNA, and dsDNA. It is closer to the spectrum of ssDNA. The CD peak in Apt5.9-32 (~268 nm) was ~8 nm different from the characteristic G-quadruplex peak (260 nm). Also, the signal from the Apt5.9-32 is much less intense than a known G-quadruplex: PW17Ext or

dsDNA control. We suspect the weak G-quadruplex-like peaks may arise from intermolecular interactions. At the recommended concentrations of oligonucleotides for the CD experiments (10 μM), the formation of intermolecular structures may be favored.

We also performed binding assays of Apt5.9-32 with ThT. We found that the average dissociation constant for Apt5.9-32 was $6.28 \pm 1.78 \mu\text{M}$ of three individual measurements (see supplementary **Figure 3.S4**). This shows a moderate binding between the dye and aptamer. This is an advantage as the aptamer can be easily denatured in the presence of ThT while it still can act as a convenient reporter in the real-time DNA circuit monitoring.

Our aptamer has several advantages over the previous aptamer¹⁹ as a reporter of enzymatic amplification. It is shorter (24 vs. 33 nucleotides). It has much higher fluorescence when bound to ThT (see supplementary **Figure 3.S5**). Additionally, the minimized aptamer does not have a strong secondary structure according to NUPACK. This is important when designing strand displacement amplification (SDA) reactions. The less competing secondary structure is crucial for DNA polymerase to efficiently generate a new strand.

3.3.3 Isothermal Strand displacement amplification

We designed a target-triggered isothermal SDA reaction to detect miR215. After optimizing the amplification, we determined that we could perform this SDA reaction at room temperature (or slightly above). It is a significant advantage: we did not require sophisticated temperature control. SDA is an enzymatic process that employed the activities of DNA polymerase and a nicking endonuclease. The microRNA miR215 acted as a primer to initiate the SDA reaction. We designed a DNA oligonucleotide to act as an SDA template. The Template215 had three specific parts. The first part at the 3' end is a sequence that was the reverse complement of the target miR-215. The second part of the SDA template was the reverse-complement of the nicking endonuclease recognition site (Nt.BstNBI). Finally, at the 5' end of Template, the sequence is the reverse complement of the reporter, Apt5.9-32.

SDA starts with the hybridization of miR215 to the template strand (or a DNA oligonucleotide with the same sequence for testing purposes, denoted Primer-215). The polymerase binds to

the 3' end of the miR-215 and extends using dNTPs as fuel. Bst polymerase is promiscuous and highly processive and can extend either an RNA or DNA primer. As the new DNA is copied from the template strand, a nicking endonuclease recognition site is generated along with Apt5.9-32. (see **Figure 3.4A** for the schematic of SDA). Once the primer strand extension is complete, the nicking endonuclease recognizes the specific nicking site and generates a single-stranded break or nick in the primer strand.

It generates a new 3' terminus on the primer strand. Bst polymerase can then extend again from this site. As it extends, it generates another copy of Apt5.9-32 and displaces the existing Apt5.9-32 into the solution with ThT. The catalytic cycle continues by nicking, extending, and releasing Apt5.9-32. The system generates many copies of Apt5.9-32 per input molecule. We estimate that every activated Template is copied ~ 30 times (based on the endpoint fluorescence and the relationship between aptamer and fluorescence in the binding curve). This gain in concentration is how we can achieve nanomolar detection limits for miR-215 despite the weak binding affinity between aptamer and dye. We controlled for any direct interaction with miR-215 (Primer-215) and Apt5.9-32 with additional fluorescence measurements.

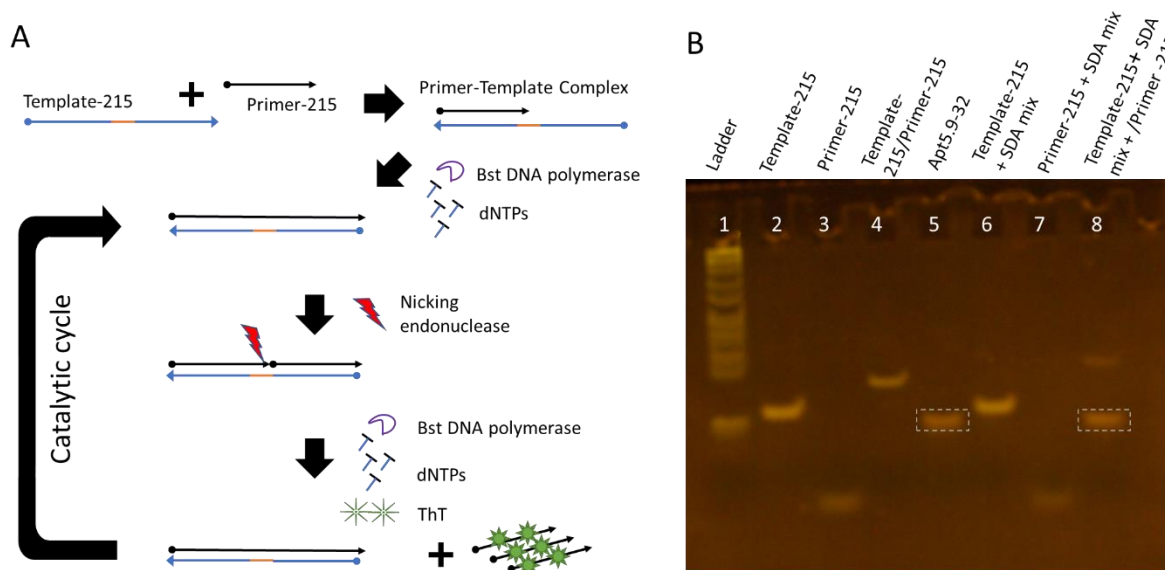


Figure 3.4. SDA with ThT aptamer (Apt5.9-32) Reporter. A) Schematic of SDA with the ThT aptamer (Apt5.9-32) reporter system. B) SDA product analysis by 12% PAGE. The white boxes indicate Apt5.9-32 bands.

We found no fluorescence generated by miR-215 in the presence of ThT. In addition to that, we also tested the same for Template and ThT and found no fluorescence. The results are shown in Supplementary **Figure 3.S6**.

We analyzed the SDA system in optimized conditions using polyacrylamide gel electrophoresis (PAGE). **Figure 3.4B** is an image of the 12% PAGE gel. Lane 1 is a DNA Ladder. Lanes 2 to 4 are the SDA reaction components (Template215, Primer 215, and Template 215/Primer 215 duplex, respectively, in Tris buffer). Lane 5 is synthetic Apt5.9-32 oligonucleotide, which the SDA reaction is designed to produce. Lane 6 and 7 contain Template-215 (no primer control) and Primer 215 (no template control) respectively in reaction conditions (i.e., including enzymes, dNTPs, Mg^{2+} , and buffer). Lane 8 shows the full SDA reaction (i.e., including Primer-215 and Template-215). All mixtures were allowed to react for 50 min at room temperature before PAGE analysis. The key result is that the product (Apt5.9-32) is generated by the reaction only when Primer-215 and Template-215 are both present. The gel image shows that the SDA product band in lane 8 is aligned with the Apt5.9-32 band in lane 5 (indicated by white boxes in **Figure 3.4B**). We interpret the slower migrating band in lane 8, which is very faint, as the Template-215/Primer-215 complex in the SDA mix. This complex in Lane 8 migrated more slowly (compare to the Template-215/Primer-215 duplex in the Tris buffer in lane 4) due to the extension of the Primer-215 and the generation of fully double-stranded DNA.

3.3.4 SDA Characterization and Optimization

We optimized the SDA reaction for reaction time as well as several parameters of the reaction composition. We determined the optimal endpoint by running the SDA reaction for 90 min while measuring fluorescence at every minute. It was found that negative control reactions were also amplified after 60 min (see supplementary **Figure 3.S7**). We determined that the best endpoint for the reaction was 50 min.

Using the fluorescence at 50 minutes, we optimized temperature, and the concentration of enzyme, dNTPs, $MgSO_4$, and ThT dye. We measured performance of the SDA based on three metrics: 1. the signal to background ratio (SBR), 2. the average rate of fluorescence increase,

and 3. the ratio of specific to non-specific product fluorescence. We focused on the SBR metric, but all three were found to be highly consistent. The analysis in terms of the rate of fluorescence increase and the ratio of specific to non-specific product fluorescence are presented in the supplementary information (see supplementary **Figure 3.S8**).

The SBR is defined as a signal over background. We defined the signal as the fluorescence intensity of the primer plus template at 50 minutes. We defined the background as the intensity of the no-primer control at the same time point under the same conditions. **Figure 3.5** shows the SBR as a function of changing each parameter. We conducted all experiments in triplicate.

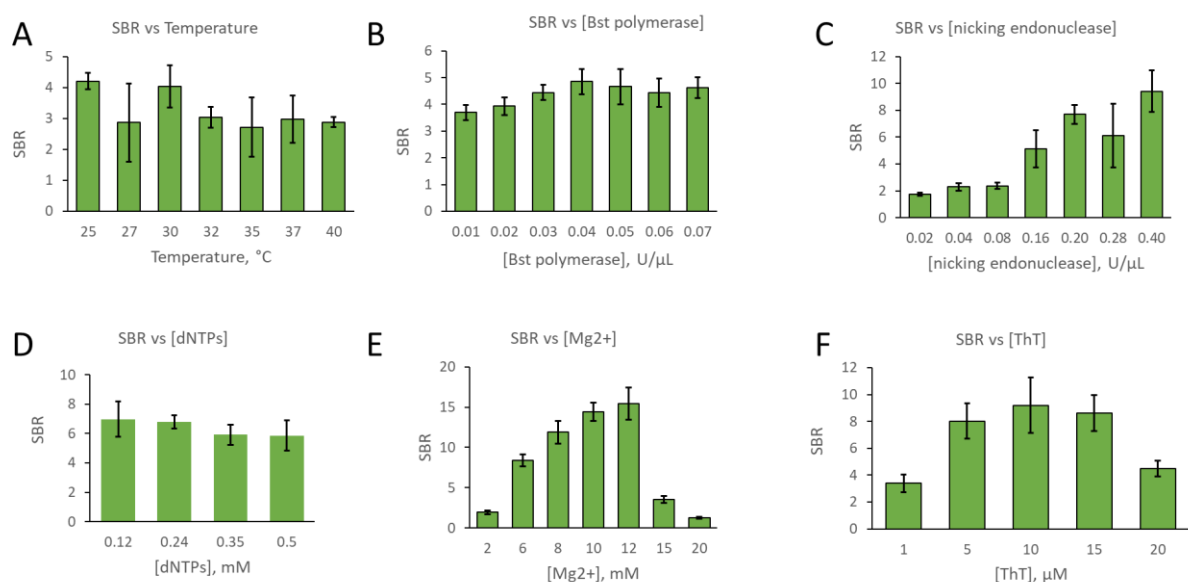


Figure 3.5. Optimization of experimental parameters. SBR as a function of (A) temperature, (B) Bst polymerase concentration, (C) nicking endonuclease concentration, (D) dNTPs concentration, (E) magnesium, and (F) ThT. (Error bars represent the standard deviation of triplicate measurements).

First, we optimized the temperature of the SDA reaction. We sought to determine a reaction temperature that generated the highest SBR. We selected seven temperature points in the range of 25-40 °C (see **Figure 3.5A**). Although we did not see a large SBR difference as a function of temperature, we noted that lower temperatures produce a slightly higher SBR. The consistent SBR over our temperature range also confirms that our SDA circuit design is a robust and flexible system able to operate at a wide temperature range. We selected 25 °C, room temperature, as the standard temperature for further experiments. This result is also

consistent with the melt curve data in **Figure 3.3C, D**. Apt5.9-32 has a fluorescence melting temperature 27 °C. At this temperature, ThT/Apt5.9-32 lost fluorescence; this reduced the SBR of the SDA reaction.

We also optimized the concentration of the reaction components. **Figure 3.5 B-F** shows the SBR as a function of the concentration of the reaction components. We interpret these results to mean that the SBR performance of the reaction was strongly dependent on nicking endonuclease concentration and magnesium ion concentration, suggesting that nick generation may be the limiting step in the catalytic cycle and that magnesium may enhance that reaction rate. The system was not strongly dependent on Bst polymerase, dNTPs concentration, or ThT concentration (within reasonable ranges). Based on these data, we standardized our conditions to 25 °C, 0.04 U/ μ L Bst polymerase, 0.2 U/ μ L Nt.BstNBI, 0.24 mM dNTPs (each nucleotide triphosphate), 10 mM Mg^{2+} , and 8 μ M ThT. When the performance was within the error of the optimal, we used the lower quantity.

3.3.5 Aptamer SDA product confers reaction specificity

We were motivated to select an efficient aptamer against ThT to add specificity to the SDA reaction without the use of covalent labels. We tested whether the fluorescence response of the SDA system was specific to the aptamer in the presence of ThT dye. Nonspecific dyes are frequently used to monitor real-time DNA amplification reactions. However, the dyes respond to any DNA product, whether it is the intended product or some undesired side-product. We set out to show that the desired product of our SDA reaction, Apt5.9-32, would produce a signal in the presence of ThT, but aberrant reactions (that produce some other DNA) would not produce a signal.

We designed two different templates, denoted Template (to produce Apt5.9-32) and nsTemplate (non-specific Template). The difference between the two sequences is that Template contains the complementary sequence of Apt5.9-32 at the 5' end which generates Apt5.9-32 in the SDA system. The nsTemplate sequence contains a random sequence at the 5' end which generates non-specific ssDNA in the system. We show that the SDA reaction

(containing the Template oligonucleotide) lights up ThT present in the reaction. The nsSDA reaction (containing the nsTemplate oligonucleotide) does not light up the ThT in the reaction (see **Figure 3.6A**).

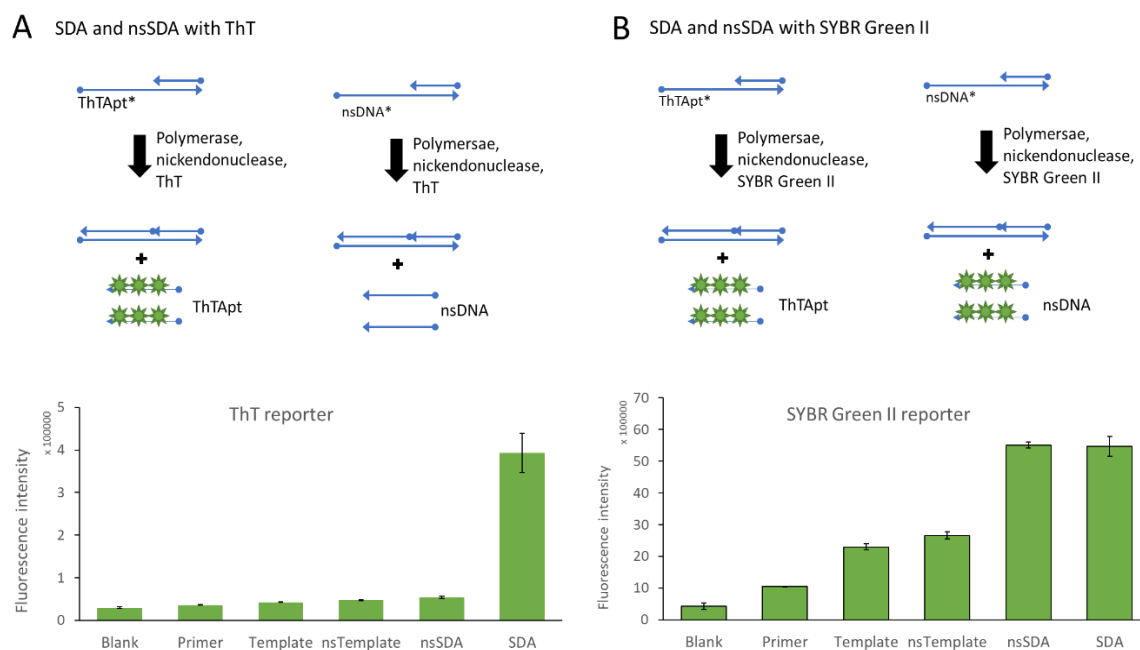


Figure 3.6. SDA product specificity. (A) A schematic diagram (top) shows how SDA (aptamer product) and nsSDA (SDA with the non-aptamer product) react in ThT. A bar graph shows fluorescence intensity at 50 min (bottom). (B) A schematic diagram (top) shows how SDA and nsSDA react in SYBR Green II. A bar graph shows fluorescence intensity at 50 min (bottom). (Error bars represent the standard deviation of triplicate measurements).

This is a significant improvement over nonspecific dye like SYBR Green II. SYBR Green II binds to any single-stranded nucleic acid (DNA or RNA). SYBR Green II is fluorescent in the SDA reaction, the nsSDA reaction, and several of the negative controls (**Figure 3.6B**). Both Apt5.9-32 and random ssDNA can generate signals. Although SYBR Green II was a brighter fluorophore under our conditions, ThT interacts specifically with the Apt5.9-32 product such that side reactions are suppressed. This confirms that our optimized SDA reaction generates an aptamer that we can detect against a background of other side products.

3.3.6 Optimization of Template-215 concentration for the detection of miR-215

The SDA reaction is designed to produce Apt5.9-32 and become fluorescent when a microRNA hybridizes to Template. We optimized the Template concentration to maximize the range and

sensitivity of the SDA system. We varied Template-215 (the Template bearing the reverse complement of miR-215) at four different concentrations (25, 50, 100, 200 nM) (See Supplementary **Figure 3.S9A**). At each template concentration, we measured the rate of fluorescence increase as a function of Primer-215 (the DNA analogue of miR-215). The system responded best to Primer-215 when Template-215 concentrations were between 100 and 200 nM. Below this range, the strand displacement reaction is constrained by a lack of substrate and does not produce strong signals. However, higher template concentration tends to generate high non-specific background. **Figure 3.S9B** shows the time-course fluorescence data of the SDA system for various Primer-215 concentrations. The reaction is nearly linear with respect to time with an increasing slope as more Primer-215 is added. **Figure 3.S9C** shows the linear relationship between endpoint fluorescence intensity and Primer-215 concentration in the SDA system. This data shows that the SDA system can act as a detector for Primer-215 with a linear range of 5-100 nM.

3.3.7 Detection of miR-215

We used our SDA system to detect miR-215 specifically. We used the optimized experimental conditions, including the optimal Template-215 concentration. **Figure 3.7A** shows excellent linearity and good sensitivity of the system. **Figure 3.7B** shows a linear relationship between fluorescence intensity at 510 nm and various miR-215 concentrations in the range of 0-20 nM. **Figure 3.7C** shows the fluorescence endpoint spectra (at time 50 min) of the SDA detection of miR-215. These results show that fluorescence intensity at 510 nm is the peak emission and increases dramatically as a function of the added miRNA. The regression equation of the linear range in **Figure 3.7B** is shown with a correlation coefficient of 0.98. For target miR-215, the limit of detection of this label-free SDA system was calculated to be approximately 2.6 nM. This limit of detection is better than a similar study of ThT based SDA based miRNA detection³.

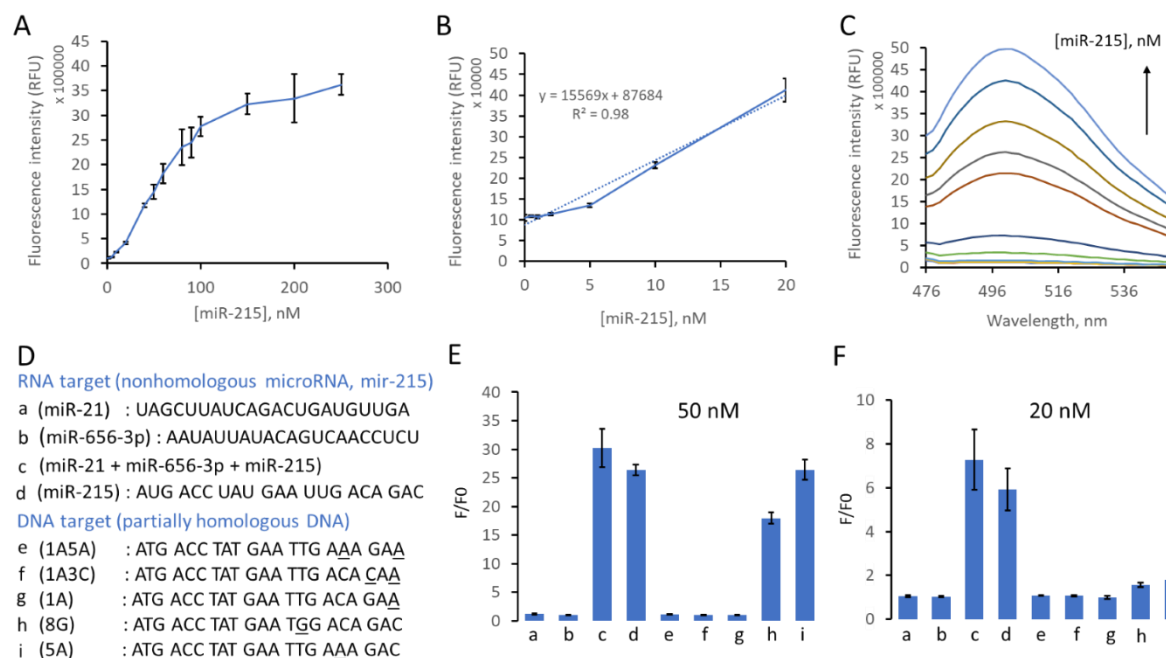


Figure 3.7 SDA Detection of miR-215. A) Fluorescence intensity (RFU) of SDA reaction (with [Template-215] =100 nM) as a function of miR-215 concentration (indicated concentrations from 0-250 nM). Fluorescence intensity was measured at 50 min. B) Relationship between fluorescence intensity and miR-215 concentrations (indicated concentrations from 0-20 nM) in the SDA system (with [Template-215] =100 nM). C) Endpoint fluorescence spectra (at 50 min of the SDA reaction) containing different concentrations of miR-215 (0, 0.5, 1, 2, 5, 10, 20, 40, 50, 60, 80, and 100 nM). D) Sequences of target oligonucleotides (a-i) used for SDA specificity including microRNA targets (a-d) and partially homologous DNA targets (e-i). Underlined bases indicate one or two bases alteration with respect to the target miR-215 sequence. E) SDA specificity with several target oligonucleotides, at 50 nM. F) SDA specificity with several target oligonucleotides, at 20 nM. F/F0 is defined as the ratio of fluorescence intensity of SDA in the presence of target sequence(F) to the fluorescence intensity of SDA mix with no target(F0, reagent blank). Error bars represent the standard deviation of triplicate measurements in all cases.

We investigated SDA specificity for the detection of miR215. We used two nonhomologous RNA targets, miR-21 and miR-656-3p, and five designed partially homologous DNA targets. We designed DNA to contain one or two altered bases from the original sequence of miR-215 (see **Figure 3.7D**). We named the partially homologous DNA sequences as 1A5A, 1A3C, 1A, 8G, and 5A, where the number indicates the position relative to the 3' end and the letter is the new base. For example, 1A5A indicates the sequence where the 1st and 5th position from the 3' end were altered to adenine. We found high specificity at 20 nM and reduced specificity at 50 nM (**Figure 3.7E**). The detection was still specific for 3' mismatched targets at the higher

concentration but not specific for all internal mismatches. Bst DNA polymerase enzyme is known to be sensitive to 3' mismatches^{37,38}.

However, at 20 nM concentration, SDA specifically detects miR-215, and no other oligonucleotides were detected (**Figure 3.7F**). The SDA shows better specificity at lower concentrations of target miRNAs. This is a more typical use case. The physiological concentrations of miRNAs are very low. SDA also successfully detected miR-215 when mixed with two other nonhomologous miRNA sequences used in the experiment. This shows that the SDA system can specifically detect miR-215 in the presence of other miRNAs.

We also investigated the potential of our system to detect miR-215 in more complex biological samples. We note that miRNA biomarkers have been measured in saliva^{39,40} and serum^{41,42}. Therefore, we verified that the reaction functions in the context of those matrices. We made simulated biological samples by spiking the SDA mix to 10% of the relevant biofluid. Even in the presence of saliva or serum, miR-215 was successfully and specifically detected by the SDA system (**Figure 3.S10A**). The fluorescence intensity in the presence of serum is lower than that of saliva, which is likely due to the presence of higher total protein concentration in the former. The overall result shows the excellent specificity of the SDA system in detecting miR-215 in a complex biological sample matrix (**Figure 3.S10B**).

3.4 Conclusion

We developed a new, light-up aptamer, Apt5.9-32, against ThT using modified GO-SELEX. This aptamer is brighter than the previously published work and is not predicted to have any base-pairing secondary structures. Isothermal nucleic acid-based amplifications are recognized for their simplicity in experiments and instruments in different bioanalytical applications⁴³ in different platforms⁴⁴. We developed a room temperature isothermal SDA reaction to generate a light-up aptamer. This reaction can successfully detect miR-215 (an important biological analyte). This label-free approach does not need covalently modified probes to report the activity of the system. Other single-stranded nucleic acid molecules (including other miRNAs) can be detected with this SDA system. The 3' end of the SDA Template

sequence simply needs to be redesigned to be complementary to the new 3' end of the analyte. Critically, the generation of Apt5.9-32 by SDA adds a layer of specificity to the system without adding a second, modified probe to the reaction.

We demonstrated this reporter with the SDA reaction. While the nanomolar LOD of the ThT aptamer reporter with SDA is modest, it can be improved by adding a stronger amplification reaction. Other reactions built by stacking and combining the SDA reaction will also be amenable to detection by producing Apt5.9-32. It has the potential to be a universal reporter for other types of DNA amplification, such as EXPAR⁴⁵, RCA^{46,47}, SDA + RCA²², asymmetric PCR⁴⁸, or EDA⁸. Input samples must be characterized to check that the sample matrix does not cause ThT to fluoresce; this can be determined with necessary controls, including no-template, no-primer, and no-enzyme controls. We hope to explore the broad applicability of this novel aptamer in future work.

3.5 Oligonucleotides used in this study

Table 3.2. Sequences of all DNA

Name	Sequences
E7N40 pool	TGCTCCGACCTTAGTCTCTG[N40] GAACCGTGTAGCACAGCAGA
P1	TGCTCCGACCTTAGTCTCTG
P1-f	/56-FAM/TGCTCCGACCTTAGTCTCTG
P2	TCTGCTGTGCTACACGGTTC
P2-Acr	/5Acryd/TCTGCTGTGCTACACGGTTC
Apt1	TCGCGTGTGCAGAGGCGAGTAGGTGGGAGATCTGTCTGGG
Apt2	GACCGGAGGGGCATCAGCTGTCCGTGAGGTTGCCGCGAG
Apt3	GCACGTCCAGGACGGGGGAGCGGTGCTAGTGTCTGGCAGG
Apt4	GACCGGAGGGGCATCAGCTGTCCGTGAGGTTGCCGCGAGT
Apt5	GCGTAGATCGAGGCTATTAGGAGGTGGGATGCGTCAGGGC
Apt5.1-24	GCGTAGATCGAGGCTATTAGGAGG
Apt5.5-28	AGATCGAGGCTATTAGGAGGTGGG
Apt5.9-32	CGAGGCTATTAGGAGGTGGGATGC
Apt5.13-36	GCTATTAGGAGGTGGGATGCGTCA
Apt5.17-40	TTAGGAGGTGGGATGCGTCAGGGC
PW17Ext	GAGGAGGAGGAGGAGAGGGTAGGGCGGGTTGGG
B-Br V4	ATCGAATCCTCCTCCTCCTCGATACTCCTCCTCCTCGATA
G-Arm V4	TATCGAGGAGGAGGAGTATCGAGGAGGAGGAGGATTCGATTCATATGT
Template	GCATCCACCTCCTAATAGCCTCGTTATGACTCAAAGATGGTACCTGCTTCTGAATT
Primer	AATTCAGAAGCAGGTACCATCTTT
nsTemplate	GTAGATATTCATACGGCTAATTGTTTATGACTCAAAGATGGTACCTGCTTCTGAATT
Template-215	GCATCCACCTCCTAATAGCCTCGTTATGACTCTTTACTGTCTGTCAATTCATAGGTCAT
Primer-215	ATGACCTATGAATTGACAGAC
miR-215	AUGACCUAUGAAUUGACAGAC
ThT.2-2	GACGACGACACAGGATTAATCTTATTAGTCGTC

3.6 Supporting information

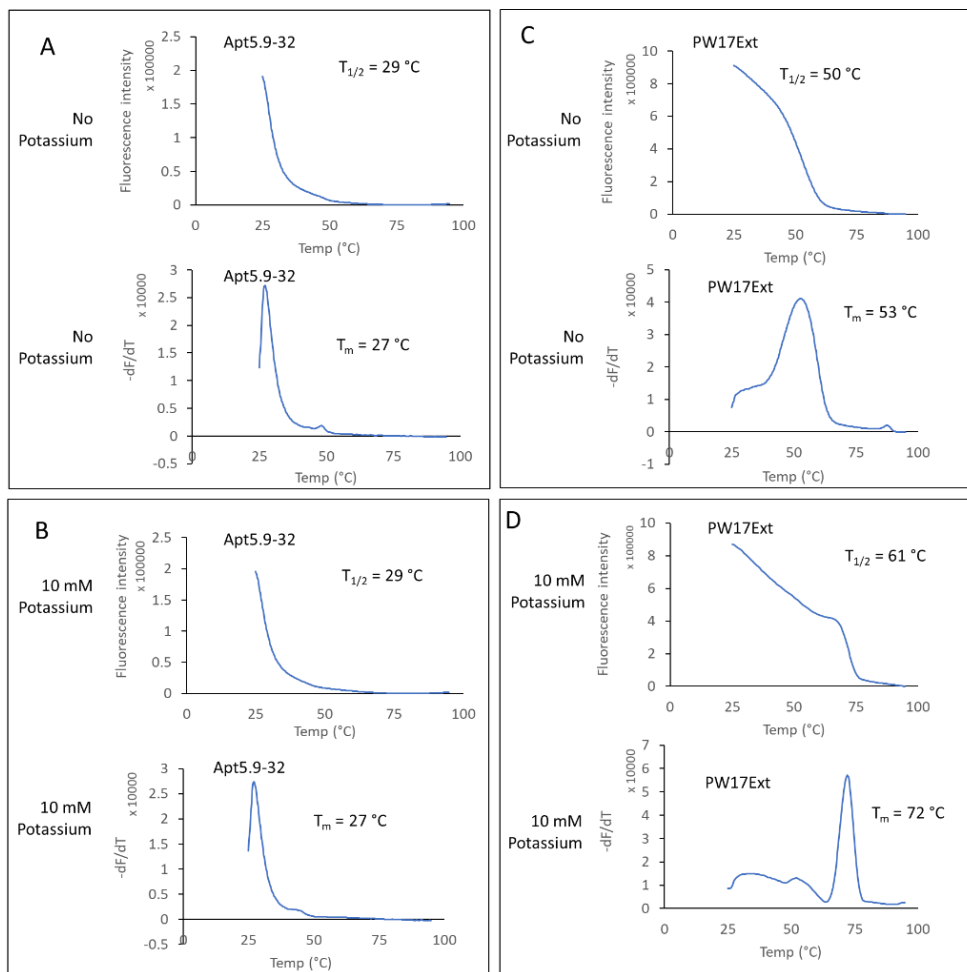


Figure 3.S1. Melt curve analysis of ThT interaction with Apt5.9-32. Top graphs show the fluorescence as a function of temperature. Bottom graphs show the first derivative of fluorescence as a function of temperature. (A) Graphs show triplicate melt curves of Apt5.9-32 in the absence of potassium. (B) Graphs show triplicate melt curves of Apt5.9-32 in the presence of 10 mM potassium. (C) Graphs show triplicate melt curves of PW17Ext in the absence of potassium and (D) Graphs show triplicate melt curves of PW17Ext in the presence of 10 mM potassium. In each case, an inset shows the temperature at which the fluorescence reached half its maximal value ($T_{1/2}$).

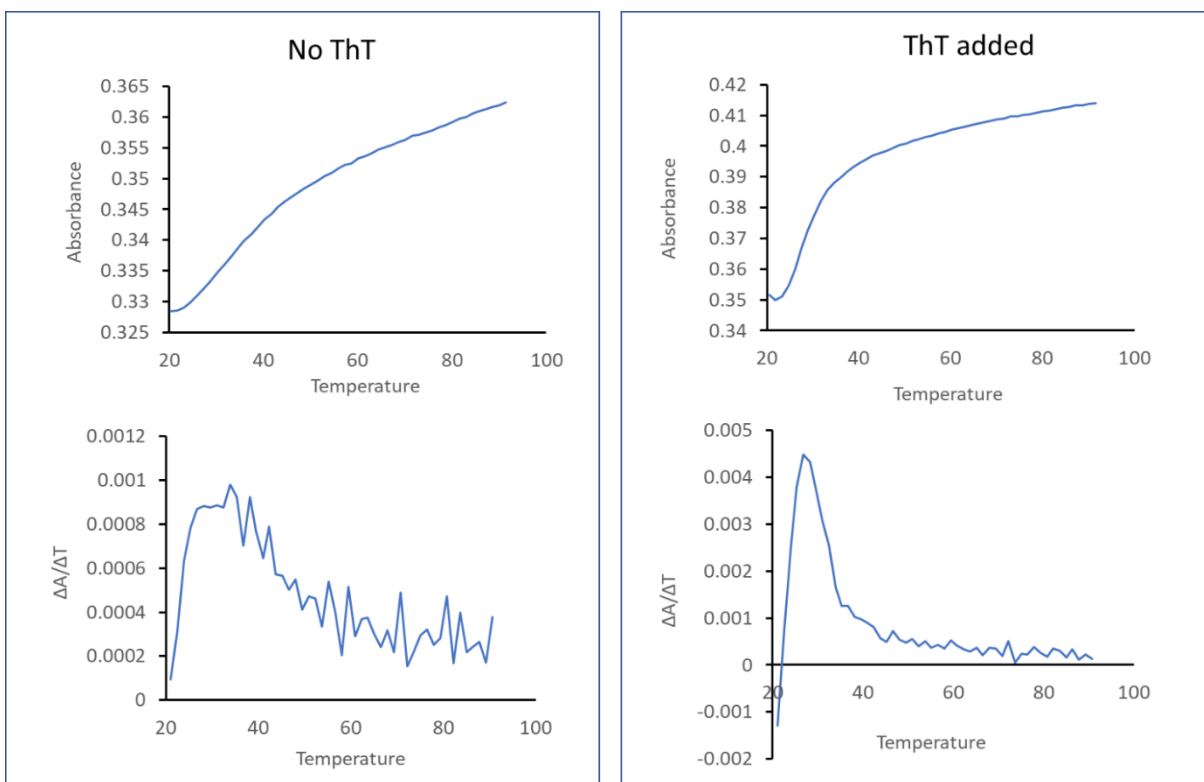


Figure 3.S2. Melt curve analysis of aptamer structure with UV absorbance at 260 nm. Top graphs show the absorbance as a function of temperature. Bottom graphs show the first derivative of absorbance as a function of temperature. Graphs show the duplicate absorbance as a function of temperature of the aptamer, Apt5.9-32 (at 1 μ M) in two conditions: In selection buffer, no ThT (left) and in selection buffer, with 5 μ M ThT (right).

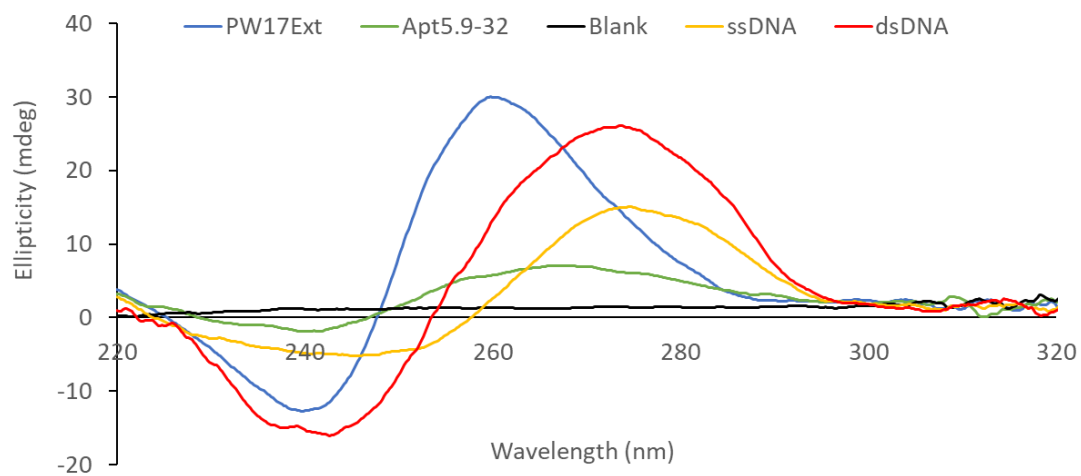


Figure 3.S3. CD spectra of the Apt5.9-32 with controls: PW17Ext (as a G4DNA), blank (buffer-no DNA), ssDNA (random), dsDNA (random)

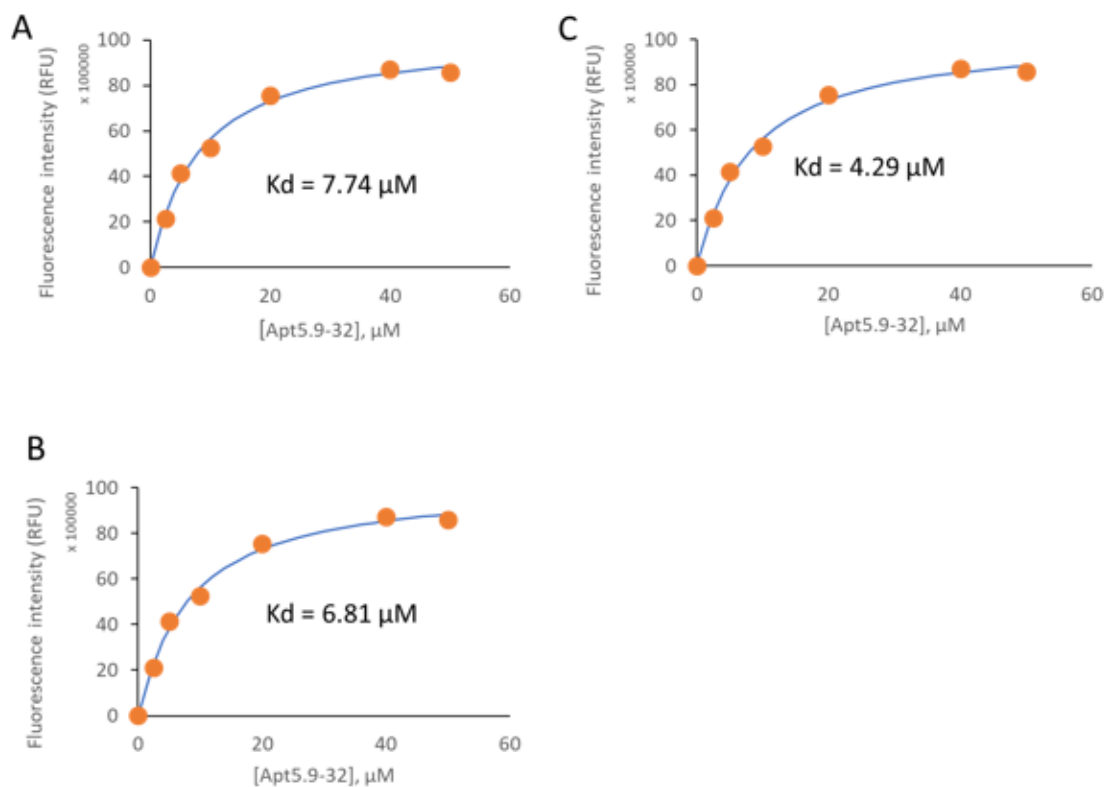


Figure 3.S4. Binding studies of Apt5.9-32, using Spectrometer Id3 platereader. Graphs show fluorescence intensity (RFU) as function of (A) Apt5.9-32 concentration, trial 1, (B) Apt5.9-32 concentration, trial 2, and (C) Apt5.9-32 concentration, trial 3. The blue line is the best fit binding isotherm used to determine dissociation constant (k_d) between Apt5.9-32 and ThT. Average $k_d = 6.28 \pm 1.78 \mu\text{M}$

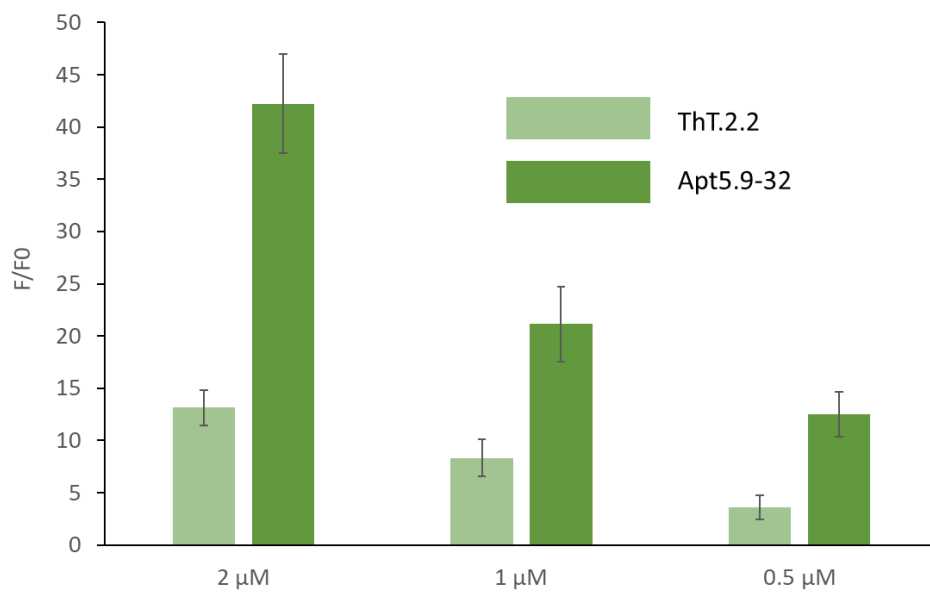


Figure 3.S5. Fluorescence enhancement of ThT comparison between Apt5.9-32(this work) and ThT.2-2 (Pei et al., Anal. Methods, 2016, 8, 8461) at several concentrations. (F0 is fluorescence of ThT only).

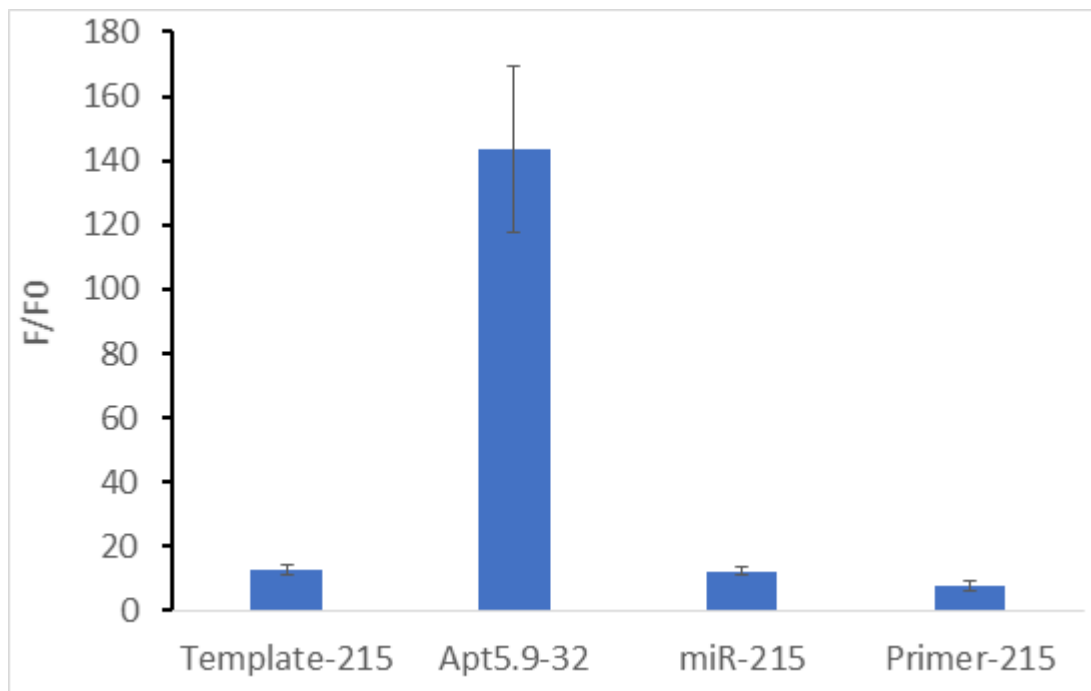


Figure 3.S6. Fluorescence enhancement of ThT (at 5 μ M) by different oligonucleotides (at 1 μ M). Comparison of fluorescence generated by Apt5.9-32, Template-215, miR-215, and Primer-215 (F_0 is fluorescence of ThT only).

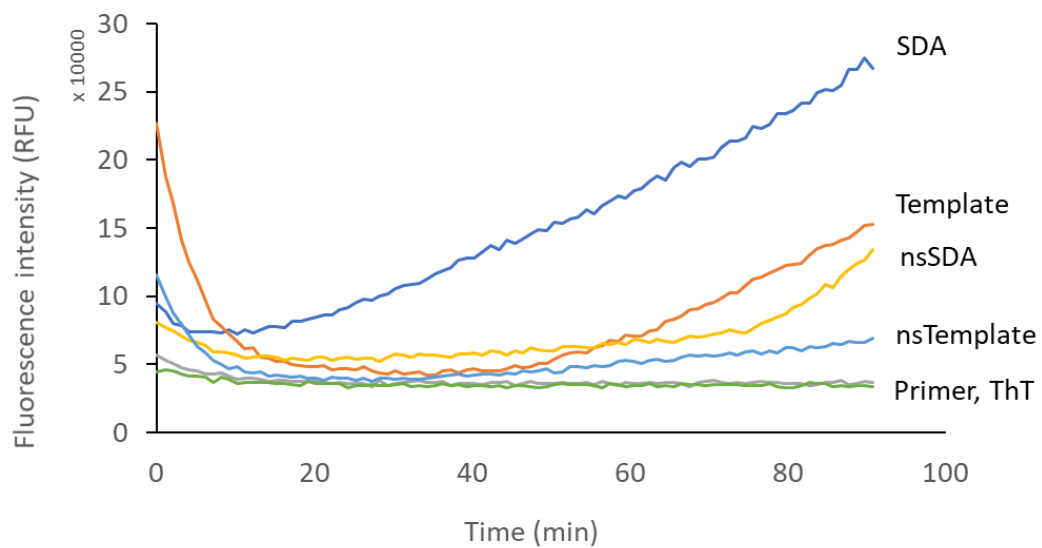


Figure 3.S7. SDA reaction time optimization. SDA was compared against necessary controls: Template, nsSDA, nsTemplate, Primer, and ThT.

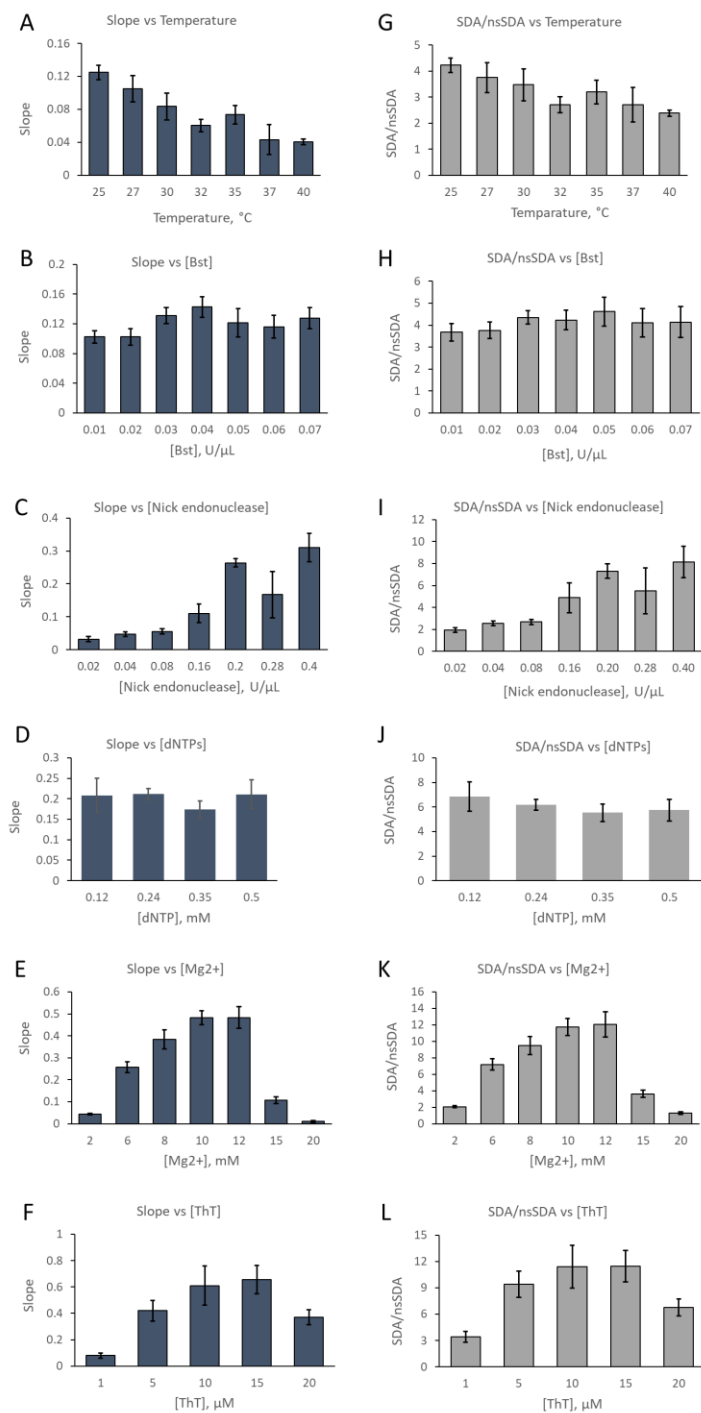


Figure 3.S8. Slope as a function of A) Temperature, B) Bst polymerase, C) Nick endo nuclease, D) dNTPs, E) Mg²⁺, and F) ThT. SDA/nsSDA as a function of G) Temperature, H) Bst polymerase, I) Nick endo nuclease, J) dNTPs, K) Mg²⁺, and L) ThT.

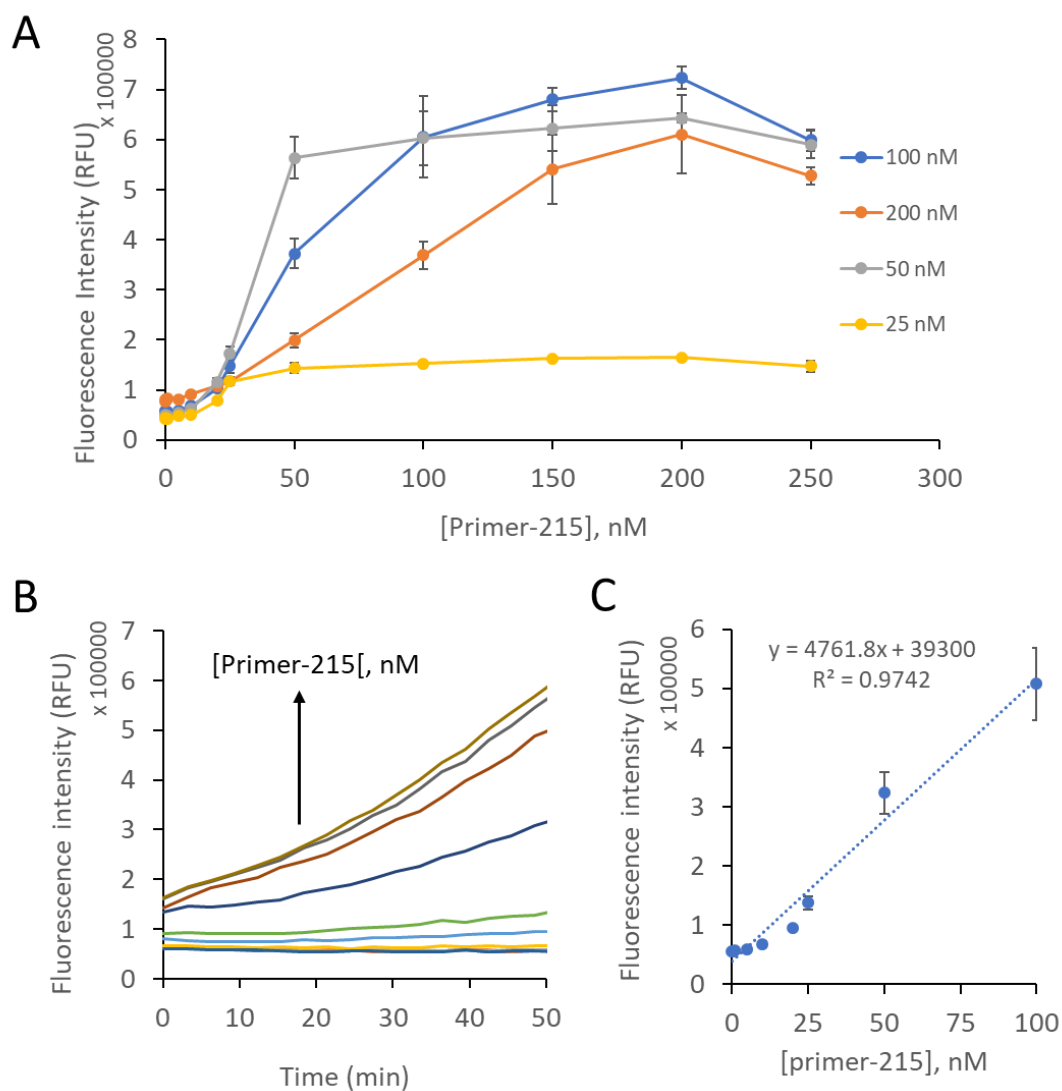


Figure 3.S9. Optimization of the Template-215 concentration. A) Fluorescence intensity of SDA reactions with four different concentrations of Template-215 (100, 200, 50, and 25 nM) as a function of various Primer-215 concentration. Endpoint fluorescence intensity was collected at 50 min. B) Fluorescence-time curves as a function of different concentration of Primer-215 (0, 0.1, 1, 5, 10, 20, 25, 50, 100, 150, and 200 nM) where [Template-215] = 100 nM. C) Linear relationship between fluorescence intensity and Primer-215 concentration in the SDA system where [Template-215] = 100 nM (error bars represent the standard deviation of triplicate measurements in all cases).

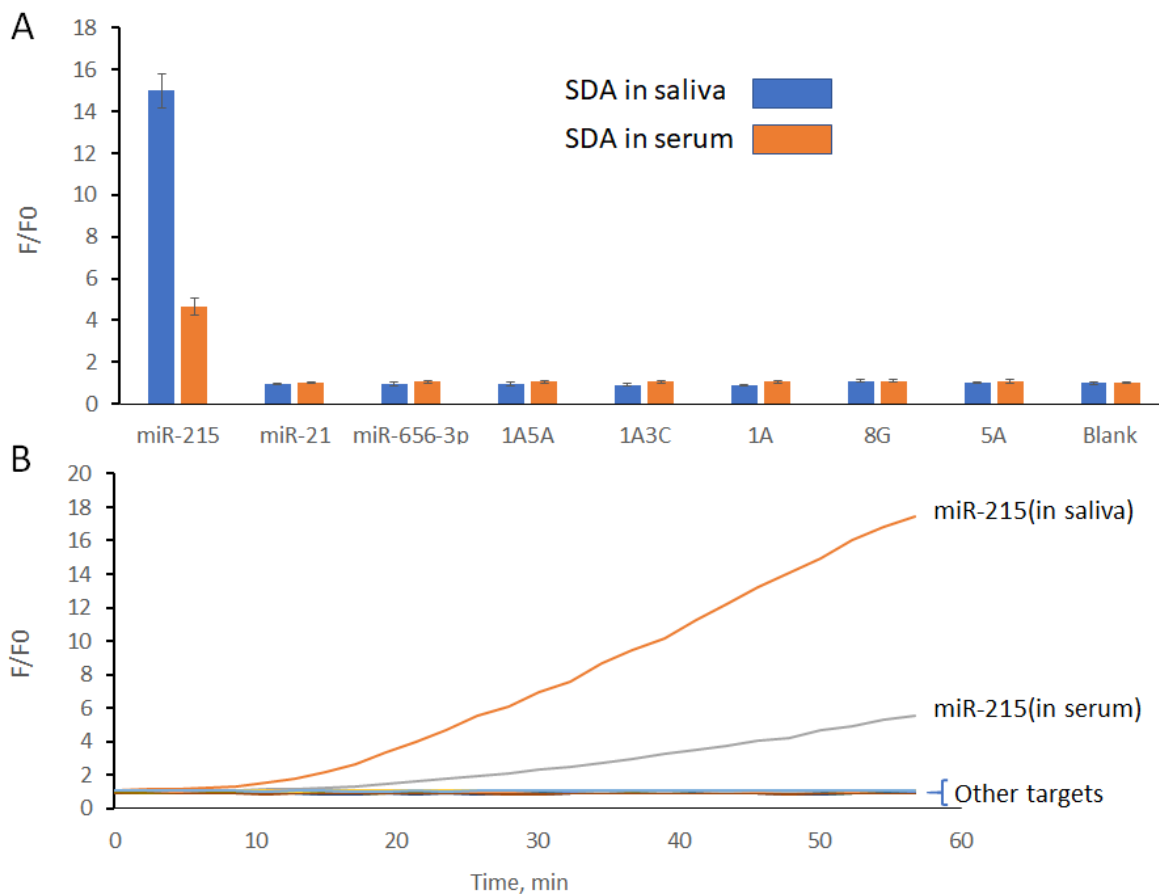


Figure 3.S10. SDA in two biofluids; saliva and serum. A) SDA comparison of 8 different oligonucleotides. Only the target miR-215 is detected both in saliva and serum. End point fluorescence intensity (F) was measured at 50 min. (error bars represent the standard deviation of triplicate measurements). B) Fluorescence-time curves as a function of 8 different oligonucleotides (triplicate measurements). Fluorescence intensity (F) from miR-215 is increased over the time in both saliva and serum sample (10% each). Other targets include miR-21, miR-656-3p, 1A5A, 1A3C, 1A, 8G, 5A, and blank in both saliva and serum samples. (F_0 is fluorescence of SDA mix with no target)

3.7 Author contributions

P B A, M M I conceptualized experiments. M M I, P B A, and V M G optimized, carried out experiments, and analyzed data. P B A, and M M I wrote the manuscript.

3.8 Notes

The authors declare no competing interests.

3.9 Reference

1. Mohanty, J. et al. Thioflavin T as an efficient inducer and selective fluorescent sensor for the human telomeric G-quadruplex DNA. *J. Am. Chem. Soc.* 135, 367–376 (2013).
2. Renaud de la Faverie, A., Guédin, A., Bedrat, A., Yatsunyk, L. A. & Mergny, J.-L. Thioflavin T as a fluorescence light-up probe for G4 formation. *Nucleic Acids Res.* 42, e65–e65 (2014).
3. Zhou, H. et al. Stable and label-free fluorescent probe based on G-triplex DNA and Thioflavin T. *Anal. Chem.* 90, 3220–3226 (2018).
4. Zhu, J. et al. Lighting up the Thioflavin T by parallel-stranded TG(GA)_n DNA homoduplexes. *ACS Sens.* 3, 1118–1125 (2018).
5. Liu, L., Shao, Y., Peng, J., Liu, H. & Zhang, L. Selective recognition of ds-DNA cavities by a molecular rotor: switched fluorescence of thioflavin T. *Mol. Biosyst.* 9, 2512–2519 (2013).
6. Sugimoto, S., Arita-Morioka, K., Mizunoe, Y., Yamanaka, K. & Ogura, T. Thioflavin T as a fluorescence probe for monitoring RNA metabolism at molecular and cellular levels. *Nucleic Acids Res.* 43, e92 (2015).
7. Xu, S. et al. Thioflavin T as an efficient fluorescence sensor for selective recognition of RNA G-quadruplexes. *Sci. Rep.* 6, 24793 (2016).
8. Damase, T. R., Islam, M. M., Shipley, M. & Allen, P. B. Thioflavin T as a noncovalent reporter for a label-free, non-enzymatic, catalytic DNA amplifier. *Methods Appl. Fluoresc.* 8, 045001 (2020).

9. Chang, W. et al. Molecular AND logic gate for multiple single-nucleotide mutations detection based on CRISPR/Cas9n system triggered signal amplification. *Anal. Chim. Acta* 1112, 46–53 (2020).
10. Park, J.-W., Tatavarty, R., Kim, D. W., Jung, H.-T. & Gu, M. B. Immobilization-free screening of aptamers assisted by graphene oxide. *Chem. Commun.* 48, 2071–2073 (2012).
11. Xing, L., Zhang, Y. & Yang, J. Graphene oxide-assisted non-immobilized SELEX of chiral drug ephedrine aptamers and the analytical binding mechanism. *Biochem. Biophys. Res. Commun.* 514, 134–139 (2019).
12. Bhattacharyya, D., Arachchilage, G. M. & Basu, S. Metal cations in G-quadruplex folding and stability. *Front. Chem.* 4, 38 (2016).
13. Li, W. et al. Insight into G-quadruplex-hemin DNAzyme/RNAzyme: adjacent adenine as the intramolecular species for remarkable enhancement of enzymatic activity. *Nucleic Acids Res.* 44, 7373–7384 (2016).
14. Zadeh, J. N. et al. NUPACK: analysis and design of nucleic acid systems. *J. Comput. Chem.* 32, 170–173 (2011).
15. Kikin, O., D’Antonio, L. & Bagga, P. S. QGRS Mapper: a web-based server for predicting G-quadruplexes in nucleotide sequences. *Nucleic Acids Res.* 34, W676–W682 (2006).
16. Belmonte-Reche, E. & Morales, J. C. G4-iM Grinder: when size and frequency matter. G-Quadruplex, i-Motif and higher order structure search and analysis tool. *NAR Genom. Bioinform.* 2 (2020).
17. Brázda, V. et al. G4Hunter web application: a web server for G-quadruplex prediction. *Bioinformatics* 35, 3493–3495 (2019).
18. Bedrat, A., Lacroix, L. & Mergny, J.-L. Re-evaluation of G-quadruplex propensity with G4Hunter. *Nucleic Acids Res* 44, 1746–1759 (2016).
19. Wang, H. et al. Selection and characterization of thioflavin T aptamers for the development of light-up probes. *Anal. Methods* 8, 8461–8465 (2016).

20. Walter, N. G. & Strunk, G. Strand displacement amplification as an in vitro model for rolling-circle replication: deletion formation and evolution during serial transfer. *Proc. Natl. Acad. Sci.* 91, 7937–7941 (1994).
21. Shi, C., Liu, Q., Ma, C. & Zhong, W. Exponential strand-displacement amplification for detection of MicroRNAs. *Anal. Chem.* 86, 336–339 (2014).
22. Zhou, Y. et al. Fluorometric determination of microRNA based on strand displacement amplification and rolling circle amplification. *Microchim. Acta* 184, 4359–4365 (2017).
23. Li, F. et al. Single palindromic molecular beacon-based amplification for genetic analysis of cancers. *Biosens. Bioelectron.* 91, 692–698 (2017).
24. Wang, Y.-X. et al. Reduced miR-215 expression predicts poor prognosis in patients with acute myeloid leukemia. *Jpn. J. Clin. Oncol.* 46, 350–356 (2016).
25. Song, B. et al. Molecular mechanism of chemoresistance by miR-215 in osteosarcoma and colon cancer cells. *Mol. Cancer* 9, 96 (2010).
26. Braun, C. J. et al. p53-responsive microRNAs 192 and 215 are capable of inducing cell cycle arrest. *Cancer Res.* 68, 10094–10104 (2008).
27. Georges, S. A. et al. Coordinated regulation of cell cycle transcripts by p53-Inducible microRNAs, miR-192 and miR-215. *Cancer Res.* 68, 10105–10112 (2008)
28. Fesler, A. et al. Identification of miR-215 mediated targets/pathways via translational immunoprecipitation expression analysis (TriP-chip). *Oncotarget* 6, 24463–24473 (2015).
29. Senanayake, U. et al. miR-192, miR-194, miR-215, miR-200c and miR-141 are downregulated and their common target ACVR2B is strongly expressed in renal childhood neoplasms. *Carcinogenesis* 33, 1014–1021 (2012).
30. Zhou, S. et al. Aberrant miR-215 expression is associated with clinical outcome in breast cancer patients. *Med. Oncol.* 31, 259 (2014).
31. Joneja, A. & Huang, X. Linear nicking endonuclease-mediated strand displacement DNA amplification. *Anal. Biochem.* 414, 58–69 (2011).

32. Cui, Y.-X. et al. An integrated-molecular-beacon based multiple exponential strand displacement amplification strategy for ultrasensitive detection of DNA methyltransferase activity. *Chem. Sci.* 10, 2290–2297 (2019).
33. Li, N., Nguyen, H. H., Byrom, M. & Ellington, A. D. Inhibition of cell proliferation by an anti-EGFR aptamer. *PLoS ONE* 6, e20299 (2011).
34. Yoshizawa, J. M. & Wong, D. T. W. Salivary microRNAs and oral cancer detection. *Methods Mol. Biol.* 936, 313–324 (2013).
35. Damase, T. R., Miura, T. A., Parent, C. E. & Allen, P. B. Application of the open qPCR instrument for the in vitro selection of DNA aptamers against epidermal growth factor receptor and Drosophila C virus. *ACS Comb. Sci.* <https://doi.org/10.1021/acscombsci.7b00138> (2018).
36. Wang, Z. & Liu, J.-P. Effects of the central potassium ions on the G-quadruplex and stabilizer binding. *J. Mol. Graph. Model.* 72, 168–177 (2017).
37. Chen, F., Zhao, Y., Fan, C. & Zhao, Y. Mismatch extension of DNA polymerases and high-accuracy single nucleotide polymorphism diagnostics by gold nanoparticle-improved isothermal amplification. *Anal. Chem.* 87, 8718–8723 (2015).
38. Stadhouders, R. et al. The effect of primer-template mismatches on the detection and quantification of nucleic acids using the 5' nuclease assay. *J. Mol. Diagn.* 12, 109–117 (2010).
39. Setti, G. et al. Salivary microRNA for diagnosis of cancer and systemic diseases: a systematic review. *Int. J. Mol. Sci.* 21, 907 (2020).
40. Turchinovich, A., Weiz, L., Langheinz, A. & Burwinkel, B. Characterization of extracellular circulating microRNA. *Nucleic Acids Res.* 39, 7223–7233 (2011).
41. Mariner, P. D. et al. Improved detection of circulating miRNAs in serum and plasma following rapid heat/freeze cycling. *Microna* 7, 138–147 (2018).
42. Mahn, R. et al. Circulating microRNAs (miRNA) in serum of patients with prostate cancer. *Urology* 77(1265), e9-1265.e16 (2011).

43. Deng, H. & Gao, Z. Bioanalytical applications of isothermal nucleic acid amplification techniques. *Anal. Chim. Acta* 853, 30–45 (2015).
44. Islam, M. M., Loewen, A. & Allen, P. B. Simple, low-cost fabrication of acrylic based droplet microfluidics and its use to generate DNA-coated particles. *Sci. Rep.* 8, 8763 (2018).
45. Wang, L., Zhang, Y. & Zhang, C. A target-triggered exponential amplification-based DNzyme biosensor for ultrasensitive detection of folate receptors. *Chem. Commun.* 50, 15393–15396 (2014).
46. Zhao, W., Ali, M. M., Brook, M. A. & Li, Y. Rolling circle amplification: applications in nanotechnology and biodetection with functional nucleic acids. *Angew. Chem. Int. Ed.* 47, 6330–6337 (2008).
47. Jiang, H.-X., Liang, Z.-Z., Ma, Y.-H., Kong, D.-M. & Hong, Z.-Y. G-quadruplex fluorescent probe-mediated real-time rolling circle amplification strategy for highly sensitive microRNA detection. *Anal. Chim. Acta* 943, 114–122 (2016).
48. Heiat, M., Ranjbar, R., Latif, A. M., Rasaee, M. J. & Farnoosh, G. Essential strategies to optimize asymmetric PCR conditions as a reliable method to generate large amount of ssDNA aptamers. *Biotechnol. Appl. Biochem.* 64, 541–548 (2017).

CHAPTER 4: Simple, low-cost fabrication of acrylic based droplet microfluidics and its use to generate DNA-coated particles

Md. Mamunul Islam, Amanda Loewen & Peter B. Allen

*pballen@uidaho.edu

University of Idaho, Dept. of Chemistry, 001 Renfrew Hall, 875 Perimeter Dr,
Moscow, ID 83844-2343

Published in: Scientific Reports, Volume 8, Article number: 8763 (2018).

Published by: Nature

Hydrogel microparticles were copolymerized with surface-immobilized DNA. Particles derived from a microfluidic device and particles derived from mechanical homogenization were compared. The hypothesis was tested that a controlled droplet generation mechanism would produce more homogeneous particles. Surprisingly, the DNA content of both particle types was similarly inhomogeneous. To make this test possible, a simple, low cost, and rapid method was developed to fabricate a microfluidic chip for droplet generation and in-line polymerization. This method used a low-cost laser cutter (\$400) and direct heat bonding (no adhesives or intermediate layers). The flow focusing droplet generator produced droplets and hydrogel particles 10–200 μm in diameter.

4.1 Introduction

We used a low-cost microfluidic technique to test whether mechanical homogenization is responsible for inhomogeneous partitioning of cholesterol-modified DNA into droplets. In our previous work¹, we generated DNA-coated particles for use as biosensors. The particles can be generated by in situ polymerization with DNA localized to the surface by a cholesterol modification. During this work, we noticed that particles were polydisperse in size and inhomogeneous in fluorescent DNA content (even among particles of the same size). We wanted to determine if the droplet generation mechanism was responsible for the

inhomogeneity. We hypothesized that droplets would contain homogenous DNA content if dispersion occurred in a single step (instead of multiple rounds of breakup as in mechanical droplet generation). We found that mechanical homogenization and microfluidic droplet generation methods produce significant inhomogeneity in the DNA contents of the droplets. The similarity between the two results suggests that amphiphilic molecules dispersed into droplets may be partitioned unevenly irrespective of the droplet formation mechanism. This fact should be considered in future applications of droplet microfluidics and analytical methods based on water dispersed in oil.

To test this hypothesis, we required a microfluidic chip so that we could observe and control droplet generation and confirm a single step mechanism. However, we lacked the facilities to produce conventional PDMS microfluidic chips. We developed a method for generating microfluidic chips that is simple and inexpensive and may find use elsewhere. Microfluidics is the use of devices that control fluid on the 1–1000 μm scale. Microfluidic techniques are a multidisciplinary field. The advantages of microfluidics include minimizing sample and reagent, producing minimal waste, simple workflows, and enabling the miniaturization of reactions. Droplet microfluidics use various methods to create discrete volumes for analysis². This enables applications in biomedical imaging, drug discovery, biomolecule synthesis, therapeutics, and diagnostics³. Droplet-based devices generated multifunctional microparticles⁴ and aided single cell studies^{5–7}. There are many more potential future applications of droplet microfluidics⁸. However, the barriers to entry are significant.

The capital requirements to prototype a conventional photolithography-based microfluidic device are high. Photolithography requires an extremely clean environment and a UV exposure system suitable for contact lithography. The photoresists and solvents are also a significant expense. After replication molding of a lithographic master into PDMS, the device is activated with an oxygen plasma cleaner, another high-cost device. With the appropriate equipment, lithography and PDMS can achieve resolution down to $\sim 1 \mu\text{m}$ for between three and forty times higher capital cost than the procedure described here.

We are presenting a low-cost method to build microfluidic chips with resolution on the order

of ~ 100 μm . Several low-cost approaches have been demonstrated to fabricate devices for droplet microfluidics. These include paper fluidic approaches^{9–11}, thermoplastic fabrication^{12,13}, optical adhesive bonding¹⁴, glass etching^{15,16}, and 3D printing^{17–20}. Our method uses PMMA which has advantages over PDMS for generating and maintaining droplets. PDMS is an elastomer widely used in droplet microfluidics^{21–26}. However, its surface properties are variable and change in contact with different organic solvents²⁷. Furthermore, PDMS is permeable to water²⁸. PDMS can also absorb hydrophobic small molecules. Many experiments require time-consuming, expensive surface treatment²⁹. PMMA is a thermoplastic material with excellent transparency, biocompatibility, non-porosity, durability and low-cost availability. PMMA has attracted the attention of the microfluidic community^{30–34}. However, fabrication in PMMA is not as easy as PDMS. It is not elastomeric and not easy to cast. It can be cut with a CO₂ laser³⁵, and several bonding methods have been reported, i.e., adhesive bonding³⁶, solvent bonding³⁷, and thermal bonding^{38,39}. However, adhesives and solvents can occlude the channels and introduce additional (potentially unwanted) materials to the device. High-pressure thermal bonding requires an expensive heated press (e.g., a Carver press costs more than \$9,000). Our reliable method for thermal bonding uses low-cost equipment. Our chips had excellent bonding strength, durability, and optical transparency. For a comparison of this method in approximate cost and features, see **Table 1**.

Our PMMA chips made droplets and we observed the droplet formation process directly with an optical microscope. We found that the flow focusing design could produce droplets from 10 to 200 μm in diameter. After prepolymer droplet formation, the chip chemically initiated polymerization. Polymerization of the droplets produced hydrogel microparticles. We linked hydrogel microparticles to DNA by including a polymerizable modification (called an acrydite). The resulting particles were similarly homogeneous compared to previous methods. DNA coated microparticles were also generated by mechanical homogenization⁴⁰. Mechanical homogenization produces a heterogeneous mixture of bright and dim particles. We hypothesized that this might be due to the droplet formation mechanism. During mechanical homogenization, droplets experience repeated cycles of partitioning of DNA between surface

and solution followed by droplet breakup. Surface DNA may not be equally partitioned into daughter droplets. The microfluidic mechanism does not have multiple cycles of partitioning and droplet breakup. Surprisingly, both mechanisms produced inhomogeneous DNA content, suggesting that another mechanism is at work. This work demonstrates a low-cost approach to probing the particle formation mechanism. We present a low-cost microfluidic fabrication, reliable bonding without a bonding layer or adhesive, microfluidic droplet generation, and in situ polymerization to generate particles coated with DNA. The low cost and simple protocol make our process easily adaptable to any lab interested in applying droplet microfluidics. Our technique allowed us to determine that droplet generation creates inhomogeneous composition irrespective of either generation mechanism: homogenization or flow-focusing droplet formation. This fact has implications for any droplet microfluidic application where chemicals may partition to the oil-water interface. Scientists in the field should be aware that the content of their droplets may be inhomogeneous.

Table 4.1 Comparison of alternative fabrication methods for droplet microfluidic devices.

Technique	Resolution	Cost/chip	Setup Cost	Transparency	Droplet size
Photolithography ⁵¹	<1 μm	\$2	\$20,000+	Yes	\sim 1 μm
Low cost PDMS ⁵²	30 μm	\$2	\$1500+	Yes	\sim 50 μm
3D printing ⁵³	200 μm	\$2	\$3,000	Partial	\sim 100 μm
Injection molding ⁵⁴	300 μm	\$0.1	\$1,000	Yes	\sim 100 μm
Paperfluidics ⁵⁵	50 μm	\$0.01	\$400	Partial	50 μm
Pipette/tubing ⁵⁶	n/a	\$1	\$500	No	75 μm
Previous laser cut ³⁵	100 μm	\$1	\$20,000	Yes	n/a
K40 laser (this work)	100 μm	\$1	\$500	Yes	10 μm

4.2 Materials and Methods

4.2.1 Microfluidic chip fabrication

A 1mm thin cover layer (Extruded XS Acrylic, Aliexpress) and a 2mm thick channel layer (Plexiglas®, Tri-State hardware) were etched and cut to form microfluidic chips. Supplementary Fig. S11 shows the assembly for bonding the microfluidic chip components. LaserDRW software was used to create the designs for all chips. A K40 type laser cutter with

a 40-watt CO₂ laser tube was used to cut the designs into the acrylic. Model F-LM1390, by FLM, China was used for this study; comparable K40 cutters are available from various Chinese manufacturers sold on Amazon and eBay. These laser engraver/cutter devices should be treated with extreme care. Laser safety precautions must be followed including laser safety goggles and good ventilation. The device should be regarded as a laboratory or research grade laser, not a consumer device.

In the design, access holes were cut first; the deepest channels were then etched to a depth of 600 μm , and shallow channels were etched last by increasing the laser head translation rate. After the channels were etched, the chip was cut free from the bulk material. The acrylic plugs left in the access holes were punched out with a blunt syringe needle. All features were cut into the thicker 2mm acrylic (unless otherwise specified). The 1mm thick acrylic was then placed over the top to seal the channels. Paper spacer was placed around the perimeter of the press to aid in uniform pressure distribution on the chips placed at the center of a heated platform. A spacer of 32 sheets of paper with an uncompressed thickness of 3mm was used. The whole assembly was then placed in a heated press (Promo Heat, Tamarac, FL, Model HP230B) at 145 °C for 10minutes under $\sim 60\text{N}$ of force from the mass of the press plus the applied force on the handle (measured with Vernier force probe). For a schematic and image of the press and assembly, see Supplemental Information **Figure 4.S1**.

4.2.2 Characterization of the droplet generator design performance

An optical microscope (Omano, microscopes.com, Roanoke, VA) with a 10 \times objective lens and Toupview software were used to capture and analyze light microscopy images. It should be noted that the triangular profile of the channels can give the appearance of shadows, charring, or blurring under brightfield microscopy and that careful illumination adjustment is necessary. For clearer wide field images, an Olympus PEN E-PL2 with a Nikon Micro Nikkor lens was used. The acrylic chips were connected to syringe pumps by stainless steel tubing (stainless steel, 20 gauge). Stainless steel tubing was also cut and glued into the channel inlets. Polyethylene micro medical tubing (95 durometer, Scientific Commodities Inc., Lake Havasu City, AZ) was stretched over the stainless-steel tubing to act as connecting joints. Water droplets were

injected dispersed oil medium to form the droplets. 5mL HSW NORM-JECT (Henke-Sass, Wolf GmbH, Germany) syringes were used for oil injection. A 1mL SOFT-JECT latex free Luer syringe (Henke-Sass Wolf) was used for aqueous injection.

Flow rates were controlled by motor driven syringe pumps (NE-300, New Era Pump Systems, NY USA and KD Scientific 210, Holliston, MA 01756 USA). The aqueous phase consisted of blue food dye in deionized water, and the oil phases were parafin oil (Fisher Scientific Company, NJ) with 1% Span 80 (Sigma-Aldrich, St Louis, MO USA) to act as a surfactant. Each chip was placed on the light microscope under a 10× objective lens during operation. An image of the droplets produced was first taken 1.5 minutes after the flow rates were altered. Additional images were taken every subsequent 15 seconds for 75 seconds. The aqueous flow rate was varied between 1 and 10 $\mu\text{L}/\text{min}$ and the first oil flow rate were varied between 20 $\mu\text{L}/\text{min}$ and 100 $\mu\text{L}/\text{min}$. The flow rate of the second oil phase was set to 30 $\mu\text{L}/\text{min}$ and held constant for each trial. This test was repeated for chips that had been cut with wide, standard, and narrower channels.

4.2.3 Particle generation by microfluidics

A microfluidic droplet generator chip was attached directly to syringes using bent syringe needles. The needles were sealed with glue (All-Temperature Hot Glue Stick, Gorilla glue company, Cincinnati, OH, USA). The aqueous phase (dispersed phase) was composed as follows: 89 mM Tris base (Ampresco, OH); 89mM Boric Acid (Research Product Intl. Corp, IL USA); 2 mM EDTA (Thermo Fisher Scientific); 5 μM of “Acryd.F.DNA” (5' Acrydite-ATT ATA GCG GCA CAG AGA C-3' fluorescein); and 5 μM of complementary, cholesterol-modified DNA (5'-CCG ACC TTA GTC TCT GTG CCG CTA TAA T-3' Chol.). DNA was purchased from IDT, Coralville, IA USA and was used without further purification. The aqueous phase was annealed in a Thermocycler at 85 °C for 3 min then cooled slowly to room temperature. Acrylamide was added to the aqueous mixture to achieve a final concentration of wt. 10% (Research Product Intl. Corp, IL USA). Ammonium persulfate (Bio-Rad Laboratories, Hercules, CA USA) was added to achieve a final concentration of wt. 0.8%. The first oil phase (continuous phase) was composed of 1% Span 80 (Sigma-Aldrich, St Louis, MO USA) in parafin oil (Fisher Scientific

Company, NJ USA). The initiator oil phase consisted of 1% Span 80 in parafin oil mixed with 0.6% TEMED (Bio-Rad Laboratories, Hercules, CA USA). Flow rates were initially set at 1 $\mu\text{L}/\text{min}$ aqueous phase, 100 $\mu\text{L}/\text{min}$ of the first oil phase, and 30 $\mu\text{L}/\text{min}$ of the initiator oil phase. After the droplets were generated and polymerized into particles, the oil was removed by centrifugation. The collection vial was centrifuged at 16,000 \times G for 20 minutes. The supernatant oil was removed by pipette. The vial was then refilled with ethanol (Pharmco-AAPER, Brookfield CT, USA), vortexed, and centrifuged in a low-speed centrifuge for three consecutive washes to remove residual oil. The particles were then air dried for 15min and re-suspended in Tris-Chloride buffer (100 mM, pH 7.6) containing 0.1% Triton X-100 (KODAK Eastman Chemicals, Rochester NY, USA). Fluorescence micrographs were acquired using an LED fluorescence microscope (LumaScope 620, Etaluma, Carlsbad, CA USA) with a 20 \times lens.

4.2.4 Particle generation by homogenization

Polyacrylamide particles were also created using the homogenization method, as described elsewhere⁴⁰. Briefly, the DNA-bearing aqueous phase was prepared as per above. The aqueous phase was placed in a 2 mL centrifuge tube with a ¼ inch ball bearing and 1mL of parafin oil containing 1% Span 80. The vial was shaken by hand for 10 seconds to obtain droplets of comparable size to those made by the microfluidic chips. The ball bearing was removed, and 8 μL of TEMED was then added to the suspension and mixed by gentle shaking. The vial was then purged with nitrogen for 30–40 min at room temperature. The resulting particles were washed, dried, and photographed as described above.

4.3 Results and Discussion

4.3.1 Characterization of laser cutter performance

Our low-cost (\$400) laser cutter had several limitations. The CO₂ laser power was low compared to other laser cutters. The laser head showed irreproducible motion at fast cut speeds. This initially contributed to high rates of failure for small channels.

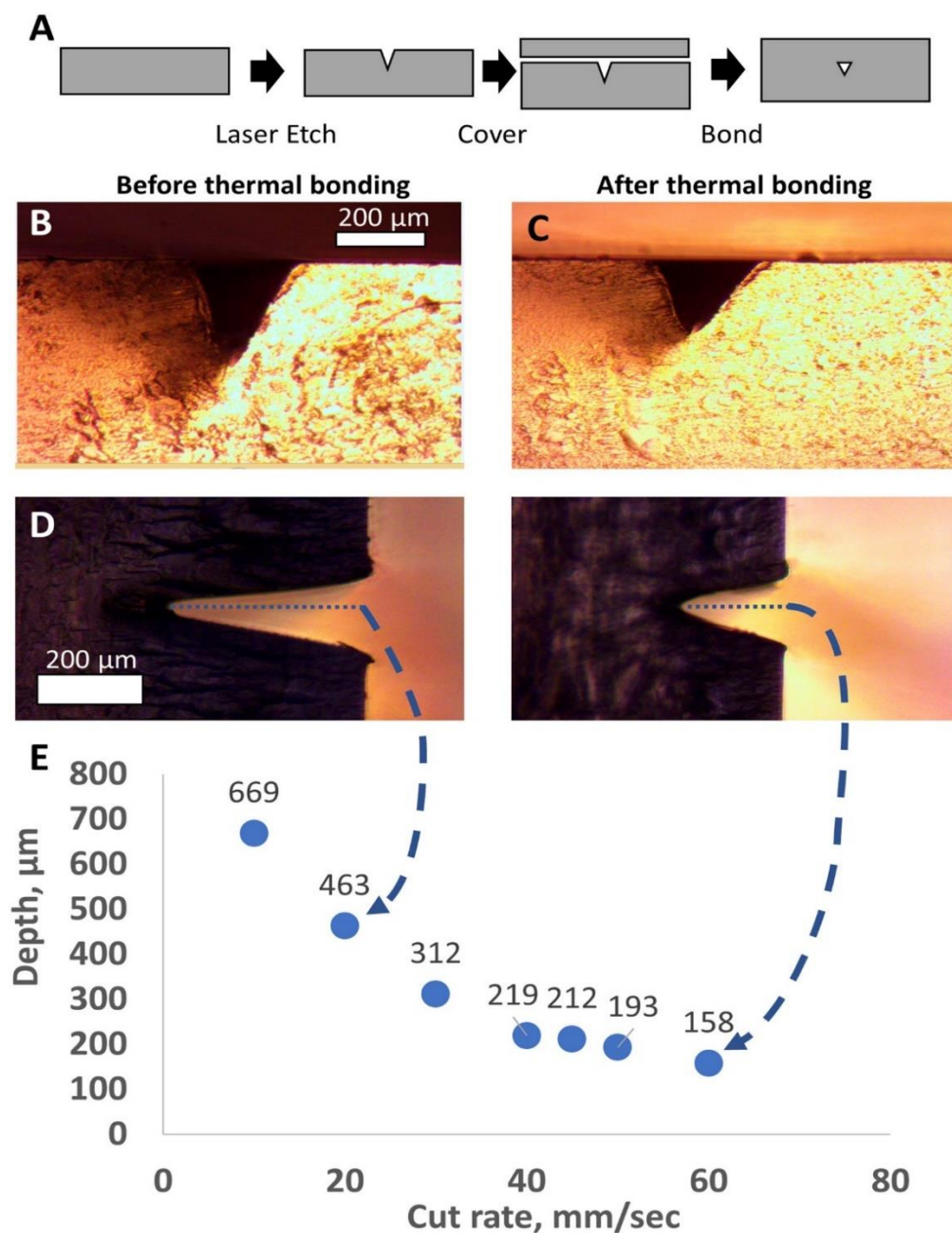


Figure 4.1. Characterization of laser etching process for generating microfluidic chips. (A) Flow diagram of the fabrication and thermal bonding process. (B) Cross-sectional images before and (C) after thermal bonding. (D) Micrographs show the measured depth of the channels in two test cases. (E) Graph shows the depth of the fluid channel as a function of laser head translation rate.

Power settings were re-calibrated weekly to achieve reproducible results. Calibration was performed by a rapid and simple operation requiring only ~ 5 minutes. A piece of PMMA sheet

of 1 mm thickness was placed in the laser cutter. Paper backing was removed from the top side only. A straight line was programmed into the software with a 10 mm/sec translation rate. The analog power knob was increased from zero until the backing paper was visibly ablated by the laser. This was easy to see. Acrylic plastic is removed without any light generated; the backing paper produces a bright yellow flare. At the calibration power setting when the laser barely penetrates 1 mm of acrylic, about 0.7 watts of power were absorbed by the target (based on the rate of acrylic vaporization and the energy of vaporization)⁴¹. Originally, this power setting was ~40% of the maximum power setting on the power knob. After 3 months, ~50% of the maximum power setting was required to achieve the same result. We note that this is significantly lower than the advertised maximum 40 watts of the laser. When operated with optimal parameters, the K40 laser cutter generated microfluidic devices with reproducible features. We set the laser to the calibrated power setting as described above. At this setting, there was an inverse correlation between the laser head translation speed and the depth of the channels produced (see **Figure 4.1E**).

We used this relationship to create chips with desired feature sizes. Before bonding, minimal feature sizes were ~200 μm wide. After bonding, shallow channels were narrower (**Figure 4.1B, C**). We could occasionally produce channels as narrow as 50 μm . Channels ~150 μm wide with 200–300 μm of space between them were produced very reliably (see reliability data in Supplementary **Figure 4.S3**). With careful calibration of temperature and time, smaller channels could be generated as the acrylic fuses and channels shrink under pressure.

4.3.2 Development of acrylic device bonding protocol

Acrylic chips were etched with a CO₂ laser and bonded with heat and pressure. Fig. 1A shows a schematic of the laser cutting and thermal bonding processes. Access holes were cut through a 2mm thick piece of acrylic and successively shallower channels were etched by adjusting laser cut speed. The cut and etched acrylic chip were then covered with a second, 1 mm thick acrylic sheet. The two pieces were bonded with a heated press using heat and pressure as described in Materials and Methods.

We optimized the fabrication protocol by varying the bonding parameters of spacer height,

time, and temperature. After numerous iterations of the protocol, we determined the spacer thickness to be the most influential factor of the bonding process. Slight changes (even two sheets of paper or $\sim 90 \mu\text{m}$) made the difference between channel collapse and incomplete bonding. With the correct number of paper spacer sheets (32 sheets for the 3 mm thick acrylic assembly), chips could be generated over a range of temperatures (135–155 °C) and times (10–20 min). We found that 145 °C for 10min yielded the most consistent results as noted in the Materials and Methods. At these temperatures, the acrylic is soft. High pressure fattens the acrylic assembly; the use of the paper spacer maintains assembly integrity.

Images of the channel were captured before and after bonding (**Figure 4.1D, E**). The channel dimensions changed less than 15% with bonding. By adjusting cutting parameters, channels with the appropriate depth can be cut in order to achieve the desired final result. The bonding temperature of 145 °C is well above the glass transition temperature T_g , 105 °C of the acrylic plastic⁴². At these temperatures, mobile polymer chains diffuse into one another at the interface, forming a strong bond.

We analyzed the applied pressure with Fujifilm pre-scale tactile pressure indicating sensor film (ultra-low range, 190 to 590 kPa). The film indicated that before bonding, the distribution of pressure was concentrated at the edges. After bonding, we found that the pressure was more evenly distributed across the chip surface (Supplemental Information, **Figure 4.S2**). We interpret these results to indicate that the acrylic assembly deformed and thinned to disperse the applied pressure.

At sub-optimal bonding parameters, the most common failure mode was channel blockage. Failure occurred most frequently within 50 μm of the inlets and at intersections. Channels of width less than 100 μm were associated with mid-channel collapse. Chips etched with large channels often showed a “ridge” of re-deposited acrylic material adjacent to the channel. This ridge was a persistent source of blockage. Blockage frequency was reduced when the deepest channels were etched first, and shallower channels etched last. Chips performed best when inlet and outlet holes were cut first, the channel network (deep before shallow) cut second, and the perimeter through-cut performed last. Re-deposition was not a problem for shallow

channels. If the etching is carried out in the preferred order, (deep followed by shallow) the small amount of re-deposition from etching shallow channels does not occlude large channels. However, if the device is produced by etching shallow channels first, the large quantity of ablated PMMA produces sufficient re-deposition to occlude the shallow channels. The laser cutter produced features with a minimum width of $\sim 50\ \mu\text{m}$ and a depth of $\sim 100\ \mu\text{m}$. However, even with optimal bonding settings, small channels showed a high rate of failure. When settings were tuned to produce an etch depth of 200–700 μm , the optimized process showed high reliability (for fabrication success rates at various channel depths, see Supplemental Information, **Figure 4.S3**).

4.3.3 Particle generator chip behavior

We designed a microfluidic device to generate and polymerize droplets into particles. Our droplet generator used a flow-focusing design. This design introduces a flow of aqueous solution (dispersed phase) into a rapid flow of oil (continuous phase) at a cross junction. The dispersed phase is forced into a narrow cone, which breaks up into droplets. Our droplet generator is shown in **Figure 4.2A**. This design was cut into acrylic sheets and bonded in the manner described above. We connected the device to syringe pumps to deliver oil and aqueous flows as shown in **Figure 4.2B**. For clarity, the aqueous phase was dyed blue, and the second oil phase was dyed red. A high-speed movie of droplet generation is also included in Supplemental Information. Our design introduces oil to the flow at two locations. In the flow-focusing system, the dispersed aqueous phase (with blue dye) and continuous oil phase (clear paraffin oil containing 1% Span 80) were mixed at a cross junction. Aqueous droplets were formed in the continuous oil phase. We left a space of 1 cm between initial droplet formation and introduction of the initiator. This allowed for droplet relaxation to a spherical shape prior to polymerization. Designs produced non-spherical particles when droplet formation and polymerization were too close. Polymerization was initiated by introducing a second oil phase containing TEMED.

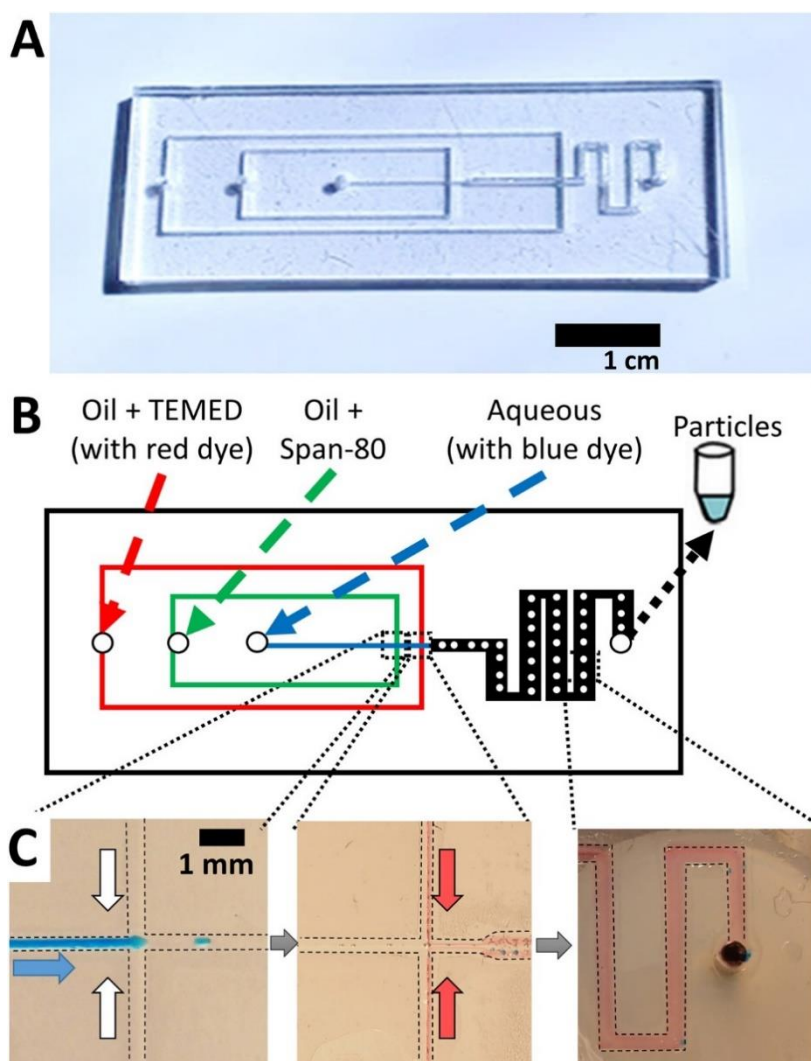


Figure 4.2. Design and operation of the microfluidic particle generator. (A) Photograph shows the finished microfluidic particle generator. (B) A schematic shows the design and identity of each fluid inlet and outlet. (C) Digital photographs show blue aqueous fluid (indicated by blue arrow) and clear or red oil (indicated by white and red arrows) flowing in the chip. Blue droplets are generated at the first junction. Red oil representing initiator is introduced at the second junction. A mixing region precedes the exit of the microfluidic chip. Dashed lines indicate margins of the channels.

In **Figure 4.2C**, this second oil phase contained Sudan red to allow confirmation of mixing the oil phases within the device. This design generated water droplets with well mixed red oil at the outlet of the device. We obtained the most homogeneous results when we used blunt syringe needles to directly connect the syringe pumps (see Supplemental Information, **Figure 4.S4** for a picture of our optimal setup).

4.3.4 Effect of flow rate on droplet size

We tested the effects of different flow rates and channel dimensions on droplet size. We generated droplets by using three microfluidic particle generator chips and variable oil and aqueous flow rates.

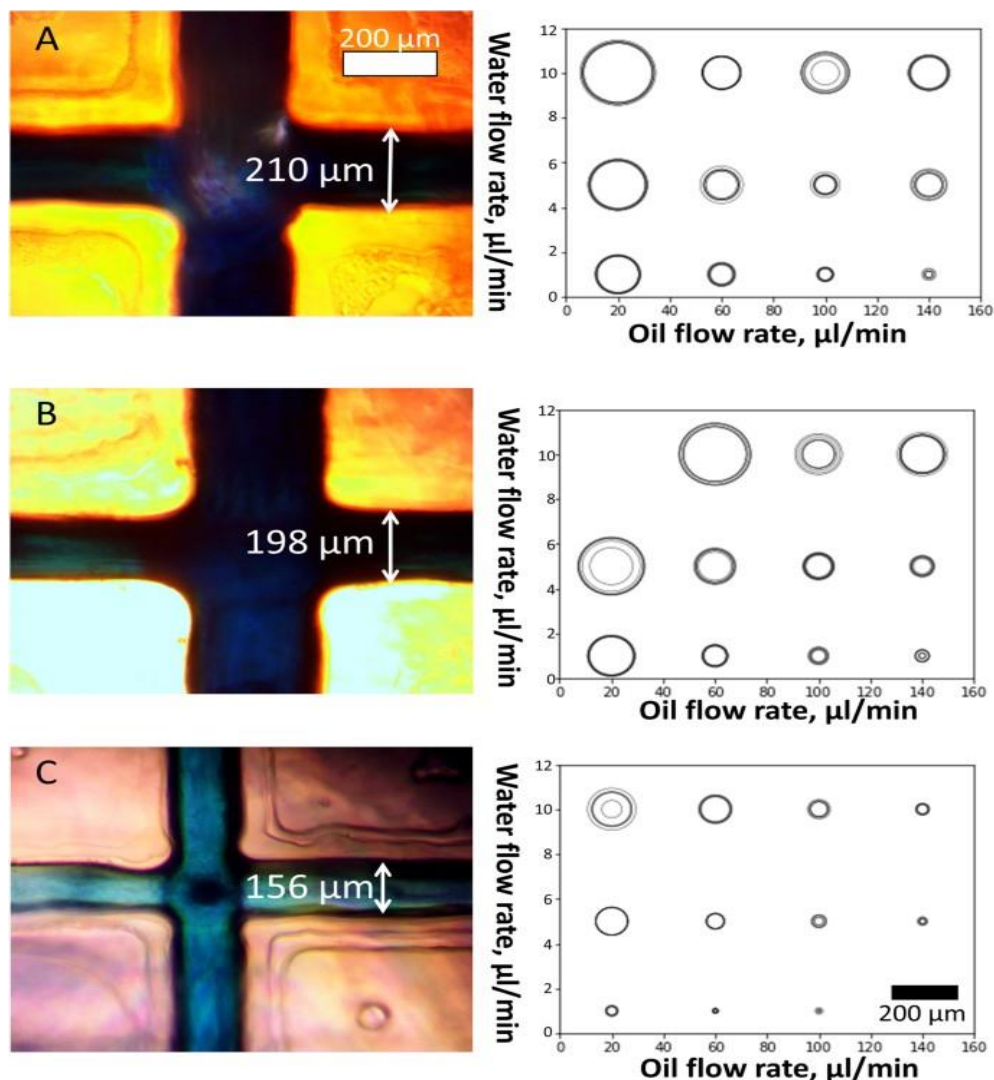


Figure 4.3. Effect of flow rate and channel size on droplet size. Droplet generator channels are shown at left.

Scatter plots at right show the effect of oil and water flow rate on droplet diameter. A 200 μm scale bar is shown in the bottom right. The size of the outlet channel in which droplets were generated was (A) 210 μm , (B) 198 μm , and (C) 156 μm at the base of the triangular channel profile. Flow rate combinations that produced oscillating droplet diameters are represented as concentric circles in the scatter plot, with circle size proportional to the range of droplet sizes produced.

The resulting data are summarized in **Figure 4.3A–C**, shown from largest to smallest (210, 198 and 156 μm wide at the surface, respectively). Some flow rate combinations produced

oscillations in the observed droplet diameters.

Flow rate had a greater influence on droplet size than channel size. The size of the droplets ranged from $\sim 10\ \mu\text{m}$ to $\sim 200\ \mu\text{m}$ for all microfluidic particle generators tested. The lower bound for droplet size was defined by the channel dimensions. Smaller channels were required to produce the smallest droplets ($<10\ \mu\text{m}$) at high oil and low aqueous flow rates. Reliable, small droplet generation occurred at an aqueous flow rate of $1\ \mu\text{L}/\text{min}$ and an oil flow rate of $100\ \mu\text{L}/\text{min}$. Once a steady state flow rate was achieved, droplet generation became stable. The continuous oil phase flow rate was then increased to $170\ \mu\text{L}/\text{min}$ and the oil containing TEMED introduced at $30\ \mu\text{L}/\text{min}$. These parameters were used to generate particles for subsequent experiments.

4.3.5 Generation of polyacrylamide particles containing DNA

DNA-coated hydrogel microparticles were synthesized by in situ polymerization of the droplets generated using the microfluidic particle generator. Acrylamide and Ammonium persulfate were included in the aqueous phase and TEMED in the second oil phase (see **Figure 4.2**).

Consecutive droplets are very similar in size. We photographed a set of droplets before they exited the chip and found a standard deviation of their diameters of less than 5% ($N=50$, see **Figure 4.4A**). However, when we generated droplets over a span of minutes or hours, the pressure slowly changes (likely due to the pulsation of the syringe pumps). Therefore, the pooled sample of particles contains a significantly higher polydispersity.

Acrylamide polymerization occurred downstream of the mixing intersection with resultant stable polyacrylamide particle formation.

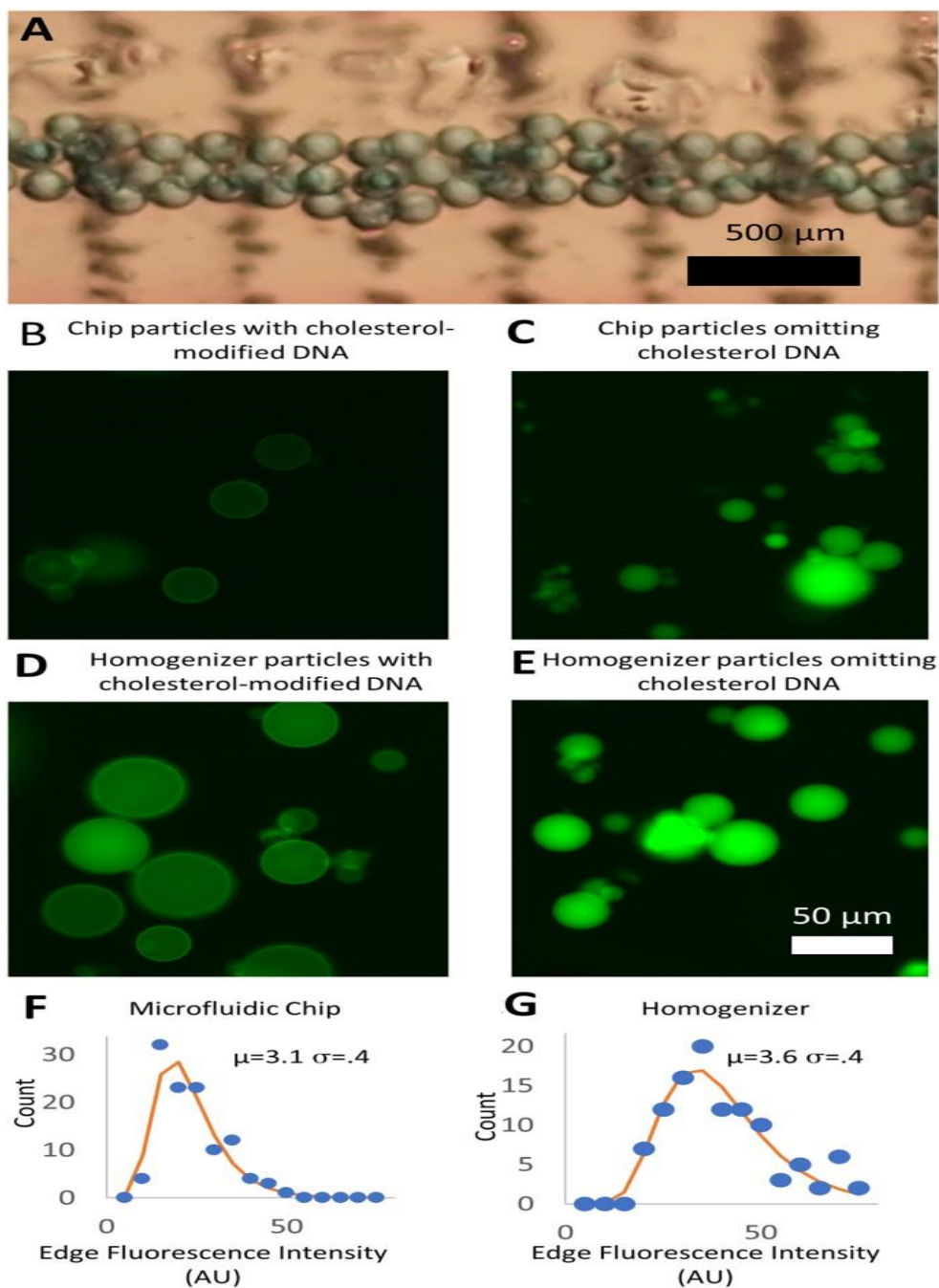


Figure 4.4. Characteristics of droplets and particles. (A) Light microscope image shows consecutive droplets within the particle generator chip connected to syringe pumps. Acrylamide droplets were then polymerized into polyacrylamide particles. (B–E) Fluorescence micrographs show polyacrylamide particles containing fluorescein-modified DNA. (B) Microparticles were generated by a microfluidic chip with cholesterol modified DNA and (C) without cholesterol-modified DNA. Polyacrylamide microparticles were also generated using mechanical homogenization (D) containing DNA with cholesterol and (E) without cholesterol. (F) Histograms show the distribution of cholesterol-modified DNA at the surface of particles manufactured using the microfluidic generator and (G) those manufactured using mechanical homogenization.

We used an oil flow rate of 150 $\mu\text{L}/\text{min}$, initiator flow of 30 $\mu\text{L}/\text{min}$ and an aqueous flow rate of 1 $\mu\text{L}/\text{min}$. The particle sizes ranged from 10–30 μm . Particles obtained from this reaction are shown in **Figure 4.4B**.

The aqueous stream contained DNA modified with fluorescein. The fluorescent DNA confers green fluorescence. The acrydite modification on the same DNA complex has a double bond, which polymerized into the polymer structure. When the DNA is also modified with cholesterol, it localizes the DNA to the surface. The cholesterol prefers the oil phase and so the DNA segregates to the oil-water interface after droplet formation. Polyacrylamide microparticles with cholesterol are shown in **Figure 4.4B** and those without cholesterol are shown in **Figure 4.4C**.

To measure the consistency of the particles' surface DNA composition, fluorescein-modified DNA at the surface of the particle was imaged using a fluorescence microscope. The fluorescence intensity at the edge of cholesterol-modified particles was quantified with ImageJ. Particles generated by microfluidic chips were similarly consistent in their DNA distribution compared to particles generated by mechanical homogenization. We fit a lognormal distribution to the histogram of particle edge intensities. The sigma (width) term of the lognormal fit was nearly the same for both cases (see **Figure 4.4F, G**).

4.4 Conclusions

DNA-coated particles have been used in diverse experiments, from studies of self assembly⁴³ to assays probing DNA methylation⁴⁴ and multiplex PCR suspension arrays⁴⁵. In our previous work, we generated DNA-coated “detector particles” by homogenization¹. In this work, we have tested the performance of a microfluidic droplet generator for generating fluorescent, DNA-coated hydrogel microparticles using low-cost microfluidics. We polymerized droplets into microparticles coated with DNA within the chip. This microfluidic technique is an alternative method for generating DNA-coated particles for capture and detection of nucleic acid analytes. This method creates droplets through a controlled mechanism that are comparable to mechanically dispersed particles.

We expected to find a difference in the particle DNA content because of the different mechanisms of droplet formation. In the case of microfluidic droplet generation, the composition of the droplet is fixed after generation; there was no subsequent coalescence or breakup. The flow focusing mechanism of droplet formation has been demonstrated in the literature; work with PDMS chips has clearly shown that the flow focusing droplet and particle generation proceeds consistently with our observations⁴⁶. In the case of mechanically homogenized droplets, a given droplet may be broken into smaller droplets multiple times. Every time an unpolymerized droplet breaks apart, there is an opportunity for uneven segregation of DNA to the daughter droplets. However, we discovered no significant difference in the DNA distribution with chip-derived particles. This suggests DNA content inhomogeneity is a result of another, more fundamental process.

Multiple analytical techniques use droplet generation to compartmentalize reactions. Our results suggest that molecules that self-segregate to the oil-water interface may not compartmentalize evenly into droplets. This may have implications for droplet-based technique such as digital PCR⁴⁷ or droplet-based directed evolution experiments⁴⁸.

To test the relationship between droplet formation mechanism and DNA content, we developed a method to create transparent PMMA microfluidic chips with an ultra-low-cost laser cutter and heated press. The device can generate microfluidic chips with features down to $\sim 100\ \mu\text{m}$ wide and $\sim 200\ \mu\text{m}$ deep with a very high success rate. Using a flow-focusing design, these devices could generate droplets and polymerized particles down to $\sim 10\ \mu\text{m}$ in diameter. This technique adds to the repertoire of rapid microfluidic fabrication alternatives such as double-sided tape and paper fluidics. It has the advantage of using only one material (no adhesives or bonding layers). Acrylic devices are well suited to droplet applications. They stretch less than PDMS and have a more stable surface. This low-cost option could help other researchers apply microfluidic approaches.

We can divide the possible mechanisms for the observed inhomogeneity in DNA content into three major categories: fluid dynamics, polymerization, and the chemistry of the oil/water interface. We anticipate that better control over fluid dynamics can produce more

monodisperse droplets. A constant pressure source will likely produce better results than the pulsatile pressure delivered by syringe pumps. When consecutive droplets are measured (as in Fig. 4A), they are monodisperse compared to pooled particles from minutes or hours of particle generation (Fig. 4D). Slight variations in pressure over time as the syringe and tubing adjust to the pulsatile pump driven flow may contribute to the observed variability. However, this is unlikely to affect the DNA composition. The dynamics of droplet formation and breakup are vastly different between the homogenized and microfluidically generated droplets. As such, fluid dynamics seem to be an unlikely cause of the common inhomogeneity in surface DNA.

The polymerization and surfactants are the same in both the mechanical and microfluidically generated droplets. The polymerization process was initiated by external TEMED in both methods for particle generation. According to Quong et al.⁴⁹, the initiation of gelation from internal chemistry (e.g. with UV photo initiators as per Yuet et al.⁵⁰) can have different effects as compared to external initiation (as in this design). This may be offset by the relatively small particles and short diffusion lengths. The third possibility is that the oil and surfactant chemistry is the cause of the inhomogeneity. In future work, it will be valuable to use mechanical homogenization to explore the possibility of internal initiation of polymerization and a survey of several combinations of oil and surfactant to resolve this question.

4.5 Supplementary information

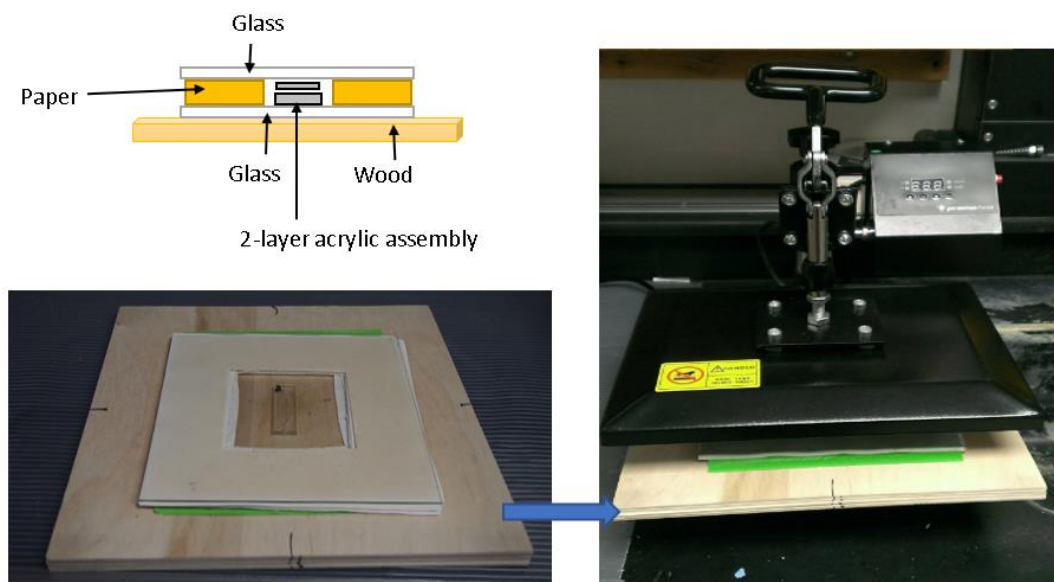


Figure 4.S1. Heated press assembly. Top left shows a diagram of the assembly used in the heated press. Bottom left shows the assembly before being placed in the heated press. Right shows the assembly after being placed in the heated press.

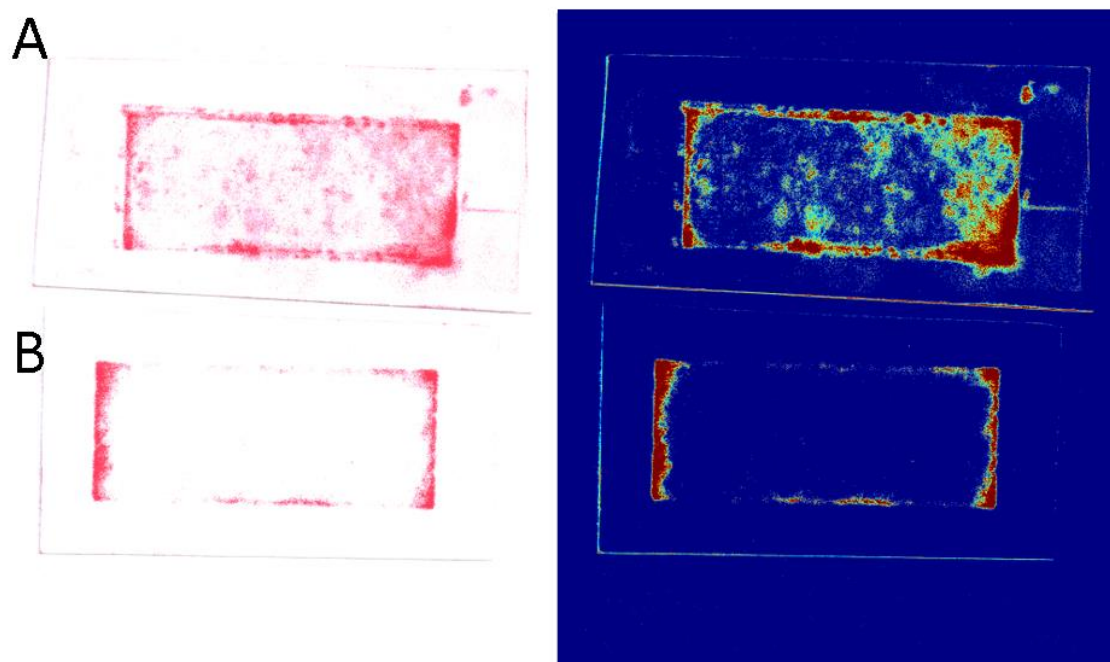


Figure 4.S2. Pressure after and before chip sealing. (A) Photograph of pressure sensitive film (28 - 85 PSI dynamic range) placed between the glass and the chip in the heated press after heat bonding the chip and cooling. Left is true color; right is false color to show contrast. (B) Photograph of pressure sensitive film placed between the glass and the chip in the heated press before heat bonding the chip. Left is true color; right is false color to show contrast.

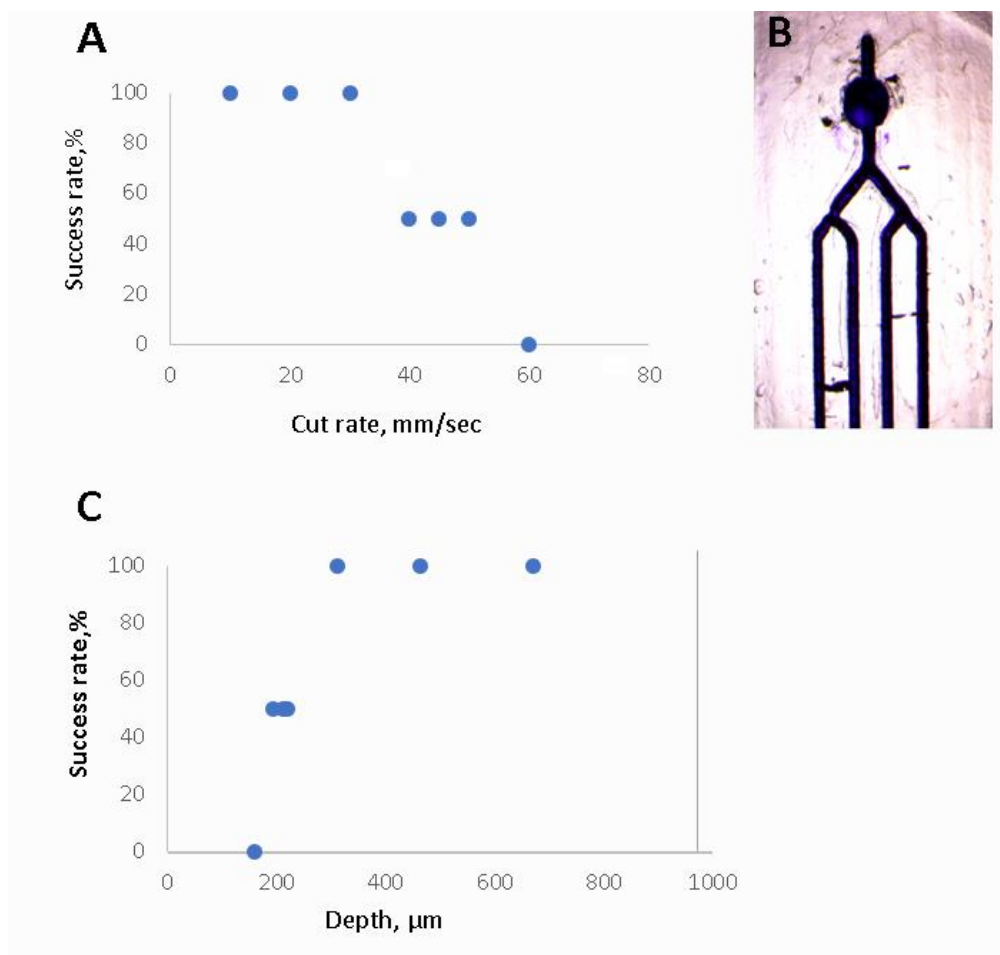


Figure 4.S3. Success rate of channels at various conditions. (A) Graph of successful channels as a function cut rate used to fabricate channels. (B) Photograph of the 4-channel chip filled with blue dye. Successful channels filled through to the end; failed channels were blocked. (C) Successful channel % as a function of the channel depth calculated based on the cut rate and calibration curve described above.



Figure 4.S4. Photograph of particle generation chip in operation. Left syringe contains the aqueous phase; top syringe contains the oil phase; right syringe contains the initiator solution.

4.6 Acknowledgements

Undergraduate fellowship support was provided through the Renfrew Scholarship at the University of Idaho.

4.7 Author Contributions

P.B.A. and M.M.I. wrote the main manuscript text; M.M.I. prepared Figures 4.1, 4.2 and 4.4. A.L. prepared Figure 4.3 and contributed to the preparation and design of microfluidic chips. All authors contributed to the design and execution of experiments.

4.8 Competing Interests

The authors declare no competing interests.

4.9 References

1. Damase, T. R., Spencer, A., Samuel, B. & Allen, P. B. Biomimetic Molecular Signaling using DNA Walkers on Microparticles. *Sci. Rep.* 7, 4081 (2017).
2. Hong, J. W. & Quake, S. R. Integrated nanoliter systems. *Nat. Biotechnol.* 21, 1179–1183 (2003).
3. Teh, S.-Y., Lin, R., Hung, L.-H. & Lee, A. P. Droplet microfluidics. *Lab. Chip* 8, 198 (2008).
4. Prasad, N., Perumal, J., Choi, C.-H., Lee, C.-S. & Kim, D.-P. Generation of Monodisperse Inorganic–Organic Janus Microspheres in a Microfluidic Device. *Adv. Funct. Mater.* 19, 1656–1662 (2009).
5. Brouzes, E. et al. Droplet microfluidic technology for single-cell high-throughput screening. *Proc. Natl. Acad. Sci. USA* 106, 14195–14200 (2009).
6. Konry, T., Golberg, A. & Yarmush, M. Live single cell functional phenotyping in droplet nano-liter reactors. *Sci. Rep.* 3, 3179 (2013).
7. Mazutis, L. et al. Single-cell analysis and sorting using droplet-based microfluidics. *Nat. Protoc.* 8, 870–891 (2013).
8. Sackmann, E. K., Fulton, A. L. & Beebe, D. J. The present and future role of microfluidics in biomedical research. *Nature* 507, 181–189 (2014).
9. Yang, J. et al. Paper-fluidic electrochemical biosensing platform with enzyme paper and enzymeless electrodes. *Sens. Actuators B Chem.* 203, 44–53 (2014).

10. Carrilho, E., Martinez, A. W. & Whitesides, G. M. Understanding Wax Printing: A Simple Micropatterning Process for Paper-Based Microfluidics. *Anal. Chem.* 81, 7091–7095 (2009).
11. Jenkins, G. et al. Printed electronics integrated with paper-based microfluidics: new methodologies for next-generation health care. *Microfluid. Nanofluidics* 19, 251–261 (2015).
12. Agresti, J. J. et al. Ultrahigh-throughput screening in drop-based microfluidics for directed evolution. *Proc. Natl. Acad. Sci.* 107, 4004–4009 (2010).
13. Najah, M. et al. Droplet-Based Microfluidics Platform for Ultra-High-Throughput Bioprospecting of Cellulolytic Microorganisms. *Chem. Biol.* 21, 1722–1732 (2014).
14. Wägli, P. et al. Microfluidic Droplet-Based Liquid–Liquid Extraction and On-Chip IR Spectroscopy Detection of Cocaine in Human Saliva. *Anal. Chem.* 85, 7558–7565 (2013).
15. Nabavi, S. A., Vladisavljević, G. T., Gu, S. & Ekanem, E. E. Double emulsion production in glass capillary microfluidic device: Parametric investigation of droplet generation behavior. *Chem. Eng. Sci.* 130, 183–196 (2015).
16. Gundabala, V. R., Martinez-Escobar, S., Marquez, S. M., Marquez, M. & Fernandez-Nieves, A. Celloidosomes® via glass-based microfluidics. *J. Phys. Appl. Phys.* 46, 114006 (2013).
17. Benjamin, H. C. M., Huan, N. S., Holden, L. K. H. & Yoon, Y.-J. 3D printed microfluidic for biological applications. *Lab. Chip* 15, 3627–3637 (2015).
18. Zhang, J. M., Aguirre-Pablo, A. A., Li, E. Q., Buttner, U. & Toroddsen, S. T. Droplet generation in crossflow for cost-effective 3D-printed “plug-and-play” microfluidic devices. *RSC Adv.* 6, 81120–81129 (2016).
19. Kang, D.-K. et al. 3D Droplet Microfluidic Systems for High-Throughput Biological Experimentation. *Anal. Chem.* 87, 10770–10778 (2015).
20. Morgan, A. J. L. et al. Simple and Versatile 3D Printed Microfluidics Using Fused Filament Fabrication. *Plos One* 11 (2016).

21. Duffy, D. C., McDonald, J. C., Schueller, O. J. A. & Whitesides, G. M. Rapid Prototyping of Microfluidic Systems in Poly(dimethylsiloxane). *Anal. Chem.* 70, 4974–4984 (1998).
22. Bawazer, L. A. et al. Combinatorial microfluidic droplet engineering for biomimetic material synthesis. *Sci. Adv.* 2, e1600567 (2016).
23. Trantidou, T., Elani, Y., Parsons, E. & Ces, O. Hydrophilic surface modification of PDMS for droplet microfluidics using a simple, quick, and robust method via PVA deposition. *Microsyst. Nanoeng.* 3, micronano201691 (2017).
24. Bardin, D. & Lee, A. P. Low-Cost Experimentation for the Study of Droplet Microfluidics. *Lab. Chip* 14, 3978–3986 (2014).
25. Li, Z., Hou, L., Zhang, W. & Zhu, L. Preparation of PDMS microfluidic devices based on drop-on-demand generation of wax molds. *Anal. Methods* 6, 4716–4722 (2014).
26. Velve-Casquillas, G., Le Berre, M., Piel, M. & Tran, P. T. Microfluidic tools for cell biological research. *Nano Today* 5, 28–47 (2010).
27. Lee, J. N., Park, C. & Whitesides, G. M. Solvent compatibility of poly(dimethylsiloxane)-based microfluidic devices. *Anal. Chem.* 75, 6544–6554 (2003).
28. Zheng, B., Roach, L. S. & Ismagilov, R. F. Screening of Protein Crystallization Conditions on a Microfluidic Chip Using Nanoliter Size Droplets. *J. Am. Chem. Soc.* 125, 11170–11171 (2003).
29. Toepke, M. W. & Beebe, D. J. PDMS absorption of small molecules and consequences in microfluidic applications. *Lab. Chip* 6, 1484–1486 (2006).
30. Hong, T.-F. et al. Rapid prototyping of PMMA microfluidic chips utilizing a CO₂ laser. *Microfluid. Nanofluidics* 9, 1125–1133 (2010).
31. Yu, H., Chong, Z. Z., Tor, S. B., Liu, E. & Loh, N. H. Low temperature and deformation-free bonding of PMMA microfluidic devices with stable hydrophilicity via oxygen plasma treatment and PVA coating. *RSC Adv.* 5, 8377–8388 (2015).
32. Ogilvie, I. R. G. et al. Reduction of surface roughness for optical quality microfluidic devices in PMMA and COC. *J. Micromechanics Microengineering* 20, 065016 (2010).
33. Tsao, C. W., Hromada, L., Liu, J., Kumar, P. & DeVoe, D. L. Low temperature bonding of

- PMMA and COC microfluidic substrates using UV/ozone surface treatment. *Lab. Chip* 7, 499–505 (2007).
34. Klank, H., Kutter, J. P. & Geschke, O. CO₂-laser micromachining and back-end processing for rapid production of PMMA-based microfluidic systems. *Lab. Chip* 2, 242–246 (2002).
 35. Prakash, S. & Kumar, S. Fabrication of microchannels on transparent PMMA using CO₂ Laser (10.6 μm) for microfluidic applications: An experimental investigation. *Int. J. Precis. Eng. Manuf.* 16, 361–366 (2015).
 36. Tsao, C.-W. & DeVoe, D. L. Bonding of thermoplastic polymer microfluidics. *Microfluid. Nanofluidics* 6, 1–16 (2009).
 37. Brown, L., Koerner, T., Horton, J. H. & Oleschuk, R. D. Fabrication and characterization of poly(methylmethacrylate) microfluidic devices bonded using surface modifications and solvents. *Lab. Chip* 6, 66–73 (2006).
 38. Du, L., Chang, H., Song, M. & Liu, C. The effect of injection molding PMMA microfluidic chips thickness uniformity on the thermal bonding ratio of chips. *Microsyst. Technol.* 18, 815–822 (2012).
 39. Kelly, R. T. & Woolley, A. T. Thermal Bonding of Polymeric Capillary Electrophoresis Microdevices in Water. *Anal. Chem.* 75, 1941–1945 (2003).
 40. Damase, T. R., Stephens, D., Spencer, A. & Allen, P. B. Open source and DIY hardware for DNA nanotechnology labs. *J. Biol. Methods* 2, e24 (2015).
 41. Malhotra, S. L., Minh, L. & Blanchard, L. P. Thermal Decomposition and Glass Transition Temperature of Poly(methyl Methacrylate) and Poly(isobutyl Methacrylate). *J. Macromol. Sci. Part - Chem.* 19, 579–600 (1983).
 42. Teng, H. et al. High glass transition temperatures of poly(methyl methacrylate) prepared by free radical initiators. *J. Polym. Sci. Part Polym. Chem.* 47, 315–317 (2009).
 43. Allen, P. B., Khaing, Z., Schmidt, C. E. & Ellington, A. D. 3D Printing with Nucleic Acid Adhesives. *ACS Biomater. Sci. Eng.* 1, 19–26 (2015).
 44. Bibikova, M. et al. High density DNA methylation array with single CpG site resolution.

- Genomics 98, 288–295 (2011).
45. Aydin, M. et al. Molecular identification of common Salmonella serovars using multiplex DNA sensor-based suspension array. *Anal. Bioanal. Chem.* 1–10, <https://doi.org/10.1007/s00216-018-0938-5> (2018).
 46. Lee, S. H. et al. On-Flow Synthesis of Co-Polymerizable Oligo-Microspheres and Application in ssDNA Amplification. *Plos One* 11, e0159777 (2016).
 47. Vogelstein, B. & Kinzler, K. W. Digital PCR. *Proc. Natl. Acad. Sci. USA* 96, 9236–9241 (1999).
 48. Meyer, A. J., Ellefson, J. W. & Ellington, A. D. Directed Evolution of a Panel of Orthogonal T7 RNA Polymerase Variants for in Vivo or in Vitro Synthetic Circuitry. *ACS Synth. Biol.* 4, 1070–1076 (2015).
 49. Quong, D., Neufeld, R. J., Skjåk-Bræk, G. & Poncelet, D. External versus internal source of calcium during the gelation of alginate beads for DNA encapsulation. *Biotechnol. Bioeng.* 57, 438–446 (2000).
 50. Yuet, K. P., Hwang, D. K., Haghgoie, R. & Doyle, P. S. Multifunctional Superparamagnetic Janus Particles. *Langmuir* 26, 4281–4287 (2010).

Appendix A: Copyright permission



SPRINGER NATURE

A CRISPR–Cas9-triggered strand displacement amplification method for ultrasensitive DNA detection

Author: Wenhua Zhou et al

Publication: Nature Communications

Publisher: Springer Nature

Date: Nov 27, 2018

Copyright © 2018, The Author(s)

Creative Commons

This is an open access article distributed under the terms of the [Creative Commons CC BY](#) license, which permits unrestricted use, distribution, and reproduction in any medium, provided the original work is properly cited.

You are not required to obtain permission to reuse this article.

To request permission for a type of use not listed, please contact [Springer Nature](#)



Cascade Transcription Amplification of RNA Aptamer for Ultrasensitive MicroRNA Detection



Author: Mengxi Zhou, Xucong Teng, Yue Li, et al

Publication: Analytical Chemistry

Publisher: American Chemical Society

Date: Apr 1, 2019

Copyright © 2019, American Chemical Society

PERMISSION/LICENSE IS GRANTED FOR YOUR ORDER AT NO CHARGE

This type of permission/license, instead of the standard Terms and Conditions, is sent to you because no fee is being charged for your order. Please note the following:

- Permission is granted for your request in both print and electronic formats, and translations.
- If figures and/or tables were requested, they may be adapted or used in part.
- Please print this page for your records and send a copy of it to your publisher/graduate school.
- Appropriate credit for the requested material should be given as follows: "Reprinted (adapted) with permission from {COMPLETE REFERENCE CITATION}. Copyright {YEAR} American Chemical Society." Insert appropriate information in place of the capitalized words.
- One-time permission is granted only for the use specified in your RightsLink request. No additional uses are granted (such as derivative works or other editions). For any uses, please submit a new request.

If credit is given to another source for the material you requested from RightsLink, permission must be obtained from that source.

[BACK](#)

[CLOSE WINDOW](#)

**SPRINGER NATURE****Graphene oxide assisted light-up aptamer selection against Thioflavin T for label-free detection of microRNA****Author:** Md Mamunul Islam et al**Publication:** Scientific Reports**Publisher:** Springer Nature**Date:** Feb 22, 2021*Copyright © 2021, The Author(s)***Creative Commons**

This is an open access article distributed under the terms of the [Creative Commons CC BY](#) license, which permits unrestricted use, distribution, and reproduction in any medium, provided the original work is properly cited.

You are not required to obtain permission to reuse this article.

To request permission for a type of use not listed, please contact [Springer Nature](#)



Simple, low-cost fabrication of acrylic based droplet microfluidics and its use to generate DNA-coated particles

Author: Md. Mamunul Islam et al

SPRINGER NATURE

Publication: Scientific Reports

Publisher: Springer Nature

Date: Jun 8, 2018

Copyright © 2018, The Author(s)

Creative Commons

This is an open access article distributed under the terms of the [Creative Commons CC BY](#) license, which permits unrestricted use, distribution, and reproduction in any medium, provided the original work is properly cited.

You are not required to obtain permission to reuse this article.

To request permission for a type of use not listed, please contact [Springer Nature](#)